

University of Science and Technology of China

A dissertation for doctor's degree



**Surface Modification of Biaxially Oriented
Polypropylene Membrane for Oily Wastewater
Separation**

Author: Most Zubaida Rukhsana Usha

Specialty: Chemistry

Supervisor: Prof. Li Liangbin

Finished time: May, 2023

中国科学技术大学学位论文原创性声明

本人声明所呈交的学位论文,是本人在导师指导下进行研究工作所取得的成果。除已特别加以标注和致谢的地方外,论文中不包含任何他人已经发表或撰写过的研究成果。与我一同工作的同志对本研究所做的贡献均已在论文中作了明确的说明。

作者签名: _____

签字日期: _____

中国科学技术大学学位论文授权使用声明

作为申请学位的条件之一,学位论文著作权拥有者授权中国科学技术大学拥有学位论文的部分使用权,即:学校有权按有关规定向国家有关部门或机构送交论文的复印件和电子版,允许论文被查阅和借阅,可以将学位论文编入《中国学位论文全文数据库》等有关数据库进行检索,可以采用影印、缩印或扫描等复制手段保存、汇编学位论文。本人提交的电子文档的内容和纸质论文的内容相一致。

保密的学位论文在解密后也遵守此规定。

公开 保密 (____年)

作者签名: _____

导师签名: _____

签字日期: _____

签字日期: _____

ACKNOWLEDGMENTS

ACKNOWLEDGEMENTS

This thesis is a result of the work done in **Prof. Liangbin Li** research group. I wish to express my special heartfelt gratitude to **Prof. Liangbin Li** for being my supervisor, advisor and motivator throughout the research work. It was a great honor to conduct successful research with him and gain more professional and academic research skills. **Dr. Xin Chen** is well acknowledged for being a big sister and friend, and for her various supports and guidance related to the research work. I thank the **Soft matter group** members including all teachers, colleague students, and supporting staff for providing a conducive research environment during my study period.

I owe my parents, sister, and other relatives too much for their endless efforts and support; I should not have become who I am today. I am grateful to all my other friends, my country mates, and all others of different nationalities with whom we shared social life in China through various activities, cultural events, etc. I also thank any other individual who contributed in one or another way to the realization of this thesis.

I sincerely acknowledge the **University of Science and Technology of China** for admitting me to its excellent research environment through the **National Synchrotron Radiation Laboratory**. This work would not have been possible without financial support. I thank the **Chinese Academy of Sciences (CAS)**, and **The World Academy of Sciences (TWAS)** for providing the fellowship grant.

ABSTRACT

ABSTRACT

The massive amounts of untreated oily wastewater produced by industrialization are directly discharged into the environment, causing a severe ecological issue. To address these issues, choosing the appropriate separation material is a highly effective method of separating water from oily wastewater. Polymeric based membrane-separation technologies can be employed as an ideal separation membrane, giving a reliable, efficient, and sustainable solution for oily wastewater separation. Among them, biaxial-oriented polypropylene membrane (PP) can replace widely used other conventional membranes due to their high mechanical strength in both machine and transitional directions. Such mechanical stability provides long service life with outstanding reusability. Unfortunately, the PP membrane's intrinsic hydrophobicity makes it easily clogged by oil droplets during separation, reducing permeability, efficiency, and reusability. To get rid of oil fouling and lessen the toxicity of oily wastewater, several effective surface modification techniques have been studied. Irradiation-induced graft polymerization approaches have been found to be the most successful and effective. This dissertation work aimed to construct a high-performance biaxial PP membrane separation technology using the influence of different monomers on the irradiation-induced graft polymerization method.

The first work modified the hydrophobic biaxial PP membrane using electron beam irradiation and subsequent chemical grafting utilizing acrylic acid and polyvinyl alcohol monomers. This simple surface modification approach considerably enhanced wettability and thermal and mechanical properties. Special attention has been given to increasing the anti-fouling phenomena, which can enhance the membrane's service life during oily

ABSTRACT

wastewater separation areas. The deposition of acrylic acid and polyvinyl alcohol as grafting monomers constructs a micro-nano rough structure to enhance the wettability with an amount of carboxyl and hydroxyl functional groups.

The second work developed a robust modified biaxial PP membrane that can withstand high operating pressure. A facile and scalable two-step surface modification method was developed by employing electron beam irradiation and grafting reaction using acrylic acid and sodium hydrogen carbonate monomers. This modification method aims to develop excellent underwater superoleophobicity, which can separate any kind of surfactant-stabilized emulsion with high separation efficiency. During the NaHCO_3 reaction process, a unique formation of super hydrophilic $-\text{COONa}$ functional groups are covalently attached and evenly distributed on a smooth biaxial PP surface thus creating a multi-scale stable rough surface through the grafting process. Such achieved rough surface assured oil droplets' aggregation upon contact and permitted straightforward water separation from oil/water emulsion. The robustness of the engineered super-wetting rough surfaces was studied under different harsh environments.

The third work focused on developing a super hydrophilic biaxial PP membrane modified via corona discharge treatment, followed by a grafting reaction with hydrophilic acrylamide monomer. Different acrylamide parameters (such as concentration, reaction temperature, and grafting duration) were studied comprehensively to find acceptable conditions for acrylamide monomer grafting reaction to produce surface nanostructures with permanent super hydrophilicity and underwater super oleophobicity. Significant separation performances were achieved for layered mixtures, surfactant-free, and

ABSTRACT

surfactant-stabilized emulsions by the highly energy-saving gravity- driven separation method.

The fourth work developed an advanced PP membrane through a highly efficient layer-by-layer modification technique using corona treatment, polyethylene imine and levo-3,4 dihydroxyphenylalanine crosslinked multi-layer assembling process. Through this synergistic development of the modification method, advanced antibacterial properties were generated. Modified PP membrane is antibacterial against *S. aureus* and *E. coli* bacteria. Notably, this highly efficient modified membrane was designed to remove multi pollutants (oil particles and bacteria) from oily wastewater in a more energy-efficient way. The improved properties of all modified biaxial PP membrane surfaces can anticipate being a substantial and prospective mass-scale industrial application for long-term oily wastewater separation.

Keywords: Biaxial polypropylene membrane, surface modification, super wetting, rough surface, oily wastewater separation

ABBREVIATIONS AND SYMBOLS

ABBREVIATIONS AND SYMBOLS

<i>Symbols</i>	Abbreviations
PP	Polypropylene
SFE	Surfactant free emulsion
SSE	Surfactant stabilized emulsion
μm	Micrometer
mm	Milimeter
nm	Nanometer
cm	Centimeter
t	Time
CA	Contact Angle
θ_y	Contact angle in young's model
γ_{sv}	Interfacial energy at the solid-vapor
γ_{sl}	Interfacial energy at the solid-liquid
γ_{lv}	Interfacial energy at the liquid-vapor
γ_{o-g}	Oil-gas interface tension
θ_1	Oil contact angle in the air
γ_{w-g}	Water-gas interface tension
θ_2	The water contact angle in the air
γ_{o-w}	Oil-water interface tension
θ_n	Oil contact angle in the water

ABBREVIATIONS AND SYMBOLS

Θ_w	Contact angle in Wenzel model
r	Solid surface roughness
f	Fraction area
θ_c	Contact angle in Cassie model
D_{pore}	Pore size of membrane
D_{drop}	Oil droplet size
$\gamma_{l_o l_w}$	Interfacial tension of the oil and water
$\cos\theta_{l_o l_w}$	Contact angle of the oil and water
\vec{F}_g	Gravity force
\vec{F}_j	Permeate force
\vec{F}_b	Bouncing force
\vec{F}_d	Driving force
γ_o	Surface tension of oil
θ_w	Water Contact Angle (WCA)
θ_o	Under Water Oil Contact Angle (UWOCA)
ΔP_i	Intrusion pressure
V	Speed of oil droplets
g	Gravity
P_w	Density of water
P_o	Density of oil
p	Porosity
r_p	Pore radius

ABBREVIATIONS AND SYMBOLS

Δl	Membrane thickness
τ	Pore tortuosity
ΔP	Pressure
J	Permeate flux
J_0	Pure permeability/flux
J_f	Final permeability/flux
2D	Two dimensional
3D	Three dimensional
ATRP	Atom transfers radical polymerization
UV	Ultraviolet
E.B	Electron beam
LBL	Layer-by-layer assembly
Ar	Argon
wt	Weight
%	Percentage
h	hour
min	Minute
s	Second
μL	Microliter
MPa	Megapascal
mL	Mililiter
L	Liter
gL^{-1}	Gram/liter

ABBREVIATIONS AND SYMBOLS

<i>R</i>	Efficiency
ppm	Parts per million
g	Gram
<i>HM-PP</i>	Hydrophilic modified-polypropylene
MD	Machine Direction
TD	Transverse Direction
<i>S</i>	Measured area
<i>z</i>	Relative profile height
Å	Angstrom
DFT	Density Functional Theory
DLS	Dynamic Light Scattering
W	Watt
η	Viscosity
CATB	Cetyltrimethylammonium Bromide
SDS	Sodium dodecyl sulfate

TABLE OF CONTENTS

TABLE OF CONTENTS

<i>ABSTRACT</i>	<i>I</i>
<i>ABBREVIATIONS AND SYMBOLS</i>	<i>IV</i>
<i>TABLE OF CONTENTS</i>	<i>VIII</i>
<i>LIST OF FIGURES</i>	<i>XII</i>
<i>LIST OF TABLE</i>	<i>XXIII</i>
<i>CHAPTER 1. General introduction and literature review</i>	<i>1</i>
<i>1.1. Introduction</i>	<i>1</i>
1.1.1. Environmental impact of oily wastewater	<i>3</i>
1.1.2. Sources and importance of oily wastewater separation	<i>4</i>
1.1.3. Types of different oily wastewater	<i>6</i>
1.1.4. The general concept of surface wettability in terms of oil/water separation	<i>9</i>
1.1.5. Basic requirements of membranes for oil/water separation.....	<i>14</i>
1.1.6. Widely used polymeric membranes for oil/water separation	<i>19</i>
1.1.7. Advanced properties of polymeric membranes.....	<i>22</i>
1.1.8. Surface modification process.....	<i>28</i>
<i>1.2. Objectives and motivation of the study</i>	<i>37</i>
<i>1.3. Organization of the thesis</i>	<i>39</i>
<i>CHAPTER 2. Fouling-resistant biaxial polypropylene membrane for pressure driven separation</i>	<i>42</i>
<i>2.1. Introduction</i>	<i>42</i>
<i>2.2. Experimental</i>	<i>46</i>
2.2.1. Materials.....	<i>46</i>

TABLE OF CONTENTS

2.2.2.	Electron beam irradiation process -----	46
2.2.3.	Preparation of AA-g-PP membranes -----	47
2.2.4.	Preparation of PVA/AA-g-PP membranes -----	48
2.2.5.	Membrane characterization-----	48
2.2.6.	Anti-oil fouling performance-----	49
2.3.	<i>Results and discussion</i> -----	50
2.3.1.	The effect of electron beam irradiation -----	50
2.3.2.	Acrylic acid grafting on PP membrane -----	51
2.3.3.	PVA graft polymerized PP membrane -----	54
2.3.4.	Surface microstructure -----	55
2.3.5.	Chemical structure-----	57
2.3.6.	Mechanical and thermal properties -----	59
2.3.7.	Anti-oil fouling behavior-----	62
2.4.	<i>Conclusions</i> -----	63
<i>CHAPTER 3. Robust super-wetting multi-scale rough biaxial polypropylene membrane for pressure driven separation</i> -----		65
3.1.	<i>Introduction</i> -----	65
3.2.	<i>Experimental</i> -----	69
3.2.1.	Materials-----	69
3.2.2.	Membrane characterization-----	69
3.2.3.	Calculation of water adsorption energy-----	69
3.2.4.	HM-PP membrane fabrication -----	70
3.2.5.	Surfactant-stabilized oil/water emulsion preparation-----	70
3.3.	<i>Results and discussion</i> -----	70

TABLE OF CONTENTS

3.3.1.	Hydrophilic modified (HM-PP) membrane -----	70
3.3.2.	Surface microstructure and chemical compositions -----	71
3.3.3.	Multi-scale surface roughness -----	76
3.3.4.	Membrane wettability -----	78
3.3.5.	Membrane stability performance -----	79
3.3.6.	Anti-oil fouling properties -----	83
3.3.7.	Emulsion separation performances -----	84
3.4.	<i>Conclusions</i> -----	88
<i>CHAPTER 4. Super hydrophilic modified biaxial polypropylene membrane for gravity-driven separation</i> -----		90
4.1.	<i>Introduction</i> -----	90
4.2.	<i>Experimental</i> -----	95
4.2.1.	Materials and chemicals -----	95
4.2.2.	Modification process of C/AM-g-PP membrane -----	95
4.2.3.	Calculation of water adsorption energy -----	96
4.2.4.	Preparation of different oil/water emulsion and separation performances -----	96
4.3.	<i>Results and discussion</i> -----	97
4.3.1.	Fabrication of super hydrophilic C/AM-g-PP membrane -----	97
4.3.2.	Chemical structure and compositions -----	101
4.3.3.	Surface morphology & macroscopic properties -----	103
4.3.4.	Membrane wettability behavior and stability performances -----	104
4.3.5.	Theoretical mechanism of underwater oleophobicity and super hydrophilicity -----	106
4.3.6.	Emulsion separation performances -----	108

TABLE OF CONTENTS

4.4. Conclusions -----	116
CHAPTER 5. Advanced super-wetting multipollutant removal biaxial polypropylene membrane for gravity driven separation -----	118
5.1. Introduction -----	118
5.2. Experimental -----	122
5.2.1. Materials -----	122
5.2.2. Preparation of monomer solutions -----	123
5.2.3. Layer-by-Layer assembling modification process -----	123
5.2.4. Oil/water emulsions preparation and separation experiments -----	124
5.3. Results and discussion -----	125
5.3.1. Micro-morphology and chemical compositions -----	125
5.3.2. Relation between surface roughness and membrane wettability -----	126
5.3.3. Environmental stability of the membrane -----	129
5.3.4. Separation performances of oily wastewater -----	131
5.3.5. Anti-bacterial performance -----	136
5.4. Conclusions -----	136
CHAPTER 6. Summary and future perspectives -----	138
LIST OF PUBLICATIONS -----	142
REFERENCES -----	143

LIST OF FIGURES

Figure 1.1: a) Distribution and reserves of unconventional oil resources ^[26], b) Number of research paper publications on oil/water emulsion separation from 2010 to 2022 (collection source: web of science, search word: emulsion separation).....**5**

Figure 1.2: Schematic illustration of different forms of oily wastewater- a) Light oil/water mixture b) Heavy oil/water mixture, c) Oil/water emulsion; (d-e) Optical microscopy images of a surfactant-free and surfactant stabilized emulsion ; (f-g) Stability of a surfactant-free and surfactant stabilized emulsion during separation ^[33].....**8**

Figure 1.3: a) Different wetting states, and b) Emulsion separation mechanism.**11**

Figure 1.4: a)1-3. Schematic illustration of the switchable wettability properties membrane and wettability performances ^[75]; b)1-4. Proposed mechanism of photocatalytic degradation and their corresponding degradation performances ^[80]; c)1-3. Schematic diagram of physical damage; corresponding contact angle; digital and SEM imagines of the damaged membrane surface before and after self-healing ^[82]; d)1-3. Inhibitory zones against *E. coli* and *S. aureus*; corresponding digital images, and antibacterial performances of using different membranes ^[84].....**26**

Figure 1.5: Widely used different surface modification methods applied for oily wastewater separation.....**29**

Figure 1.6: a) Strategies of different grafting methods-grafting-to, grafting-from, grafting-through ^[92]; Schematic illustration of the b)1-2. Brush-functionalized chemical-induced grafted PAN membrane using ATRP initiator ^[94], and two step chemical-induced grafted PVDF membrane using alkali initiator ^[95]; Schematic illustration of the irradiation-induced

LIST OF FIGURES

graft polymerization using c)1-2. Ar plasma and acrylic acid grafting ^[96], and corona treatment and acrylamide grafting ^[44].**30**

Figure 1.7: Schematic illustration of a)1-3. the dip coating modification process and the modified membranes' wettability and separation performances ^[100]; b)1-3. the immersion process and their wettability with separation performances ^[101]; c)1-2. the spray coating method and separation efficiency values ^[76]; d)1-2. the vacuum coating method and cross-sectional micrographs of modified and unmodified membrane ^[102]; e)1-2. the rub and spin coating method and the wettability of the modified membrane ^[103].**31**

Figure 1.8: Schematic illustration of a) the plasma (Ar) irradiation process ^[110]; b)1-3. the UV-irradiation method, WCA values, and corresponding water flux and rejection rate ^[111]; c)1-3. the gamma irradiation process, flux and oil rejection of the gamma irradiated membrane with recycling properties ^[112].**33**

Figure 1.9: Schematic illustration of the a)1-3. LBL modification process, flux and rejection ratio of different LBL modified membrane ^[82]; b)1-3. mineralized LBL modification process, SEM images of different cycles membrane, and WCA and UWOCA values ^[115]; c)1-4. electrostatic LBL self-assembly process, underwater chloroform sliding angles and self-cleaning tests, water permeances, flux recovery ratio and oil content in permeances ^[116].**34**

Figure 1.10: Illustration of the a)1-2. crosslinking modification process of PVDF/GO membrane and their separation performances ^[117]; b)1-3. in-situ cross-linking modified membrane, oil demulsification process, and separation performances of modified membrane ^[118]; c)1-3. crosslinking process, corresponding separation flux and flux recovery ^[119].**35**

LIST OF FIGURES

- Figure 2.1:** Schematic illustration of the a) Fabrication process of biaxially oriented microporous PP membrane, b) Hydrophilic surface modification of hydrophobic PP membrane by pre-irradiation-induced graft polymerization method with possible chemical structures.....**46**
- Figure 2.2:** SEM micrographs of electron beam irradiated PP membrane with high and low resolution, (a1-b1) 0 kGy irradiated PP, (a2-b2) 5 kGy irradiated PP membrane, (a3-b3) 30 kGy irradiated PP membrane, and c) ESR spectra of the E.B irradiated membrane.**51**
- Figure 2.3:** Grafting ratio of AA on the PP membrane surface and Water contact angle measurement in different variable parameters a) Temperature (50 °C - 90 °C), b) Concentration (5% - 25%), c) Grafting heating time (3 min – 15 min), and d) Electron beam dose (5 kGy- 30 kGy).**52**
- Figure 2.4:** FTIR spectra for a) Effect of temperature, b) Effect of concentration, c) Effect of grafting heating time, and d) Effect of electron beam dose.....**53**
- Figure 2.5:** a) A linear relation between WCA and pore sizes of different AA-g-PP membranes; b) a linear relation between grafting ratio and UWOCA of different PVA loaded membranes; c) WCA measurement at 100 s wetting time, d) corresponding dynamic photographs at 0 s and 100.**55**
- Figure 2.6:** SEM micrographs of a1) unmodified PP, a2) AA-g-PP, a3) PVA/AA-g-PP-1, a4) PVA/AA-g-PP-3, and a5) PVA/AA-g-PP-5 membrane; b) a relation graph of membrane wettability and surface roughness; AFM 2D and 3D images of the (c1-c2) unmodified PP, and (d1-d2) PVA/AA-g-PP-5 membrane.**56**
- Figure 2.7:** Surface chemical compositions of PP, AA-g-PP, and PVA/AA-g-PP membrane. a) ATR-FTIR spectra; b) Wide scan XPS spectra; High-resolution C1s fitting

LIST OF FIGURES

curve of, c) unmodified PP membrane, d) AA-g-PP membrane and e) PVA/AA-g-PP-5 membrane; and High-resolution O1s fitting curve of, c) unmodified PP membrane, d) AA-g-PP membrane and e) PVA/AA-g-PP-5 membrane.58

Figure 2.8: Mechanical and thermal properties of PP, AA-g-PP, and PVA/AA-g-PP membranes; a) stress-strain curve at MD direction, b) stress-strain curve at TD direction, c) TGA thermographs, and d) DSC heating curve.61

Figure 2.9: a) Permeability and rejections of PP, AA-g-PP, and PVA/AA-g-PP membranes; b) long-term permeability with anti-oil fouling properties of PVA/AA-g-PP membrane, c) FRR and FDR value of different membranes.63

Figure 3.1: Schematic illustration of the a) conversion process of hydrophobic biaxial PP membrane to super-wetted HM-PP membrane and b) emulsion separation method through unmodified and rough surface structured modified PP membrane.68

Figure 3.2: WCA data of NaHCO₃ treatment in different variable parameters a) temperature, b) concentration, and c) heating time.71

Figure 3.3: (a-c) Surface microstructure of PP, AA-g-PP, and HM-PP membranes, d) EDS mapping images of HM-PP membrane with elemental percentile, e) average pore diameter, f) ATR-FTIR, and g) Survey XPS spectra.....72

Figure 3.4: Cross-sectional micrographs of a) unmodified PP, b) AA-g-PP, and c) HM-PP membrane73

Figure 3.5: a) N₂ adsorption/desorption curves and b) porosity value of PP, AA-g-PP and HM-PP membrane.73

LIST OF FIGURES

Figure 3.6: (a-f) High-resolution C 1s, O 1s, and Na1s, XPS spectra of PP, AA-g-PP, and HM-PP membranes.	75
Figure 3.7: 3D AFM values measured in the (a1-c1) air condition, (a2-c2) underwater condition; Multiscale roughness value in X and Y direction; (d1-d2) unmodified PP membrane, (e1-e2) AA-g-PP membrane, (f1-f2) HM-PP membrane; g) linear graph of average roughness value, and h) digital images of a membrane with marking X and Y directions.....	78
Figure 3.8: a) Dynamic WCA images and values, b) membrane wetting images; c) UWOCA of HM-PP membrane; (d-f) DFT optimized geometries of water adsorbed by CH ₃ , COOH, and COONa group of PP, AA-g-PP, and HM-PP membrane respectively (an orange dashed frame marks the water molecule and grey, white, red, and purple represents C, H, O, and Na respectively), and i) corresponding electrical energy values in Hartree unit (1Ha=2565.5 kJ/mol=627.5094 kcal/mol) to calculate the water-binding energy.	79
Figure 3.9: a) Thermal stability; (b-c) mechanical stability in MD and TD directions; d) UWOCA at harsh environments with corresponding dynamic UWOCA images; e) variation of UWOCA of the HM-PP membrane after being abraded by different sandpapers; f) the schematic illustration of sand abrasion test; g) scotch tape peeling, h) membrane bending and i) UV irradiation time.	81
Figure 3.10: SEM images of sand paper abraded HM-PP membrane using (a1-a2) 120 mesh, (b1-b2) 220 mesh, and (c1-c2) 320 mesh sandpaper.	82
Figure 3.11: SEM images of HM-PP membrane after a) scotch tape peeling, h) bending and i) UV irradiation.	82

LIST OF FIGURES

Figure 3.12: a) Anti-oil adhesion properties by the approach-compress-detach method; dynamic photographs of underwater soybean oil contamination by b) unmodified PP membrane, c) modified HM-PP membrane; d) excellent self-oil cleaning properties of HM-PP membrane.**83**

Figure 3.13: Schematic illustration of the emulsion separation device, b) optical microscope and digital images of feed and filtered water, (c-d) oil droplet sizes of feed and filtered water measured by DLS, e) digital photographs of HM-PP membrane before and after 10 cycles emulsion separation.**85**

Figure 3.14: a) Surface microstructure and b) cross-sectional micrographs of HM-PP membrane after 10 cyclic separations.**86**

Figure 3.15: Separation performances of HM-PP membrane - a) various oil/water emulsions, b) different soybean oil content emulsion, c) cyclic performances; FRR value using d) various oil/water emulsions, e) different soybean oil content emulsion, f) cyclic performances.**86**

Figure 4.1: Schematic illustration of the (a) preparation of commercial biaxially oriented PP membrane and the transformation process of hydrophobic PP membrane to super hydrophilic C/AM-g-PP membrane, (b) emulsion separation mechanism through unmodified hydrophobic and modified super hydrophilic PP membrane.**95**

Figure 4.2: Wettability behavior of C/PP membrane by dynamic water contact angle experiment at different power over the different treatment times. a) power-300 W (treatment time-60 s, 120 s, 180 s, 240 s, and 300 s; b) power-400 W (treatment time- 30 s, 60 s, 90 s, and 120 s); c) power-500 W (treatment time- 10 s, 20 s, and 30 s); d) optical

LIST OF FIGURES

images of water contact angle of C/PP membrane at different power and treatment time.	97
Figure 4.3: SEM micrographs of C/PP membrane using different treatment power and time, 300 power (a1-a4)- 60s, 120s, 180s, 240s treatment time; 400 power (b1-b4)- 30s, 60s, 120s, and 180s treatment time; 500 power (c1-c3)- 10s, 20s, and 30s treatment time; and d) unmodified PP membrane.	99
Figure 4.4: The grafting ratio value of a) monomer concentration at 90 °C temperature and 45 min grafting time, b) temperature using 10 % (v/v) monomer concentration and 45 min grafting, c) monomer grafting time using 10 % (v/v) monomer concentration at 90 °C temperature.	100
Figure 4.5: Water contact angle values of using different a) monomer concentration, b) temperature, c) grafting time; WCA images of different wetting times represent the wetting behavior of C/AM-g-PP membrane for d) 45 min and e) 60 min grafting time.	101
Figure 4.6: Surface chemical compositions of PP, C/PP, and super hydrophilic C/AM-g-PP membrane. a) Possible chemical structure with new functional groups of C/AM-g-PP membrane, b) ATR-FTIR spectra, c) wide scan XPS spectra; High-resolution C1s fitting curve of d) unmodified PP membrane, e) C/PP membrane, and f) C/AM-g-PP membrane.	102
Figure 4.7: (a1-c1) SEM surface microstructure, (a2-c2) cross-sectional micrographs, (a3-c3) nitrogen adsorption/desorption properties of unmodified PP membrane, C/PP membrane, and C/AM-g-PP membrane, respectively and d) EDS scanning images of C, O, and N elements of C/AM-g-PP membrane.	103

LIST OF FIGURES

- Figure 4.8:** a) Under water-oil contact angle value with optical images of oil droplets (Petroleum ether, Hexane, Toluene, and Soybean oil), b) WCA and UWOCA values of C/AM-g-PP membrane at different complex conditions, c) dynamic oil (Soybean oil) adhesion properties of C/AM-g-PP membrane by the approach-compress-detach method. **105**
- Figure 4.9:** Water adsorption energy calculation, (a-c) DFT optimized geometries of water adsorbed by COOH, CONH₂, and CH₃ groups respectively, and corresponding calculated water adsorption energy. The water molecule is marked by a yellow dashed frame and grey, white, red, and blue represent C, H, O, and N respectively. **107**
- Figure 4.10:** Digital photographs of the oil and water separation process a) layered mixture separation, b) surfactant stabilized emulsion separation, c) digital image of the water spreading over unmodified PP and modified C/AM-g-PP membrane, and d) photographs of the different emulsion separated membrane. **109**
- Figure 4.11:** Permeate flux and separation efficiency of C/AM-g-PP membrane for the separation of various oil (Petroleum ether, Hexane, Toluene, and Soybean oil) from water; a) oil/water layered mixture, b) surfactant-free emulsion, c) surfactant stabilized emulsion, d) flux recovery ratio values, d) changes of the permeate fluxes of the layered mixture, surfactant-free emulsion, and surfactant stabilized emulsion for Petroleum ether over 10 recycle numbers, and f) permanent hydrophilicity and underwater oleophobicity (P. ether) behavior of C/AM-g-PP membrane measured over 10 weeks. **111**
- Figure 4.12:** Permeate flux and corresponding separation efficiency performance of C/AM-g-PP membrane of different oil/water layered mixture, a) petroleum ether; b) hexane, c) toluene, and d) soybean oil over 10 recycle number. **113**

LIST OF FIGURES

Figure 4.13: Surface morphology in low and wide resolutions of C/AM-g-PP membrane after surfactant stabilized oil-in-water emulsion separation, (a1-a2) Petroleum ether, (b1-b2) hexane, (c1-c2) toluene, and (d1-d2) soybean oil.	114
Figure 4.14: Optical microscopy and digital photographs of a) surfactant-free and b) surfactant-stabilized feed emulsion and permeate water of Petroleum ether, Hexane, Toluene, and Soybean oil.	115
Figure 4.15: Comparison of separation efficiency and permeate flux of various membranes with our work, a) layered mixture, b) surfactant-free emulsion, and c) surfactant stabilized emulsion.....	116
Figure 5.1: Schematic illustration of the a) possible chemical reaction mechanism and, b) modification process of the super-wetting membrane.	122
Figure 5.2: L-dopa solution a) before and b) after self-polymerization.	123
Figure 5.3: a) Polymerization yields, b) Digital photographs of unmodified and different layer assembled PP membranes.	124
Figure 5.4: Surface microstructure of (a1-a5) unmodified PP membrane, PP/3 L, PP/5 L, PP/10 L, and PP/15 L membrane; (b) EDS mapping images of PP/15 L membrane with elemental percentile; c) ATR-FTIR spectra; (d-f) high-resolution C1s, O1s, and N1s XPS spectra of PP/15 L membrane.	125
Figure 5.5: (a-b) A relation graph of surface roughness with WCA and UWOCA values, respectively; (c1-c2) 2D AFM images and (d1-d2) surface topography profiles of PP and PP/15 L membrane.	127

LIST OF FIGURES

- Figure 5.6:** a) Differences of wetting time with different modification layers, b) underwater oil contact angle of PP/15 L membrane using different oils, c) a comparison of underwater oil contact angle value with our work and other reported literature, d) a schematic illustration of the inner pore structure of unmodified and different layered modified membranes with anti-oil fouling performances. **129**
- Figure 5.7:** Water contact angle and underwater oil contact angle value of PP/15 L membrane in various complex conditions; a) sandpaper abrasion, b) membrane bending, c) scotch tape peeling, d) UV radiation exposure; e) different pH values, f) membrane storage over 8 weeks. All UWOCA experiments were carried out using vegetable oil. **130**
- Figure 5.8:** a) Permeate flux and corresponding separation efficiency, b) membrane cycling performances of PP/15 L membrane using petroleum ether/water emulsion. **132**
- Figure 5.9:** Separation fluxes and efficiency of PP/15 L membrane using various oil/water as a) free oil layer mixture, b) surfactant stabilized emulsion, c) a relation curve of flux in regards to different oil viscosity; d) a continuous separation flux, e) flux recovery ratio f) a comparison of surfactant-stabilized emulsion separation performances of our work with other literature. **134**
- Figure 5.10:** a) Oil demulsification and aggregation properties of the surfactant-stabilized emulsion; DLS oil droplet information with digital photographs of surfactant stabilized feed emulsion and permeate water; (b1-b4) petroleum ether and (c1-c4) vegetable oil. **135**
- Figure 5.11:** Anti-bacterial activities on *S. aureus* and *E.coli* bacteria incubated with PP and PP/15 L membranes, and b) their corresponding digital images. **136**

LIST OF FIGURES

Figure 6.1: Schematic graph of the recent progress of the different modification methods for constructing super wetting biaxial PP membrane surface and the need for more effective and universal strategies.....	141
--	------------

LIST OF TABLE

LIST OF TABLE

Table 1.1: Chemical structure of widely used different commercial polymeric membranes for oil/water separation.	21
Table 1.2: Separation performances of the advanced polymeric membranes in oil/water separation.	27
Table 1.3: A details comparison of separation performances using different surface modifying polymeric membranes for oil/water separation.	36
Table 2.1: Chemical composition of unmodified PP, modified AA-g-PP, and PVA/AA-g-PP-5 membrane	58
Table 3.1: BET surface area of PP, AA-g-PP, and HM-PP membrane.....	74
Table 3.2: A comparison of various membrane separations of emulsified oil/water emulsion.....	88
Table 5.1: The viscosity of different oils that are used in this work.	133

CHAPTER 1. General introduction and literature review

1.1. Introduction

The scarcity of freshwater by water pollution has become a significant challenge in the 21st century ^{[1][2]}. According to reports, the earth contains 2.5% fresh water, of which only 1% is accessible. More than two billion people worldwide are thus without access to fresh water. Such insufficiency of fresh water occurs due to the enormous amounts of untreated oily wastewater produced by industrialization (food, textile, leather, petrochemical, pharmaceutical, metal, etc.) ^{[3][4]}. In addition, our ecosystem and human health are seriously threatened by the industrial contribution of the free discharge of oily wastewater ^[5]. Developing an economically and highly efficient favorable technique to treat oily wastewater has recently attracted many researchers to ameliorate such environmental and fresh water scarcity issues ^[6].

Numerous techniques have been developed by many industries to treat oily wastewater due to their significant negative impacts on the environment and human health. Therefore, the commonly widely used traditional approaches are- adsorption ^[7], biological treatment ^[8], floatation ^[9], and coagulation ^[10]. The primary drawbacks of conventional procedures are- a) contamination and devaluation of remaining oil, b) the requirement for both sophisticated control and skilled operators, c) high operating expenses, and d) remaining significant environmental impact ^[11]. Membrane-separation technology has been appreciated as a versatile approach that can address the shortcomings of traditional treatment methods and emerged as a result of the quick development in separation technology ^[12]. The membrane-based technology distinct many advantages such as high

CHAPTER 1

separation efficiency, low cost, fast operation, simple separation process, and economical^[6] and can successfully separate layered mixtures, surfactant-free emulsion, and surfactant-stabilized emulsion. The most extensively used membrane technology for treating oily wastewater are- polymeric membranes^[13], ceramic membranes^[14], graphene oxide-based membranes^[15], mixed-matrix membranes^[16], etc.

Polymeric membrane-based technology now commands the most interest among other membrane-based technologies in the emulsion separation area and is incredibly adaptable in industry verticals. Oil/water separation performance can be greatly enhanced by polymeric membranes with high water flux, separation efficiency, and antifouling properties. Therefore, dealing with trade-off relationships between efficiency and flux as well as membrane fouling and scaling is one of the main problems with the use of polymeric membranes in the treatment of oily wastewater^[1]. Several researchers highlight the fouling issues of polymeric membranes thus declining the separation performances and their uses commercially^[17]. Therefore, Thus to enlighten the raised issues of polymeric membranes, a few important parameters should be present in the membrane before applying for oil/water separation- a) surface roughness, b) nanoscale pore size, c) super wettability (hydrophilicity and underwater oleophobicity), d) chemical stability, and e) mechanical durability. Unfortunately, all polymeric membranes are facing a lack of some of these above-required properties.

Surface modification is only the most effective process thus can enhance all of these required features, overcome the fouling issues and dominate the modified polymeric membrane in the oil/water separation area. Various surface modification processes can apply, such as surface coating, grafting, irradiation (gamma^[18], electron beam^[19], plasma,

CHAPTER 1

etc.), cross-linking, layer-by-layer method, etc. Many variable parameters need to take care of during the surface modification process such as temperature, modifying materials concentration, reaction time, etc. Using polymeric membranes as the foundation, recent oil/water separation technology is focused on creating advanced properties, including-switchable wettability, self-cleaning, antibacterial, and self-healing capacities. Such advanced features are still in the early stages of development and use. Therefore, considerable work needs to be done before they can be used in real-world applications.

1.1.1. Environmental impact of oily wastewater

Oily wastewater must be appropriately treated and disposed of in order to have the least negative environmental impact possible, which generated by industrial development and causes oil splits and production of huge amount of oily wastewater ^[4]. This may entail removing contaminants using cutting-edge treatment techniques and making ensure that any leftover waste is disposed of safely and sustainably. Additionally, through improved manufacturing processes and waste reduction techniques, efforts should be made to lessen the amount of oily wastewater generated in the first place. Therefore, it can be concluded that oily wastewater pollution is mainly manifested in the following main aspects ^[20].

- **Water pollution:** The discharge of untreated or inadequately treated oily wastewater into water bodies can cause serious harm to aquatic life. Hydrocarbons, heavy metals, and other toxic chemicals can accumulate in fish and other aquatic organisms, leading to reduced growth rates, reproductive problems, and even death. In addition, oily wastewater can disrupt the ecological balance of water bodies by depleting oxygen levels and altering pH levels.

CHAPTER 1

- **Soil contamination:** When oily wastewater seeps into the soil, it can contaminate the ground and pose a risk to plants, animals, and humans. Hydrocarbons and other pollutants can accumulate in the soil and reduce its fertility, leading to reduced crop yields and plant growth. In addition, contaminated soil can pose a health risk to animals and humans that consume plants grown in the contaminated soil.
- **Air pollution:** The treatment and disposal of oily wastewater can release harmful gases into the atmosphere, contributing to air pollution. Methane, a potent greenhouse gas, can be released during the treatment of oily wastewater if anaerobic conditions are present. In addition, volatile organic compounds (VOCs) can be released into the air during the storage and transportation of oily wastewater.
- **Climate change:** Oily wastewater can contribute to climate change if it contains methane, a potent greenhouse gas. Methane is released during the treatment and disposal of oily wastewater if anaerobic conditions are present.

The environmental impact of oily wastewater can be significant, but there are various approaches that can be used to mitigate this impact. By implementing proper treatment with advanced membrane-based separation technology can reduce the toxicity amount of oily wastewater, can minimize the negative impact on the environment.

1.1.2. Sources and importance of oily wastewater separation

Oily wastewater discharge without any pre-treatment has negative consequences on the ecosystem, including soil, groundwater, and surface water. Additionally, wastewater elements such as hydrocarbons, oils, fats, and petroleum fractions may also contribute to air pollution by evaporation ^[21]. Oil-water emulsions have severely polluted many regions, seas, and oceans. Repeated industrial effluent releases, maritime activities, and oil spills

CHAPTER 1

are the main causes of these pollutions. Over a million tons of oil have been released into the sea annually in the last fifteen years, according to the US National Research Council [22]. As a result, given the current rise in oil discharge at this level, it is imperative to address this issue and build an oil wastewater treatment system that complies with national restrictions while ensuring safety leakage. Therefore, many international organizations and countries have established strict guidelines for the safe dispensing of oil-water emulsions. Such as- in Australia, the allowed concentration of oil in water streams at the discharge limit is just 30 ppm per day and 50 mg per liter at any given time [23]. According to the emission standard of Malaysia, the emission is only allowed 10 mg/L for discharge into any other inland or Malaysian waterways and 5 mg/L for discharging into any inland waters within defined catchment regions [1]. The People's Republic of China is permitted to release water with a maximum oil level of 10 ppm, which increased to 29 ppm in the United States [24][25]. On the other hand, restoring of unconventional oils is also a concerning issue and thus can create frequent oil spills.

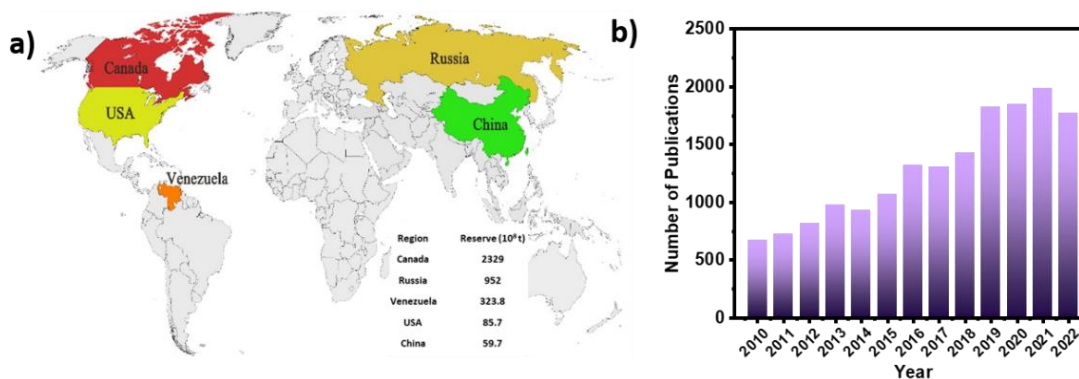


Figure 1.1: a) Distribution and reserves of unconventional oil resources [26], b) Number of research paper publications on oil/water emulsion separation from 2010 to 2022 (collection source: web of science, search word: emulsion separation).

CHAPTER 1

According to the obtained data **Figure 1.1a**, large regions including North America, Eastern Europe, Latin America, and China reserves more than 6 trillion barrels of unconventional oil ^[26]. Therefore, the above national restrictions and the possibility of unconventional oil spills accident create a pressing need for technological advancement that may meet the objectives of environmental legislation while still being reasonably priced. It is crucial to have in-depth knowledge of oily wastewater separation, which leads the researchers actively investigate the developments of state-of-art oily wastewater separation. **Figure 1.1b** shows the publication database of the last 12 years by different researchers on oily wastewater separation. The increasing trend of the given data indicates the potentiality of conducting research on oily wastewater separation due to its severe toxicity.

1.1.3. Types of different oily wastewater

The fast expansion of industrial operations in the oil and gas, petrochemical, pharmaceutical, metallurgical, and food industries has resulted in significant challenges due to the massive production of organic solvents and oily wastewater. Furthermore, purified water supplies are critical for human survival and progress. Due to the variety and complexity of oil/water combinations, the separation of oily wastewater is fraught with difficulties in real-world applications. To achieve efficient separation for all sorts of oily wastewater, it is crucial and required to re-conceptualize the types of oily wastewater and grasp their distinct characteristics and properties.

1.1.3.1. Free oil/water mixture

The free oil/water separation is easier due to its formation as a free oil cake layer on top of the water. Due to the super hydrophilic properties, water can easily penetrates the

CHAPTER 1

membrane by gravity force whereas the free oil layer is left over at the top of the membrane. It assumes that free oil in water can be separated by a gravity-driven process without applying any external pressure. Free oil/water mixtures can be classified as light oil/water or heavy oil/water mixtures based on the density differential between oil and water. Furthermore, if water has a higher density than oils and organic solvents is considered a light oil/water mixture. On the contrary, if water has a lower density than oils and/or organic solvents, which is considered a heavy oil/water mixture. However, the light oil layer is easy to remove due to its floating behavior, which prevents oil from spreading and passing through the membrane. Whereas, high-viscosity oils are difficult to remove due to the high surface tension of oil than water. Such adhering oils are difficult to separate, which often gathered at the membrane surface, causing pore clogging and sharp decline at permeate flux, resulting in a limited number of reusability.

1.1.3.2. Oil/water emulsion

Oil/water emulsions can be categorized as surfactant-free and surfactant-stabilized emulsions. Both surfactant-free (SFE) and surfactant-stabilized (SSE) emulsion separation is more difficult than oil/water mixture separation. However, as compared with surfactant-free, surfactant-stabilized is distinguished as an extremely challenging and complex one to separate due to their very stable oil droplets in water^[27]. The oil droplet sizes in surfactant-free emulsions are (20 μm –150 μm) and surfactant-stabilized emulsions are below 20 μm ^{[28][29]}. However, the reason for such micro nano-sized oil droplets in SSE is due to using surfactants, which break the oil droplets into tiny sizes during magnetic stirring, such differs from the oil droplet sizes in SFE and SSE^{[30][31]}. Therefore, membranes with micro/mili meter-sized pores, in addition to different typical and traditional procedures are

CHAPTER 1

not suitable for emulsion separation ^[32]. As a result, the controllability of the pore-sized membrane provides significant benefits in the field of emulsion separation. The theoretical foundation "size-sieving" mechanism can be applied for larger oil droplets and smaller membrane pore sizes during emulsion separation. However, particular pore sizes are required to allow the continuous phase to move through the membrane fast. In addition, SFEs and SSEs provide different stabilities. *Li et al.* showed that in the same amount of time, ($t=230$ s), an SFE demulsified and aggregated into large oil droplets, while the particle size of an SSE showed almost no change ^[33], which proves the strong stability of SSE as than SFE.

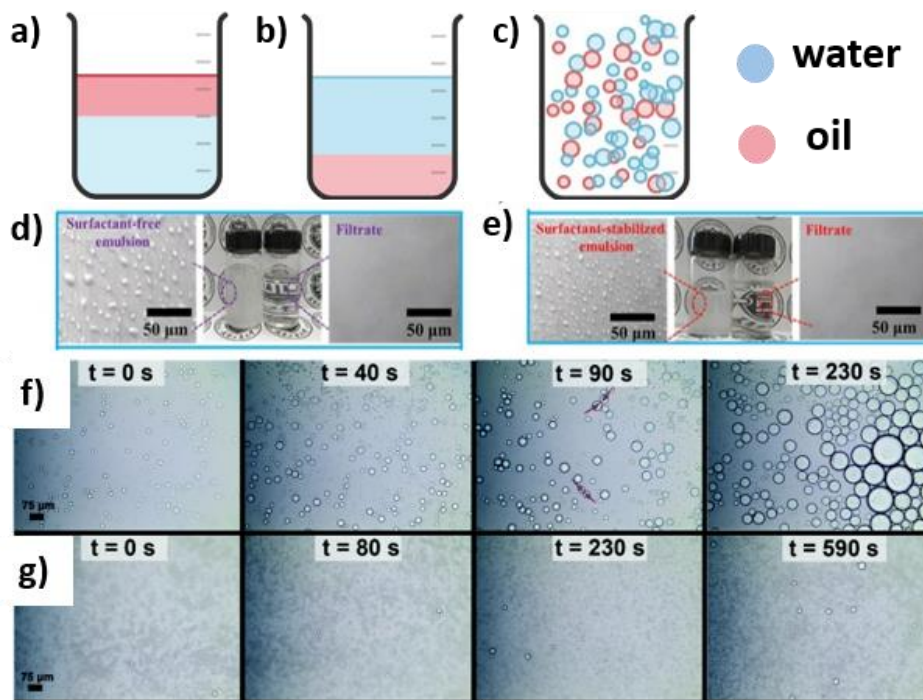


Figure 1.2: Schematic illustration of different forms of oily wastewater- a) Light oil/water mixture b) Heavy oil/water mixture, c) Oil/water emulsion; (d-e) Optical microscopy images of a surfactant-free and surfactant stabilized emulsion ; (f-g) Stability of a surfactant-free and surfactant stabilized emulsion during separation ^[33].

CHAPTER 1

1.1.4. The general concept of surface wettability in terms of oil/water separation

The surface wettability is considered the foremost criterion for oil/water separation, which depends on their physicochemical properties. Wetting refers to the interaction of the oil, water, air, and solid (membrane surface) phases when oil/water separation is discussed with the separation mechanism (**Figure 1.3a-b**). Understanding the concept of dynamics that initiative wettability can help us to better understand the utilization of simple and effective membrane technology for oil/water separation.

1.1.4.1. Wetting models

The interfacial tension of different mediums (solid, liquid, and vapor) can determine the contact angle. Thomas Young first explained the equilibrium condition of vapor, liquid, and solid in terms of a liquid droplet on a solid surface by the following equation ^[34].

$$\cos \theta_y = \frac{\gamma_{SV} - \gamma_{SL}}{\gamma_{LV}} \quad (1.1)$$

Where θ_y represents the CA in young's model and γ_{SV} , γ_{SL} , and γ_{LV} are the corresponding interfacial energy at the solid-vapor, solid-liquid, and liquid-vapor interfaces, respectively. Under the same atmospheric conditions and for the same solid surface, the lower the γ_{SL} is responsible to achieve the smaller the CA. Additionally, an oil droplet's wetting state on a solid surface under water can also be studied by the following Young's Equation ^[35].

$$\cos \theta_n = \frac{(\gamma_{o-g} \cos \theta_1) - (\gamma_{w-g} \cos \theta_2)}{\gamma_{o-w}} \quad (1.2)$$

Where γ_{o-g} and θ_1 represent the oil-gas interface tension and the oil contact angle in the air interface. γ_{w-g} and θ_2 represent the symbol of the water-gas interface tension and the

CHAPTER 1

water contact angle in the air interface. γ_{o-w} and θ_n is the interface tension of the oil-water interface and the oil contact angle in the water interface.

The ideal solid surface, which has a smooth topography and is chemically homogeneous, is the only one for which Young's model is relevant. Whereas, the Wenzel and Cassie model can describe the condition of wetting for a liquid droplet on a rough solid surface. In the Wenzel model, the droplet can be inserted into the grooves of the solid rough surface, and the CA can be stated as per the following equation ^[36].

$$\cos \theta_w = r \cos \theta_y \quad (1.3)$$

Where θ_w is the CA in the Wenzel model and r represents the solid surface roughness factor. Due to the r value is always being larger than 1, the rough structure will enhance the solid surface wettability. If $\theta_y > 90^\circ$, the surface roughness further increases the θ_w ; if $\theta_y < 90^\circ$, the surface roughness decreases the θ_w .

The liquid will not fill into the grooves of the rough surface as the surface roughness increases, and these solid surface grooves will be filled with air instead. Based on this, the Cassie model depicts the liquid balance between contacting the rough surface and contacting the air layer in the rough structure. The liquid contacting the air layer of the total solid area will be $1-f$ if the liquid contacting the solid surface across the entire solid area is f , and then the Cassie model's CA may be stated as the following equation ^[37].

$$\cos \theta_c = f \cos \theta_s + (1 - f) \cos \theta_v \quad (1.4)$$

CHAPTER 1

where θ_c is the CA in the Cassie model, θ_s corresponds to the CA of the liquid on the smooth solid surface, and θ_v corresponds to the CA of the liquid on the vapor surface ($\theta_v=180^\circ$). Hence, the equation can be expressed as ^[34]–

$$\cos \theta_c = f \cos \theta_s + f - 1 \quad (1.5)$$

Again in terms of solid rough surface, surface roughness, r should be noted and the above equation can be further written as the following condition ^[38]–

$$\cos \theta_c = r f \cos \theta_s + f - 1 \quad (1.6)$$

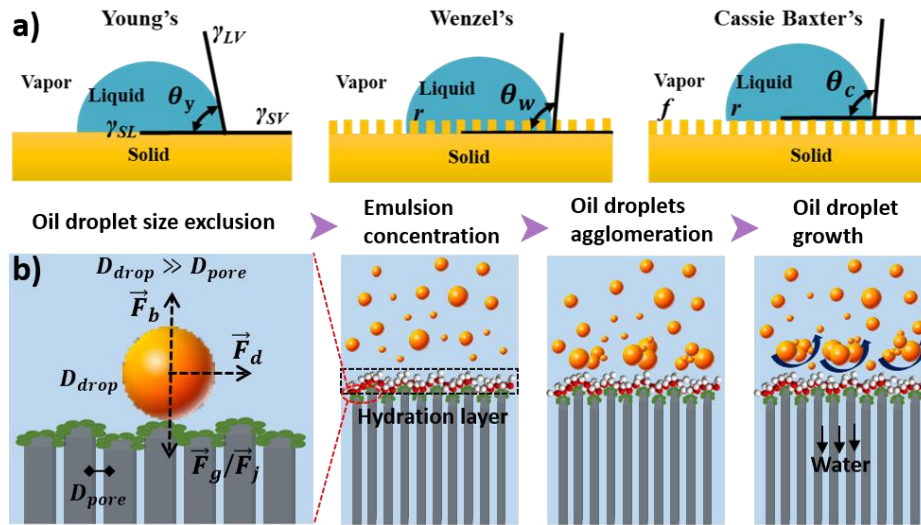


Figure 1.3: a) Different wetting states, and b) Emulsion separation mechanism.

1.1.4.2. Emulsion separation mechanism

Pore sizes (D_{pore}) of membrane surfaces contribute a core relation with oil droplet size (D_{drop}) thus mainly defines the performances of separation. When the oil droplet size is much smaller than the membrane pore size ($D_{drop} \ll D_{pore}$), the oil particles can enter the membrane pores and thus decrease separation efficiency by contributing to intrapore fouling. On contrary, if the oil droplet size is larger than the membrane pores ($D_{drop} \gg$

CHAPTER 1

D_{pore}) will initially reject oil droplets by size exclusion. Nevertheless, the stability of the emulsified emulsion will also have a separation performance effect. However emulsified oil droplets are less likely to coalesce, which allows the water to travel around individual droplets to reach the membrane surface. These circumstances happen only when the applied transmembrane pressure is higher. Therefore, the following equation can be applied regarding the relation between membrane pores and pressure ^[39].

$$\Delta P = -\frac{4 \cos\theta_{l_o l_w} \gamma_{l_o l_w}}{D_{pore}} \quad (1.7)$$

Where $\gamma_{l_o l_w}$ is the interfacial tension and $\cos\theta_{l_o l_w}$ is the contact angle of the oil and water phase. Membrane pore sizes are inversely related to pressure, which designates that larger membrane pore requires less pressure and smaller pores require higher pressure. However, uniform smaller pores are essential to obtain high separation efficiency. In addition, due to the flow mechanism, while oil-containing emulsion makes a contact with the membrane surface, three different forces are working to spread the emulsions quickly on the separation membrane surface ^[40]. During this mechanism, gravity force (\vec{F}_g) and permeate force (\vec{F}_j) drives water to permeate while bouncing force (\vec{F}_b) and strong oil flow/driving force (\vec{F}_d) dominating the oil droplets agglomerates in underwater ^[41], which is estimated according to the following equation ^[33].

$$\vec{F}_d = \gamma_o (\cos\theta_w - \cos\theta_o) \quad (1.8)$$

Where γ_o is the surface tension of oil, θ_w and θ_o is the WCA and UWOCA. Therefore, excellent WCA and UWOCA values lead to flow force that drives the oil droplets' agglomeration. Additionally, the collision between the oil droplets and the hydrated surface

CHAPTER 1

under flow/driving force also contributes to the agglomeration and coalescence of oil droplets. Hence, the agglomerated oil droplets are formed into larger droplets and are quickly repelled off while water easily diffuses and penetrates through the membrane. Theoretically, this mechanism can be explained through the following equation ^[42].

$$\Delta P_i = -\frac{2\gamma\cos\theta}{d} \quad (1.9)$$

Where ΔP_i , γ , θ , d represent intrusion pressure, the oil/water surface tension, the contact angle, and the radius of the meniscus. In contrast, the water phase could constantly permeate through the interspace between the membrane pores under the influence of external pressure and positive capillary force when $\Delta P < 0$ and $\theta < 90^\circ$. Additionally, the spontaneous agglomeration of oil droplets thus gradually coalesces into greater radius oil droplets further explained by following Stokes' resistance law ^[43].

$$V = \frac{D_{drop}^2 g(P_w - P_o)}{18\mu_w} \quad (1.10)$$

Where V is the speed of oil droplets rising, D_{drop} is the diameter of oil droplets, g is the acceleration of gravity, P_w and P_o represent the density of water and oil, respectively, and μ_w represents the viscosity of water. It can be seen from the above formula that the rising speed of the oil droplet is positively correlated with the oil droplet diameter and the density difference between water and oil thus showing significant relation with separation performances, which can be further explained through the following Hagen-Poiseuille equation ^[44].

$$J = \frac{p\pi r_p^2 \Delta P}{8\eta \Delta l \tau} \quad (1.11)$$

CHAPTER 1

Where porosity (p), pore radius (rp), membrane thickness (Δl), pore tortuosity (τ), and pressure (ΔP) can be neglected due to using the same membrane separation. However, viscosity (η) is the key parameter that leads to the increasing and decreasing of permeate flux (J).

1.1.5. Basic requirements of membranes for oil/water separation

The main goal to be accomplished through the separated membranes are excellent oil/water separation performances. As a result, the aforementioned goals are linked to several fundamental requirements of the membrane materials that have a significant impact on separation efficiency and permeate flux ^[45]. Surface roughness, pore size, surface wettability, chemical stability, mechanical durability, membrane thickness, and scale-up and commercialization are some of the fundamental needs that will be covered in more detail in this section.

1.1.5.1. Surface roughness

Surface roughness is a key parameter typically identified by topography images obtained using atomic force microscopy (AFM). Surface roughness also impacts increasing the membrane wettability, which increases water permeability and decreases the fouling problems by enhancing the separation efficiency ^[1]. However, recently many studies have concentrated on the influence of surface roughness for oil/water emulsion to achieve outstanding emulsion separation performances and to minimize the fouling issue. *Li et al.* investigated that creating a micro-nano hierarchical rough structure on the membrane surface is advantageous to increase the membrane's super-wetting ability ^[46]. In addition, these microstructures largely decrease the membrane's ability to hold oil droplets by creating a strong hydration layer. Furthermore, the Wenzel and Cassie-Baxter models also

CHAPTER 1

theoretically suggest that a membrane's wettability could be enhanced by creating a suitable multiscale roughness structure on the membrane surface ^{[47][48]}. It can be said that the roughness value shows a linear relation with the inherent wetting properties, which proves that the higher roughness value causes a higher surface wetting.

1.1.5.2. Membrane pore size

Membrane pore sizes are considered as further key parameters for oil/water separation. Depending on the technique employed to measure the pore size, the real membrane pore size is approximated differently. The most common method for measuring membrane pore size is the bubble pressure test, the gas adsorption method, the porosimetry test, computer tomography, and mean-flow pore size methods. However, membrane pore size contributes a core relation with oil droplet size thus defining the performances of separation. Such as, when the oil droplet size is much smaller than the membrane pore size, the oil particles can enter the membrane pores and thus decrease flux and separation efficiency by contributing to intrapore fouling. Therefore, the size of the membrane pore should be less than the size of the oil droplet to prevent such intrapore fouling. However, the oil may still pass through membrane pores, but only if the transmembrane pressure is higher than the critical pressure. In general, a small pore-sized membrane will initially reject large oil droplets through the size exclusion method. Therefore, controlling the membrane pore size and selecting membrane materials with the proper pore size is highly appreciable to enhance the separation performances as well as to avoid oil-fouling issues. In this regard, polymeric membrane surfaces are considered ideal membranes due to their uniform nano/micropore size distribution ($<0.3 \mu\text{m}$). Whereas, pore sizes of widely used other traditional materials especially- made mesh (0.25-0.038 mm) ^[49], porous sponge

CHAPTER 1

(100-200 μm)^[50], fabric (6.64-18.9 μm)^[51] are much larger than the emulsified oil droplet sizes (0.1-20 μm)^{[52][53]}. Hence, due to their larger pore diameters, the sizes of emulsified oil droplets are not suitable candidates for emulsion separation^{[54][44]}.

1.1.5.3. Surface wettability

The membrane materials selected for separation purposes must meet the desired wettability properties (super hydrophilicity and underwater superoleophobicity) to achieve high separation performances of oily wastewater emulsion. There has been a lot of interest in generating super-wetting properties from both theoretical and practical viewpoints. The presence of different hydrophilic functional groups such as, $-\text{OH}$, $-\text{SO}-$, $-\text{NH}_2$, $-\text{SO}_2-$, $-\text{NO}_2$, $-\text{COOH}$, $-\text{C}-\text{O}-$ makes the membrane surface superhydrophilicity^[55]. As the mechanism, the membranes with superhydrophilicity ensure water permeation and shield the hydrophobic parts of membrane materials from being exposed^[13]. However, simply increasing hydrophilicity can boost permeability, but this does not always lead to high oil rejection. Therefore, it is essential to generate underwater superoleophobicity in the meanwhile to achieve high separation efficiency by rejecting oil droplets. The superhydrophilicity is measured through water contact angle (WCA; in air $<10^\circ$), and underwater superoleophobicity is measured through oil contact angle (UWOCA; in water $\geq 150^\circ$). However, constructing a micro/nano-rough structure is a highly intriguing solution also for generating surfaces with great hydrophilicity and underwater superoleophobic properties^{[56][57]}. It is reported that rough surface functions as a technique to reduce the underwater contact area between oil and membrane surfaces by producing a strong hydration layer^{[58][59]}.

CHAPTER 1

1.1.5.4. Chemical stability

Modified membrane surfaces can experience wide and complex environments during emulsion separation. Weak chemical bonding can arise in such harsh environments and can lead to a severe decrease in hydrophilicity and underwater oleophobicity behavior. Destruction of chemical stability results in severe flux decline and a tremendous decrease in separation efficiency by irreversible membrane fouling during the separation process. Such chemical stability is extensively important for long-term oil/water separation. However, membranes' chemical stability is investigated using sand paper abrasion, scotch-tape peeling, membrane bending, UV-irradiation exposure, long storage time, immersion in hot water, and different pH values, etc. Although complicated situations would result in a deterioration in wettability properties, employing an efficient surface modification process and selecting the perfect membrane material can help to limit such damage. *Zhan et al.* introduced chemically stable halloysite nanotubes material to develop a graphene oxide/poly(arylene ether nitrile) nanofibrous membrane, which shows excellent separation performances in harsh environments (high-temperature, strong corrosive acid, and basic solutions) ^[60]. Whereas, *Li et al.* developed acid, alkali, and salt-tolerant stable modification process by zeolite imidazole framework (ZIF-8) on polytetrafluoroethylene (PTFE) nanofibrous membrane ^[61].

1.1.5.5. Mechanical durability

The reliability of materials upon usage is significantly affected by the mechanical characteristics of membranes. The mechanical strength of the membranes and their longevity is considerably influenced by how well pressure-driven membrane separation procedures work. Tensile strength, Young's modulus, and elongation at break are examples

CHAPTER 1

of mechanical strength characteristics that demonstrate the membrane's capacity to withstand tensile stress, elastic deformation and resist dimension change when an external force is applied. However, some separations may need high operating pressure due to several factors-smaller pore size, materials' inner structure, and high concentration of oil and surfactants in the emulsion. In such situations, membrane materials must hold any operating pressure that needs during separation. High operating pressure may increase the chance that membranes will physically compress and such can result in an irreversible loss of water flux. *Qin et al.* stated that adding nanoparticles to polymer membranes is a workable way to increase mechanical performance without compromising other desirable properties ^[62]. On the other hand, some membrane materials hold natural mechanical strength as-biaxially oriented different polymeric membranes contain high mechanical strength in both machine and transverse directions and show superior performances as compared to any commercially available polymeric membranes ^[44]. Higher mechanical stability can therefore offer great membrane reusability along with prolonged service life.

1.1.5.6. Membrane thickness

Membrane thickness and separation performances have a substantial relationship. With an increase in thickness, osmotic pressure, the emulsion flow distance, and resistance all increase simultaneously ^[63]. Additionally, the thickness of the membrane will provide a steady increase in separation efficiency, but an intense decrease in flux. When the same amount of emulsions are used to separate through the membrane as in one cycle, the membrane with a less thickness first reaches separation capacity ^[64]. As a result, to achieve a higher separation flux in applications, the membrane's thickness is desired to be as thin as possible under the assumption of good separation measurements ^[65].

CHAPTER 1

1.1.5.7. Scale-up and commercialization

Commercial viability is significantly influenced by the materials used and the manufacturing process. Scaling up and making the move to the commercial realm can be made easier by currently used large-scale modification technologies, such as various coating, irradiation techniques, graft polymerization, crosslinking, etc. Apart from these widely used modification methods, membrane materials that are used for modification techniques also play a critical role. Due to environmental and regulatory concerns, high concentrations of volatile organic compounds, caustic substances, and chemicals based on heavy metals can hinder commercialization.

1.1.6. Widely used polymeric membranes for oil/water separation

Polymeric membrane-based separation technology can present a substantial solution in oily wastewater areas due to its nano and microporous orientation. Up-to-date polymeric membrane-based technologies become the most considerable attention and are highly adaptable in many industries for oil/water emulsion separation ^[66]. Such polymeric membrane separation possesses many distinct advantages such as uniform porous structure, high efficiency, low cost, low energy consumption, and simple operation ^[67]. **Table 1.1** lists the most widely used and frequently adopted polymeric membranes for oil/water separation by researchers during the past few decades. Despite all of these benefits, their inherent hydrophobicity prevents them from being used to separate water from oily wastewater. Its hydrophobicity characteristics demonstrate the adherence of oil droplets to membrane surfaces, which frequently results in significant fouling issues. Membrane fouling impacts not only water permeability and separation efficiency, but also membrane life, productivity, and permeate quality, as well as increasing operating expenses and shortening membrane

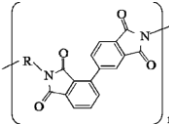
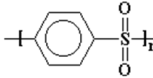
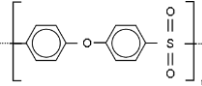
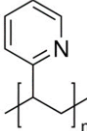
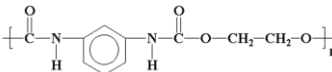
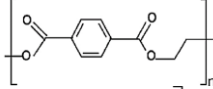
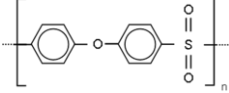
CHAPTER 1

lifetime. *Zoubeik et al.* stated that the flux decline of the membrane was divided into three stages ^[68]. The highest rate of fouling is visible in the initial stage, which displays a quick decline in flux. In the second stage, as the flow drops more gradually, the fouling rate slows down, and in the third stage, the fouling rate is nil and the flux approaches a steady-state state under constant transmembrane pressure. During the fouling process, membranes become clogged and obstructed because of oil droplets and organic pollutants. The removal of these contaminants may shorten the membrane's life. As a result, increased membrane antifouling performance and efficiency are highly desirable. Various strategies have been used to prevent fouling and optimize the membrane's hydrodynamic conditions. One of the most efficient strategies for improving membrane antifouling is surface modification.

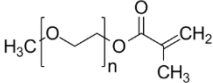
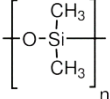
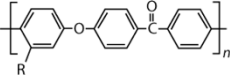
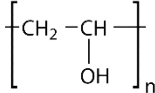
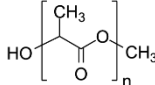
Other than commercial polymeric membranes, natural biodegradable polymers can be considered as oil/water separation as these membranes are non-toxic, environment friendly, and low cost. However, these natural biodegradable membranes are not much adopted by researchers and industrially because of their low stability performance. Still, the demand for biodegradable polymers is rapidly growing every year (about 10–20% per year) as membrane separation ^[69]. Frequently used some biodegradable polymers - cellulose ^{[70][71]}, chitosan ^[72], starch ^[73], and alginate ^[74], etc. Additionally, biodegradable polymers are naturally super hydrophilic but concern about their long-term usability limits their wide application. However, in this review, we mainly focus on different commercial polymeric membranes that are used for oil/water separation.

CHAPTER 1

Table 1.1: Chemical structure of widely used different commercial polymeric membranes for oil/water separation.

Full form	Abbreviation	Structure
Polyimide	PI	
Polyacrylonitrile	PAN	$\text{-(CH}_2\text{-CH(C}\equiv\text{N))}_n\text{-}$
Poly(vinylidene fluoride)	PVDF	$\text{-(CH}_2\text{-C(F)}_2\text{)}_n\text{-}$
Polypropylene	PP	$\text{-(CH}_2\text{-CH(CH}_3\text{))}_n\text{-}$
Polytetrafluoroethylene	PTFE	$\text{-(CF}_2\text{-CF}_2\text{)}_n\text{-}$
Poly(ether sulfone)	PES	
Polyketone	PK	$\text{-(CH}_2\text{-CH}_2\text{-C(=O))}_n\text{-}$
Polysulfone	PS	
Poly(2-vinyl pyridine)	PVP	
Polyethylene	PE	$\text{-(CH}_2\text{-CH}_2\text{)}_n\text{-}$
Polyurethane	PU	
Poly(ethylene terephthalate)	PET	
Polysulfone	PSf	
Poly(vinyl chloride)	PVC	$\text{-(CH}_2\text{-CHCl)}_n\text{-}$

CHAPTER 1

Poly(ethylene glycol methacrylate)	PEGMA	
Polydimethylsiloxanes	PDMS	
Poly(aryl ether ketone)	PAEK	
Poly(vinyl alcohol)	PVA	
Poly lactic acid	PLA	

1.1.7. Advanced properties of polymeric membranes

Recent oil/water separation technology is concentrating on developing advanced properties using polymeric membranes as the basis. Switchable wettability, self-cleaning, antimicrobial, and self-healing capabilities are a few of these features that have recently received a lot of attention. However, the development and use of advanced features are still in their infancy, and there is still much work to be done before they are used in practical application. We cover these cutting-edge features of different super-wetting polymeric membranes used for oil/water separation in this section.

1.1.7.1. Switchable wettability

Switchable oil/water separation refers to the capability of a single super wetting membrane to selectively separate various oil/water mixtures, like water-in-oil and oil-in-water emulsions, on demand. Including this functionality would open up new opportunities for the treatment of industrial oily wastes. Such switchable wettability featured membrane is known as Janus membrane, which is currently widely used to separate simultaneously water and oil both. Such a switchable separation through Janus membranes is easily

CHAPTER 1

produced by aligning their respective wetting surfaces to initially contact the oil/water mixes. Li and his co-workers developed PVDF Janus membrane by hydrophilic copolymer poly(vinylpyrrolidone-vinyltriethoxysilane) and a glycerol coating on the nonwoven fabric support the limitation of the phase separation on the bottom surface with blocking the segregation of hydrophilic copolymer (**Figure 1.4a**)^[75]. The Janus PVDF membrane displayed switchable separation performances for both oil-in-water and water-in-oil emulsions because of its anisotropic wettability against it by hydrophobic or hydrophilic PVDF membranes. *Zhang et al.* developed PTFE Janus membrane by using a polyaniline–silica nanoparticle through a facile immersion-spray coating method^[76]. Superhydrophilic with underwater superoleophobic wettability is created using polyaniline, which is applicable for oil-in-water separation. Conversely, superhydrophobicity and underwater superoleophilicity is created using silica nanoparticles and successfully can separate water-in-oil emulsions.

1.1.7.2. Self-cleaning

Huge amounts of oily wastewater must be handled with high-flux separation materials with efficiency. Very porous membranes are especially susceptible to organic contamination, which results in a substantial fall in separation efficiency and flux. Although it has been shown that porous materials with superhydrophilicity and underwater superoleophobicity are anti-oil fouling, fouling of porous membranes is nevertheless inevitable in long-term use. As a result, the most challenging issue is how to successfully remove oil contamination from the membrane's surface without sacrificing any separation performances. Several initiatives have been developed. Among the best methods used for wastewater separation is self-cleaning process that includes photocatalytic degradation,

CHAPTER 1

photo Fenton process. Oily pollutants can be effectively removed from wastewater while simultaneously being photodegraded by combining a super wettability polymeric membrane with self-cleaning technology. TiO₂-based photocatalytic separation materials have found widespread usage due to their outstanding qualities, including strong chemical stability, high catalytic activity, hydrophilicity, and low toxicity. Only under UV light can TiO₂-based photocatalytic materials create a noticeable photocatalytic effect, whereas sunlight only emits a very small quantity of UV. In addition to TiO₂, other substances (such ZnO, CeO₂, zeolite, graphene oxide etc.) can be utilized to create photocatalytic separation membranes ^{[77][78][79]}. *Xu et al.* modified polyethersulfone membrane using boron doped-graphitic carbon nitride as photocatalyst and Poly(vinylpyrrolidone) as a sacrificial pore-forming agent (**Figure 1.4b**) ^[80]. However, introducing such photo catalysis shows excellent degradation of different organic dyes and antibiotics such as- Methylene blue (MB), Rhodamine B (RhB), Methyl violet (MV), Congo red (CR), Tetracycline (TC), and Ciprofloxacin (CIP). Whereas, *Xie et al.* developed PVDF/TA/ β -FeOOH membrane, where β -FeOOH shows excellent photo-Fenton catalytic property self-cleaning with outstanding flux recovery (>98%) ^[81].

1.1.7.3. Self-healing

Laboratory scale is considered as favorable condition for a super wetting polymeric membrane to separate complex wastewater with a high separation efficiency and flux. Conversely, during a practical application, the separation performances of these polymeric membranes could be significantly diminished or lost entirely due to environmental risks including- plasma etching, corrosive situations, UV irradiation, extremely high or low temperatures, etc. If the damage is not fixed in a timely manner, these harsh environments

CHAPTER 1

will attack the membranes quickly and results in an early loss of separation performances. Currently, the majority of separation materials require artificial repair or replacement, which is both expensive and difficult. As a result, it is possible to create advanced separation membranes with self-healing qualities to boost durability, lengthen their lifespan, and retain good separation performances in a severe environment. *Feng et al.* carried out the modified PVDF membrane's physical damage by sandpaper friction and then immersed in FeCl_3 solution for 12 h to enhance the self-healing properties (**Figure 1.4c**)^[82]. The obtained data reported that, the damaged membranes successfully restored the hydration layer with Fe^{3+} linking and the corresponding hydrophilicity decreased. Additionally it is also reported that it remains irreversible process if the physical damage penetrates the inner membrane.

1.1.7.4. Anti-bacterial

Polymeric membranes used in wastewater treatment suffer from the constant issue of biofouling, which also affects their effectiveness. Fortunately, several initiatives have been made to enhance antibacterial efficiency. Such bacterial properties can be enhanced by introducing several anti-bacterial agents through surface modification techniques, which are effective ways to create an efficient antibacterial membrane. Membranes are modified to prevent the buildup of microorganisms by using bactericidal mechanisms. There are several studies reported using various antibacterial agents modified membrane for oil/water separation. However, among them, silver nanoparticles demonstrate the most effectiveness of as an antibacterial agent^[83]. *Chen et al.* modified PAA cross-linked PES membrane decorated by AgNPs to endow the membrane's excellent antibacterial properties (**Figure 1.4d**)^[84]. It is reported that introducing AgNPs shows the bacterial

CHAPTER 1

killing ratio of 93.4% and 95.7% against *E. coli* and *S. aureus*, respectively. *Vásquez et al.* also reported the effective antibacterial properties of introducing AgNPs on PDMS [85].

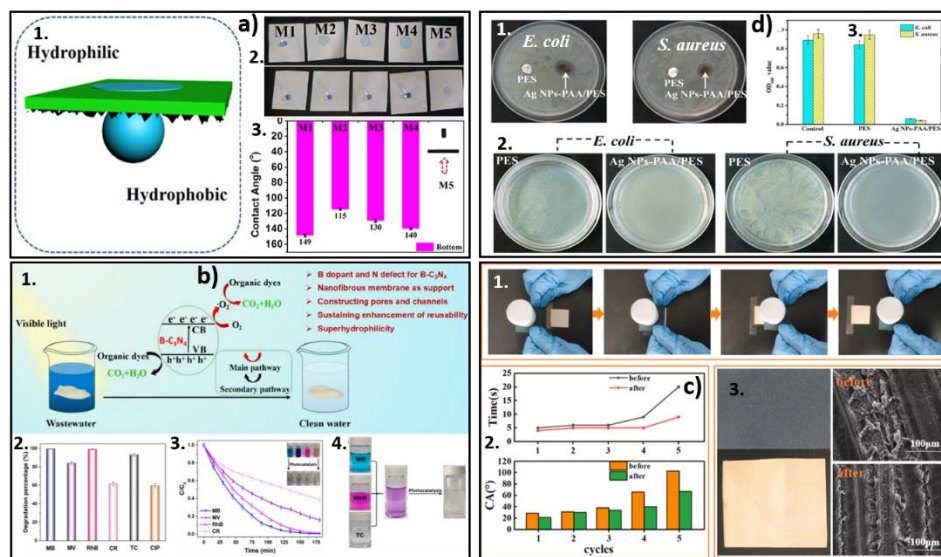


Figure 1.4: a)1-3. Schematic illustration of the switchable wettability properties membrane and wettability performances [75]; b)1-4. Proposed mechanism of photocatalytic degradation and their corresponding degradation performances [80]; c)1-3. Schematic diagram of physical damage; corresponding contact angle; digital and SEM imagines of the damaged membrane surface before and after self-healing [82]; d)1-3. Inhibitory zones against *E. coli* and *S. aureus*; corresponding digital images, and antibacterial performances of using different membranes [84].

CHAPTER 1

Table 1.2: Separation performances of the advanced polymeric membranes in oil/water separation.

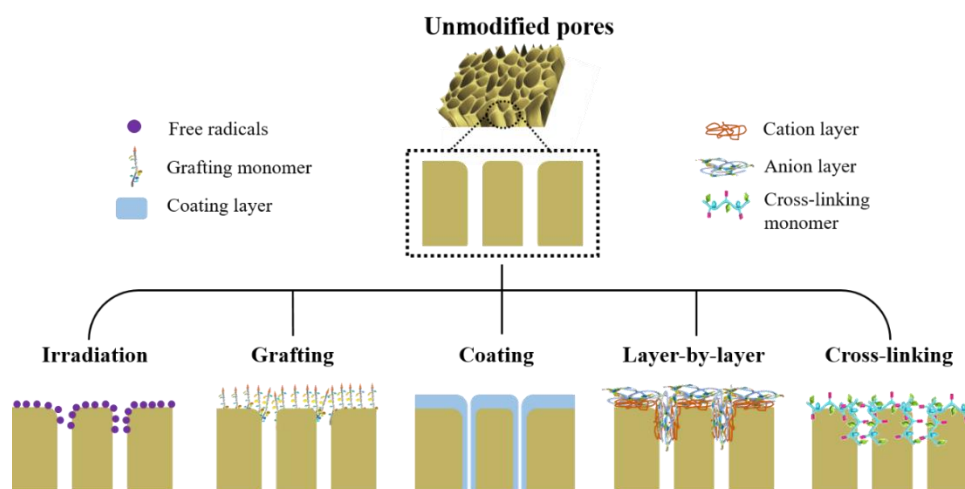
Polymeric membrane	Modifying agent	Advanced properties	Oil rejection	Flux (Lm⁻² h⁻¹)	Ref.
PVP/PVDF	TiO ₂	Self-cleaning	>99.92%	O/W=5000	[86]
PVDF	ZIF-8@ZnO	Switchable wettability, Self-cleaning	>99%	O/W=3879	[87]
PAN	TiO ₂ /amino silane	Self-cleaning	>99%	O/W=200,000	[88]
PVDF	NH ₂ -MIL-88B(Fe)	Self-cleaning	>99.4%	O/W=1970	[77]
PVDF	TA/β-FeOOH	Self-cleaning	>99.1%	O/W=2106.2	[81]
PVDF	NVP/VTES/AIBN	Switchable wettability	97.5%	O/W~4000	[75]
PLA	CNTs/SiO ₂ nanofluids	Switchable wettability	99.5%	O/W=1142.2	[62]
PTFE	polyaniline–silica nanoparticle	Switchable wettability	99.7%	O/W=1800	[76]
PAA-g-PVDF	Fe ³⁺ /SA/CCS	Self-healing	99.21%	O/W=974	[82]
PAN	bPEI-PAA/hyaluronic acid	Self-healing	>99.95%	O/W>1000	[89]

CHAPTER 1

Tungsten oxide/PAN	bPEI/PAA	Self-cleaning, Self-healing, Anti-bacterial	>99.93%	O/W=4509	[90]
PVA-co-PE	AgNPs	Switchable wettability, Anti-bacterial	>99.9%	O/W=2300	[91]
PAA/PES	AgNPs	Anti-bacterial	>99.3%	O/W=5142	[84]
PDMS	Polydopamine/AgNPs	Anti-bacterial	99.99%	O/W=4043	[85]

1.1.8. Surface modification process

Surface modification is a widely used process for modifying the surface composition and structure of membranes by adding new functionalities and without compromising their desirable macroscopic properties. Numerous surface properties, including wettability, roughness, pore size and distribution, reusability, mechanical and chemical stability etc. can be changed using various surface modification techniques according to the application (**Figure 1.5**).



CHAPTER 1

Figure 1.5: Widely used different surface modification methods applied for oily wastewater separation.

1.1.8.1. Grafting method

Grafting technique can be used to modify the surface of a polymeric membrane to reduce undesirable features or add new functionality. Three often-utilized procedures are "grafting-to", "grafting-from", and "grafting-through" ^[92]. The "grafting-to" procedure involves covalently bonding of polymer chains with reactive anchor groups at the ends or on the side chains to the membrane surface. The "grafting-from" approach makes use of active species that already exist on a membrane surface to start the polymerization of monomers from the surface, also known as graft polymerization. Functional monomers have demonstrated to be far more flexible and versatile when used in the "grafting-from" approach than when used in the "grafting-to" ^[92]. Another technique for producing side chains with precise specifications is grafting-through. A lower molecular weight monomer and free radicals are typically used to copolymerize a macro monomer with an acrylate functionalized. The ratio of the molar concentrations of the macro monomer and the monomer, as well as the activity of their copolymerization, determine the number of chains that are grafted ^[93]. The ratio of monomer to macro monomer molar concentrations as well as their copolymerization activity determines how many chains are grafted ^[93]. Out of the three chemical-induced methods, the grafting-from technique offers the most versatility for modifying a membrane in accordance to oil/water separation's surface characteristics. Grafting from/graft polymerization can supply the base membrane with permanent, advanced, and unique activities. As a result, customized membranes can be widely used for potential polymeric membrane separation technology. On contrary, chemical-induced

CHAPTER 1

graft polymerization method introduce chemical-based surface activator, which involves the development of a radical on the membrane surface. However, atom transfers radical polymerization (ATRP) is the commonly used chemical-induced "grafting-from" method. Finally, it can be said that all graft polymerization methods show excellent membrane wettability and separation performances (**Figure 1.6**).

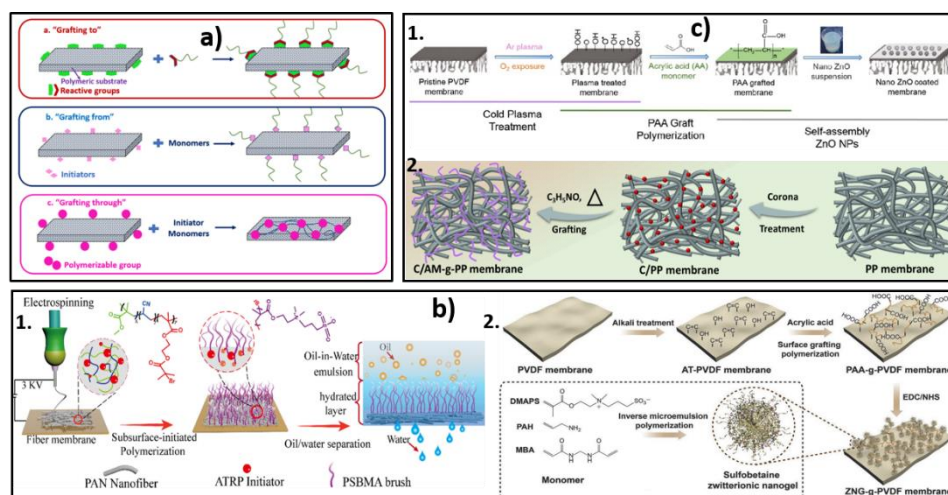


Figure 1.6: a) Strategies of different grafting methods-grafting-to, grafting-from, grafting-through ^[92]; Schematic illustration of the b)1-2. Brush-functionalized chemical-induced grafted PAN membrane using ATRP initiator ^[94], and two step chemical-induced grafted PVDF membrane using alkali initiator ^[95]; Schematic illustration of the irradiation-induced graft polymerization using c)1-2. Ar plasma and acrylic acid grafting ^[96], and corona treatment and acrylamide grafting ^[44].

1.1.8.2. Surface Coating:

One of the most prevalent and extensively used strategies for creating super wetting substances for oily wastewater separation is surface coating (**Figure 1.7**) ^{[97][98]}. To achieve the desired super-hydrophilicity or super-hydrophobicity, the substrate is immersed in a

CHAPTER 1

solution that contains either micro/nanoparticles or low-surface-energy molecules, or both. The several types of widely accepted coating processes are- immersion, dip coating, spin coating, spray coating, vacuum coating and so on. Understanding this modification process requires a microscopic perspective on how the altering layers and/or modifying monomers interact with the membrane surface. While outstanding characteristics and separation performances have been recorded employing the coating modification method, the durability of the coating layer is still indicated as being poor, demonstrating their weak interactions with the membrane surface. Therefore, to construct strong interactions such as covalent bond or electrostatic interaction, further small-molecule grafting, coating-cross-linking method can develop stabilized monomer's network with the membrane surface [99].

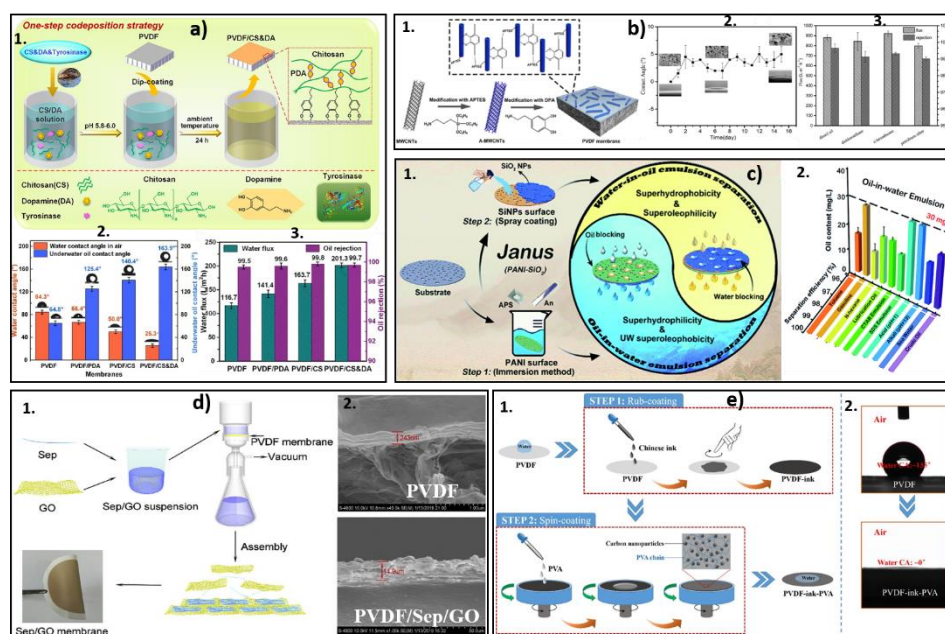


Figure 1.7: Schematic illustration of a)1-3. the dip coating modification process and the modified membranes' wettability and separation performances [100]; b)1-3. the immersion process and their wettability with separation performances [101]; c)1-2. the spray coating method and separation efficiency values [76]; d)1-2. the vacuum coating

CHAPTER 1

method and cross-sectional micrographs of modified and unmodified membrane ^[102];

e)1-2. the rub and spin coating method and the wettability of the modified membrane

^[103].

1.1.8.3. Irradiation Technology

Irradiation technology is one of the most primitive but utmost often-used methods, which is regarded as a pretreatment step for subsequent surface modifications to introduce polar groups onto an inert polymeric membrane surface. Numerous irradiation techniques, including plasma, Ultraviolet, gamma, electron beam, and microwave, are frequently utilized in the oily wastewater separation field (**Figure 1.8**). Plasma and UV BOTH treatment release of reactive oxygen species-singlet oxygen ($^1\text{O}_2$), superoxide radicals ($\text{O}_2^{\cdot-}$), or hydroxyl radicals ($\cdot\text{OH}$) in the membrane surface, which is thought to be a reliable, stable, and large-scale technique and allowing for the effective regulation of the beginning and end of the reaction ^{[99][104]}. However, membrane pores can be adjusted by continuing a specific treatment time and power level. It is reported that, only applying plasma treatment can cause the destruction of inner pore structure. However, further grafting or crosslinking method after applying plasma treatment can help to recover the inner pore structure damage ^[44]. Despite the generation of reactive oxygen species, the UV light has a strong bio toxicity and plays a vital role for as a self-cleaning contamination removal method in oil/water separation ^{[105][106]}. On the other hand, gamma-ray and electron beam both can produce large amounts of free radicals on the structural framework of substrates by directly breaking chemical bonds or indirectly attacking with radiolytic active species ^[107]. However, the usage of electron beam irradiation is limited in oil/water separation area. On the other hand, microwave irradiation has also been widely applied to

CHAPTER 1

free-radical polymerization and copolymerization reactions using various monomers. The application of microwave irradiation is widely used to accelerate the chemical reactions in chemical synthesis process, but very less works are performed as surface modification process [108]. The most exciting part is that for other irradiation process often take many hours to complete, whereas few minutes of microwave irradiation is frequently enough [109].

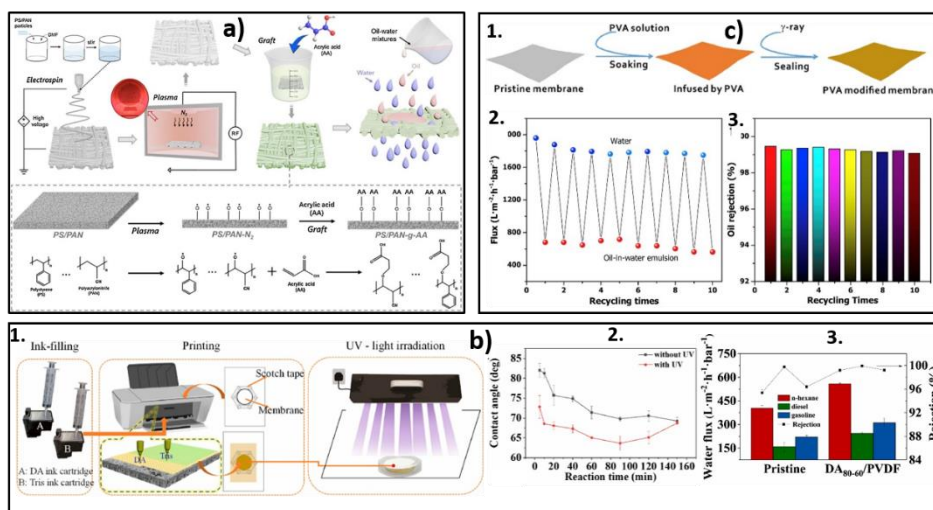


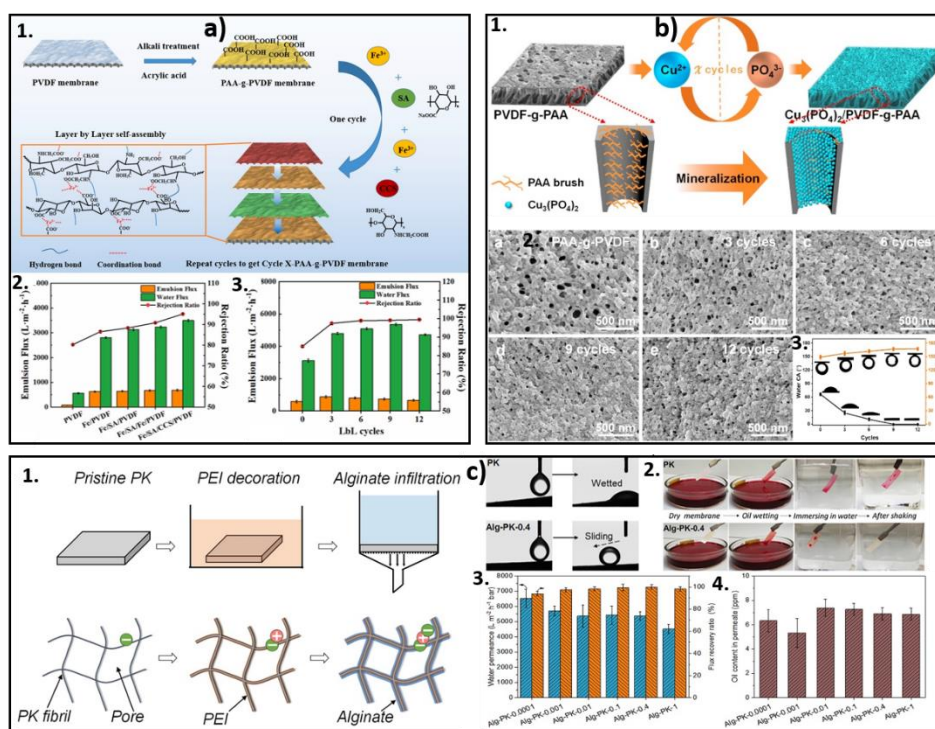
Figure 1.8: Schematic illustration of a) the plasma (Ar) irradiation process [110]; b)1-3. the UV-irradiation method, WCA values, and corresponding water flux and rejection rate [111]; c)1-3. the gamma irradiation process, flux and oil rejection of the gamma irradiated membrane with recycling properties [112].

1.1.8.4. Layer by layer

Layer-by-layer assembly (LBL) has been widely used to create super wetting interfaces with micro/nanostructure, desired components, simple operation, no matrix damage and adjustable thickness as a simple and economical bottom-up approach. For efficient oil/water separation, various super wetting particle coatings have been developed by LBL deposition (**Figure 1.9**). In a normal procedure of LBL method, pre-treatments are

CHAPTER 1

either required to activate the unmodified membrane in positively or negatively charged and then the pre-treated membrane was then immersed alternatively into several solutions containing molecules with the opposite charge to create many layers on the membrane surface ^[113]. Numerous tunable features can be adjusted such as membrane thickness, and inner pore sizes according to demand through this method ^[114].



CHAPTER 1

1.1.8.5. Cross-linking

Crosslinking is the process of affixing a covalent bond between two or more monomer molecules chemically with the membrane surface. Crosslinking modification entails joining or separating different chemical groups to change the membrane's wettability or other properties. Different surface functional groups (carbonyl, hydroxyl, amino, etc.) can generate onto the membrane surface. Those characteristics are thought to be particularly useful in producing a super-wetting membrane surface for the oil/water separation area (**Figure 1.10**). However, choosing an effective cross-linked monomer is also crucial. However, such cross-linking method provides superdrophilicity, hydrophilic stability, high separation efficiency and excellent antifouling properties.

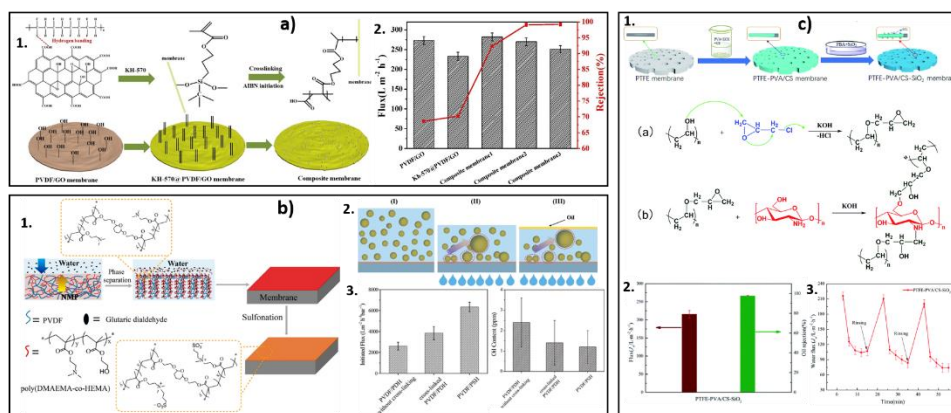


Figure 1.10: Illustration of the a)1-2. crosslinking modification process of PVDF/GO membrane and their separation performances ^[117]; b)1-3. in-situ cross-linking modified membrane, oil demulsification process, and separation performances of modified membrane ^[118]; c)1-3. crosslinking process, corresponding separation flux and flux recovery ^[119].

CHAPTER 1

Table 1.3: A details comparison of separation performances using different surface modifying polymeric membranes for oil/water separation.

Polymeric membrane	Modification Method	Flux (Lm⁻² h⁻¹)	Oil rejection	Wettability (WCA,UWOCA)	Ref.
PVDF	Grafting	2050	~94 %	<3°,UW superoleophobic	[96]
PP	Grafting	1385	99.3%	0°, > 150°	[44]
PES	Grafting	331.2	98.9	35°	[6]
PAN	Grafting	65	>99.9%	0°, > 150°	[94]
PVDF	Grafting	25 000	99.9%	0°,~160°	[95]
PVDF	Grafting	840	97	29°,	[120]
PES	Grafting	N/A	98%	45.4,	[121]
PAN	Coating	2270	<10 ppm	0°, >150°	[122]
PAN	Coating	10,000	P98%	0°	[123]
PVDF	Coating	605	99.34%	0°, 158.6°	[124]
PAN	Coating	32800	>99.6%	16.3°, 157.3°	[125]
PVDF	Coating	2237.94	<50 ppm	0°, 155.5°,	[126]
PVDF	Coating	735	95.4%	41°, 156°	[127]
PES	Coating	81	99	0°, 157.3°	[128]
PES	Coating	70	98.5	43.3°, 151.2°	[129]
PI	Coating	6038	99%	0°,150°	[130]
PI	Coating	6500	>99%	0°,161.5°	[131]

CHAPTER 1

PP	Coating	1466	<40 ppm	0°, 162.7°	[132]
PS/PAN	Irradiation	2330	>99.5%	0°, UW	[110]
				superoleophobic	
PVDF	Irradiation	2241.3	>99.0%	65°, ~100°	[111]
PVDF	Irradiation	6.9 × 10 ²	>99.5%	0°, ~159°	[133]
PES	Irradiation	99.5	91.8	53°, N/A	[134]
PVDF	Irradiation	7200	99.8%	0°, 150°	[135]
PVDF	LBL	974	99.21%	0°, 169.6°	[82]
PK	LBL	6500	6–10 ppm	0°, >158°	[116]
PVDF	LBL	1654	3 ppm	0°, 166°	[115]
PVDF	LBL	1230	99.8%	0°, 163°	[114]
PAN	Crosslinking	1293	98.2%	0°, 141°	[136]
PVDF	Crosslinking	>145	>99%	0°, 159°	[117]
PVDF	Crosslinking	6350	98%	0°, 156°	[118]
PTFE	Crosslinking	2157.6	97.67%	0°, 158.5°	[119]
PVP/PAN	Crosslinking	20,610	97%	34.4°, N/A	[137]
PAN	Crosslinking	29840	99.2%	0°, 155°	[138]
PVDF	Crosslinking	90	98.3%	0°, 153°	[139]

1.2. Objectives and motivation of the study

Water separation from oil/water emulsion continues to be a crucial problem due to the significant amount of oily wastewater discharged by industrial operations. The need for a low-cost, low-energy oil-water separation technology is essential as the requirements for the discharge of oily wastewater tighten due to an increase in environmental concerns

CHAPTER 1

around the world. Due to its straightforward operational procedure and excellent separation effectiveness, membrane technology is highly sought after in the industrial sector for this oil-water separation.

Based on the above-discussed environmental problems and the principle in developing a high-performance membrane technology for oily wastewater, we take the biaxially oriented PP microporous membrane as the basis membrane, which has the advantage of nanometer pore size, low cost, and good mechanical. Commercially available mostly polymeric membranes are reported poor mechanical strength, which causes lower self-life and reliability in the separation application area. The technology of biaxially oriented PP possesses high mechanical strength both in the machine and transitional direction as compared to other polymeric membranes prepared through thermal-induced phase separation, uniaxial stretch, and electrospinning process. Therefore, higher mechanical stability can provide long membrane service life with outstanding reusability. Despite their above-mentioned remarkable features, unfortunately biaxially stretched PP microporous membranes are hydrophobic by nature. To meet the requirement for separating water from oily wastewater, modification of the surface to super hydrophilicity is highly demanded. Being motivated by above stated problems and targeting to contribute to finding solutions, the main objectives of this work were:

- To modify the hydrophobic biaxial PP membrane by irradiation-induced graft polymerization method.
- To introduce super wetting properties (super hydrophilicity and underwater super oleophobicity) to the PP membrane through surface modification.

CHAPTER 1

- To develop a thermally and mechanically robust modified PP membrane, which can withstand both pressure-driven and gravity-driven separation.
- To achieve permanent membrane wettability and excellent stability in different complex environments.
- To understand the basic theoretical explanations of super wetting PP membrane with oily wastewater separation mechanism.

Note that, the main objective of this research is to surface modification of biaxial PP membrane for the separation of water from oily wastewater. During the surface modification process, three important key parameters are given bottomless attention- 1. Tuning the membrane pore sizes in accordance with the oil droplet size of the oily wastewater; 2. Generating not only super hydrophilicity but also paying much more attention to creating an underwater superoleophobic surface for a high percentage of oil rejections; and 3. Creating a rough membrane surface to obtain both preferred pore size and super wetting properties.

1.3. Organization of the thesis

A thorough and deep analysis of different surface-modified PP membrane's separation performances is conducted. The thesis covers a total of five chapters divided as follows-

- **Chapter 1** generates an overall introduction to oily wastewater separation. In detail, the theory of super wetting states, separation mechanism, the basic requirements of separating membranes, advanced properties of polymeric membranes, and different modification methods are discussed and reviewed.

CHAPTER 1

- **Chapter 2** reports the successful pre-irradiation-induced graft polymerization of unmodified PP membrane by applying electron beam irradiation and subsequent chemical grafting using acrylic acid and polyvinyl alcohol monomers. Through this facile surface modification process, significant wettability and excellent thermal and mechanical enhancement are discussed. Special attention has been given to increasing the anti-fouling phenomena, which can enhance the membrane's service life in oily wastewater separation areas.
- **Chapter 3** covers a highly mechanically stable biaxial PP membrane that can withstand high operating pressure. A facile and scalable two-step surface modification method has been developed by employing acrylic acid and sodium hydrogen carbonate monomer. This modification method reports excellent hydrophilicity and underwater superoleophobicity by constructing multiscale micro/nano rough surfaces with separation performances.
- **Chapter 4** describes super hydrophilic PP membrane modified via corona discharge treatment and followed by a grafting reaction with hydrophilic acrylamide monomer. Due to its excellent mechanical properties with a uniformly modified micro-nano porous structure, significant separation performances are achieved for layered mixtures, surfactant-free, and surfactant-stabilized emulsions by the energy-saving gravity-driven separation method.
- **Chapter 5** reports an advanced PP membrane modified through a highly efficient layer-by-layer modification technique using polyethylene imine and levo-3,4 dihydroxyphenylalanine cross-linked multi-layer assembled super-wetting hierarchical rough membrane surface. The synergistic development of the rough

CHAPTER 1

surfaces causes the embeddedness of wetting properties of the modified membrane with excellent separation performances by removing multi pollutants (oil particles and bacteria) from oily wastewater in a more energy-efficient way.

- **Chapter 6** concludes the existing limitations and prospective directions for future aspects of PP membrane-based separation technology.

CHAPTER 2. Fouling-resistant biaxial polypropylene membrane for pressure driven separation

The intrinsic hydrophobic behavior of biaxial oriented polypropylene microporous membrane limits its broad application area by leading the serious membrane fouling. An environment-friendly, desirable, practical, and easy to large-scale prepared surface modification process is designed to enhance the membrane wettability and oil fouling. Through the pre-irradiation-induced graft polymerization method by applying electron beam radiation and using acrylic acid and polyvinyl alcohol, the grafted membrane surface could construct some micro-nano structure to enhance the wettability with an amount of carboxyl and hydroxyl functional groups. Through this facile surface modification process, significant wettability, fouling improvement, and excellent thermal and mechanical enhancement are obtained, which further could widen the modified membrane application area in membrane separation with enhancing the service life.

2.1. Introduction

Membrane fouling is an unavoidable challenge, which can occur due to colloidal, surfactant, microbiological, and chemical (organic and inorganic) components that are clogged to the membrane surface and pores ^[140]. Different size of colloidal particles and membrane pores sizes causes various fouling such as solute adsorption on the membrane surface or in pores, solute blockage of pores, cake layer formation, and gel layer formation ^[141]. Fouling is a physicochemical phenomenon, where the material composition of the membranes and their physicochemical characteristics significantly determine their

CHAPTER 2

interactions with feed water and foulants and largely linked to reducing the separation performances such as flux decline, membrane stability, cost efficiency, and membrane lifetime ^{[142][143]}. However selecting the best membrane material can minimize these serious fouling issues. On that perspectives, the biaxially orientated polypropylene (PP) microporous membrane is chosen as a suitable substrate among other commercial polyolefin membranes due to its excellent mechanical properties, outstanding chemical and mechanical stability, high flexibility, and especially low cost ^{[144][145][146][147]}. In addition, the biaxially oriented microporous membrane exceeds all the limitations of other commercially available PP membranes and can be used in broad industrial application areas ^{[148][149][150][151][152]}. However, the intrinsic hydrophobic with low surface energy still limits the wide-ranging applications of the PP membranes ^{[153][154]} and leads to serious oil fouling during the operation. Therefore, it is crucial to find a beneficial solution to break all the limitations.

Surface modification is a highly emerging process that has attracted significant attention to achieve super wetting properties with anti-oil fouling properties and increase broad commercial application area ^{[155][156]}. Various surface modification techniques are noted as applicable processes for PP membranes to enhance the anti-oil fouling properties ^{[157][158][159][160]}. However, most of these techniques still have not shown satisfactory results in the achievement of super wettability with excellent anti-oil fouling properties ^[155]. But among them, radiation-induced graft polymerization is more frequently adopted commercially to achieve permanent hydrophilicity, by introducing a variety of polar functional groups into a polymeric chain by the direct graft polymerization of monomers ^{[161][162]}. The radiation-induced graft polymerization method can be divided into two ways:

CHAPTER 2

i) pre-irradiation and ii) simultaneous irradiation graft polymerization methods ^[163]. The membrane modification process by the radiation-induced graft polymerization technology is noted as a remarkable process due to significant enhancement in membrane wettability, and thermal and mechanical properties ^[134]. Considering the pre-irradiation process provides a robust structure with an abandoned number of free radicals generated on the membrane surface, which accelerates the attachment of more grafting monomers by grafting reaction ^[164]. The PP membrane surface modification using the pre-radiation-induced graft polymerization process could be controlled by adjusting the chemical composition and the grafting density ^[165].

To avoid serious fouling issues using different oils, and organic solvents and producing new pollution or waste during the membrane separation process, our work introduces the electron beam (E.B) radiation method as a pre-irradiation process, and acrylic acid (AA) and polyvinyl alcohol (PVA) to do the surface modification of the biaxial oriented PP microporous membrane. It is reported that 10 MeV E.B is more efficient than gamma irradiation due to its very strong energy, which accelerates homogenous reaction to build outstanding graft polymerization of the polymeric membrane ^{[166][167]}. Compared with other irradiation processes, the irradiation efficiency of E.B accelerator technology is reported as remarkable and extensively utilized in material areas in commercial industries ^[19]. Widely used Acrylic acid (AA) as a grafting monomer is noted as low toxicity with neutral pH in water solution. The AA contains many side chains in its inner chemical structure as an anionic chemical. It can easily lose its protons to acquire the negative charge, which is considered a remarkable ability to retain and absorb water ^[168]. Recently, many researchers have investigated and reported AA as an efficient grafting monomer due to the

CHAPTER 2

excellent adhesion properties and higher polymerizability of AA with the polymeric membrane ^[169]. Inspired by all reported beneficial properties of AA from previous studies, AA is selected as the first step modification monomer to enhance the hydrophilicity behavior of hydrophobic PP membrane, named AA-g-PP membrane. As the second step modification process, the AA-g-PP membrane goes through poly (vinyl alcohol) (PVA) grafting reaction. Incorporating the hydroxyl (–OH) functional group has gained significant interest in enhancing hydrophilicity, adhesion property, and surface energy ^[170]. Herein, PVA is an attractive environment-friendly hydrophilic polymer with an abandoned number of hydroxyl functional groups in its polymer chain ^[171], which is highly soluble in water and widely applied as hydrophilic surface modification material for water treatment applications ^{[172][173]}. Besides these hydrophilic properties, PVA is reported as biologically compatible with good chemical and thermal resistance and excellent binding properties in nature ^[174]. Combining the polymeric membrane substrates manufacture, electron beam pre-irradiation method, and AA and PVA grafting, this work provides the facile design of an environment-friendly, desirable, practical, easy to large-scale prepared, and successful hydrophilic functionalized anti-fouling modified membrane, which can be actively applied in the comprehensive application area.

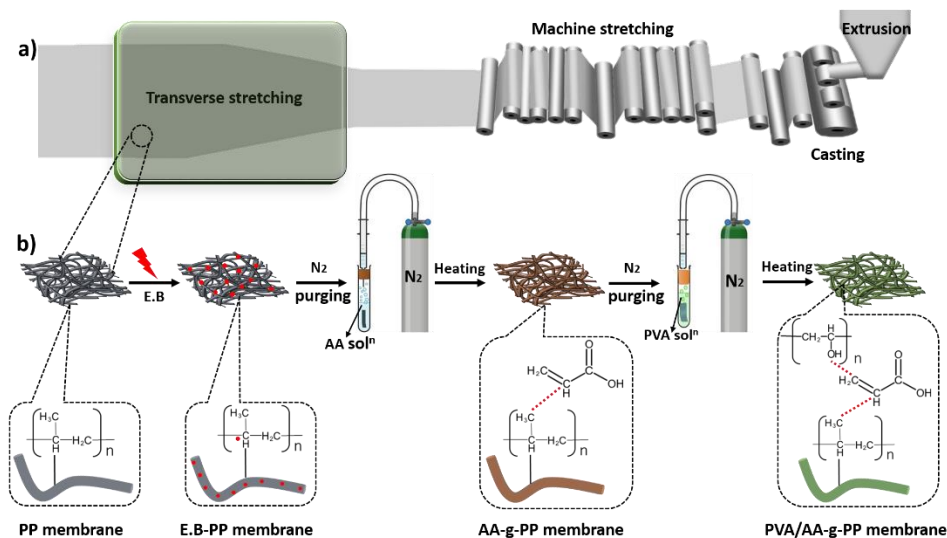


Figure 2.1: Schematic illustration of the a) Fabrication process of biaxially oriented microporous PP membrane, b) Hydrophilic surface modification of hydrophobic PP membrane by pre-irradiation-induced graft polymerization method with possible chemical structures.

2.2. Experimental

2.2.1. Materials

Biaxial oriented commercial polypropylene microporous membrane with a reported thickness of 80 μm was supplied from Tongling Jingneng Electronics Co., Ltd. Acrylic acid, Ethanol, Acetone, Polyvinyl alcohol, petroleum ether was supplied from Sinopharm chemical reagent Co., Ltd. (Shanghai, China). All chemicals were used without any further purification.

2.2.2. Electron beam irradiation process

The polypropylene membrane was first cut into 5 cm \times 5 cm in size and washed twice with ethanol for 30 min for removing all the contamination. Finally, the washed

CHAPTER 2

membranes were kept in the oven for drying at 60 °C overnight. The dried PP membranes were placed in zip-lock bags separately to prevent contamination. Electron beam irradiation was performed at Anhui Times Innovation Technology Investment Development Co. Ltd., (Hefei, China). PP membranes were exposed to 10 MeV E.B irradiation by applying 5-30 kGy doses. After irradiation exposure, membranes were kept in the refrigerator until used and all the experiments were performed within two days after irradiation. The irradiated membranes were tested by electron spin resonance spectroscopy (ESR, Bruker EMX) to confirm the existence of generated free radicals.

2.2.3. Preparation of AA-g-PP membranes

E.B irradiated PP samples were immersed into a closed glass tube containing a mixed solution of acrylic acid and deionized water with different AA concentrations (5, 10, 15, 20, 25 % (v/v)). After adding nitrogen gas to the reaction mixture for 30 minutes in a glass tube, the glass tube was heated in a water bath for 3, 6, 9, 12, and 15 minutes at various temperatures (50 °C-90 °C). After the grafting reaction, the samples were instantly rinsed with acetone and distilled water by an ultra-sonication process for 10 min to remove the homopolymer. Finally, the samples were put in a vacuum oven for drying at 60 °C overnight. The grafting ratio in percentage was calculated as per the following expression [153].

$$\textit{Grafting ratio} (\%) = (W_a - W_b) / W_b \times 100 \quad (2.1)$$

Where, W_b and W_a represent the symbol of the corresponding weight of the unmodified PP membrane and modified AA-g-PP membrane, respectively.

CHAPTER 2

2.2.4. Preparation of PVA/AA-g-PP membranes

PVA powder was diluted in deionized water to make three different concentrations (1, 3, 5 wt %) homogeneous solution at 90 °C by continuous stirring. AA-g-PP samples were immersed into a glass tube containing PVA solution and purged by nitrogen gas for 30 min. Then the purged glass tube was placed into the water bath for 30 min at 90 °C. However, to avoid the brittle structure of the membrane after the grafting reaction followed by the acrylic acid grafting parameters, less PVA concentration range (1-5 wt %) with high temperature (90 °C) and high reaction time (30 min) was maintained. After completion of the reaction, the samples were instantly washed with deionized water three times by ultrasonication (15 min) to remove the unreacted reactant and finally dried in the oven, maintaining a constant temperature (60 °C) for 24 h.

2.2.5. Membrane characterization

ATR-FTIR spectra (Attenuated Total Reflection Fourier Transform Infrared) of the unmodified PP, AA-g-PP, and PVA/AA-g-PP were obtained from an ATR-FTIR mode (Bruker Tensor 27, Germany). Scanning Electron Microscopy (SEM, Zeiss Libra, Germany) was performed to investigate the surface morphologies of the modified and unmodified membranes. BJH method was applied for the measurement of average membrane pore sizes using Micro metrics ASAP 2020 adsorption instrument at 77 K. Water contact angle (WCA) and underwater oil contact angle (UWOCA) were measured by SDC-350 (Shengding, China) contact angle machine at room temperature by dropping 2 μ L of both water and oil droplets. The average measurement of three samples was reported as the final contact angle value. In addition, each sample was measured 5 times from a different area. Chemical and elemental composition and identification were

CHAPTER 2

performed by X-ray photoelectron spectroscopy (XPS, ESCALAB 250), The thermal stability behavior of the membrane samples under the N₂ atmosphere was performed by thermo-gravimetric analysis (TGA, Q5000IR, USA). Mechanical performances of PP, 5 kGy-PP, AA-g-PP, and PVA/AA-g-PP samples were performed by an HD-B604-S universal testing machine supplied by Dongguan, China.

2.2.6. Anti-oil fouling performance

Surfactant stabilized emulsions are prepared by using a 1:100 (v/v) ratio of petroleum ether and water with 0.04 wt % tween 20 as non-ionic surfactant by continuous magnetically stirring for 24 h. emulsion separation experiment was carried out at a dead-end ultrafiltration cup using 0.8 MPa operating external pressure. 500 mL emulsion is poured into the upper glass tube, and permeate water was collected from the bellow glass beaker. The following equation was used to compute the pure permeability (J_0), emulsion permeability (J), and final permeability after 60 min (J_f)^[175]:

$$\text{Permeate flux } (J) = \frac{\Delta V}{\Delta A \times \Delta T \times \Delta P} \quad (2.2)$$

Where, ΔV (L), ΔA (m²), ΔT (h), and ΔP (MPa), denote the permeate water, membrane area, permeate time and applied pressure respectively. The membrane was extensively cleansed with water and ethanol after emulsion separation and further calculate the pure water flux (J_1). Therefore, using the pure permeability value before (J_0) and after (J_1) emulsion separation, the following equation was used to calculate the flux recovery ratio (FRR) and flux decline ratio (FDR)^{[176][177]}:

$$FRR(\%) = \frac{J_1}{J_0} \times 100 \quad (2.3)$$

CHAPTER 2

$$FDR(\%) = 1 - \frac{Jf}{J_0} \times 100 \quad (2.4)$$

Feed oily wastewater (1L) was poured through a modified PP/15 L membrane and the permeate water was collected after 15 min separation to calculate the permeate flux, cyclic performances, and flux rejection recovery. Furthermore, the efficiency (R) of oil rejection from permeate water was calculated by the following equation ^[178] using the feed C_0 (gL⁻¹) and permeate C (gL⁻¹) oil concentrations, which is determined by utilizing Thermo Evolution 600 UV-Visible Spectrophotometer:

$$R (\%) = \frac{C_0 - C}{C_0} \times 100 \quad (2.5)$$

2.3. Results and discussion

2.3.1. The effect of electron beam irradiation

The surface changes in the effect of the E.B irradiated PP membranes are investigated by applying different E.B doses (5-30) kGy. The E.B dose is considered an essential parameter for AA grafting reaction. When the PP membrane is irradiated by E.B irradiation, an abundant number of free radicals are generated on the membrane surface. These free radicals are cross-linked with the molecular chain of the PP membrane. Differences of SEM surface micrographs of unmodified membranes with lower (5 kGy) and higher (30 kGy) E.B dose irradiation are studied and shown in **Figure 2.2(a1-b3)**. It is observed that a lower E.B dose irradiated membrane surface has negligible effect, while a higher E.B dose irradiated membrane surface leads to a decrease in membrane pores. A higher E.B dose produces more free radicals, which are meant to react with more AA monomers by forming strong chemical bonds. Herein, **Figure 2.2c** showed the ESR spectra of E.B generated free radicals of high (30 kGy) and low (5 kGy) absorbed doses. PP

CHAPTER 2

membrane without any E.B dose (0 kGy) showed no ESR signal. In contrast, ESR signal intensity increased with the increase of E.B dose, which indicates that more radicals are generated on the membrane surface. However, different E.B doses (5-30) kGy have a significant effect on AA grafting reaction, which is analyzed in detail.

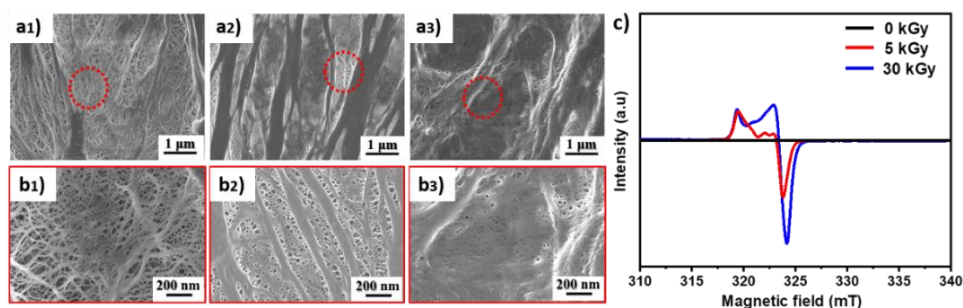


Figure 2.2: SEM micrographs of electron beam irradiated PP membrane with high and low resolution, (a1-b1) 0 kGy irradiated PP, (a2-b2) 5 kGy irradiated PP membrane, (a3-b3) 30 kGy irradiated PP membrane, and c) ESR spectra of the E.B irradiated membrane.

2.3.2. Acrylic acid grafting on PP membrane

The main objective of the AA grafting reaction is to immobilize the AA monomers on the unmodified membrane to enhance surface hydrophilicity. Details grafting experiment is performed to finalize the suitable variable parameters according to the observed surface wettability changes. Four variable parameters are applied to investigate the grafting reaction effect of AA on the PP membrane surface, noted as temperature, concentration, grafting heating time, and electron beam dose. The results are displayed in **Figure 2.3**. It can be seen the tremendous increasing effect of all the variable parameters on the grafting ratio data. A series of AA-g-PP membranes with a continuously increasing grafting ratio is fabricated by gradually increasing the four variable parameters. The results

CHAPTER 2

revealed that the grafting ratio increases with temperature, concentration, grafting heating time, and electron beam dose. The higher temperature helps to increase the reaction rate, and the higher concentration of monomer provides much more AA monomer for the reaction. In general, more grafting heating time results in a higher grafting ratio by increasing the graft polymerization rate due to the diffusion of more AA monomers. Further, increasing the electron beam dose generates more radicals to react with more AA monomers.

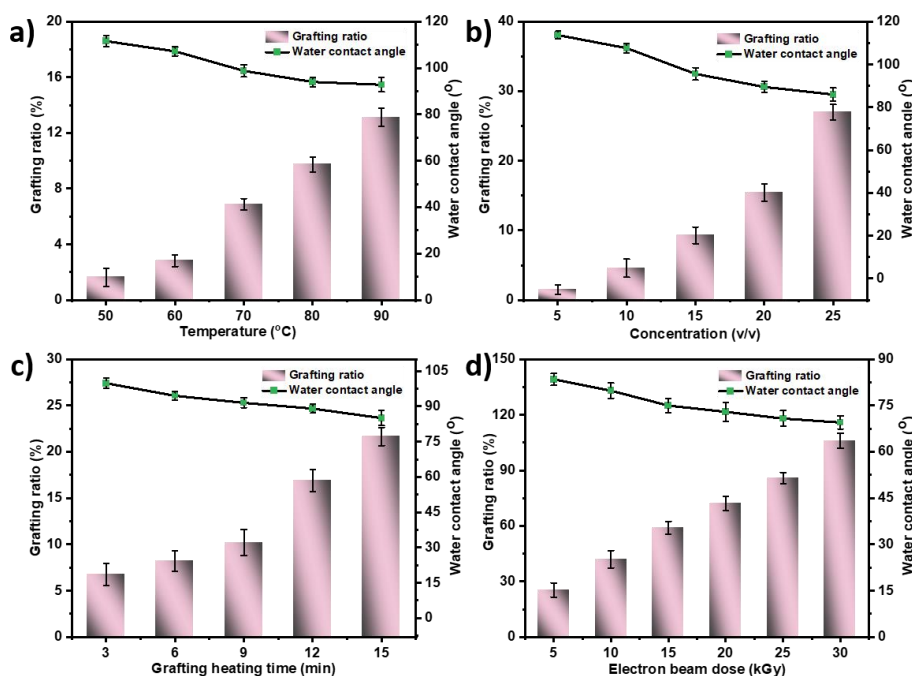


Figure 2.3: Grafting ratio of AA on the PP membrane surface and Water contact angle measurement in different variable parameters a) Temperature (50°C - 90°C), b) Concentration (5% - 25%), c) Grafting heating time (3 min – 15 min), and d) Electron beam dose (5 kGy- 30 kGy).

The highest grafting ratio (106 ± 4.1)% is achieved by applying the highest electron beam dose (30 kGy). AA-g-PP membrane using an E.B dose rate above 30 kGy leads to

CHAPTER 2

the rigid and transparent membrane surface after grafting that limits the E.B dose to 5-30 kGy. Compared to the growing trend of grafting ratio data, a similar but downward decreasing trend is observed for WCA data. The lowest WCA value (69°) is achieved for a high electron beam dose grafted membrane with the highest grafting ratio value. FTIR has confirmed the successful grafting reaction of AA-g-PP membrane for all variable parameter samples, presented in **Figure 2.4**.

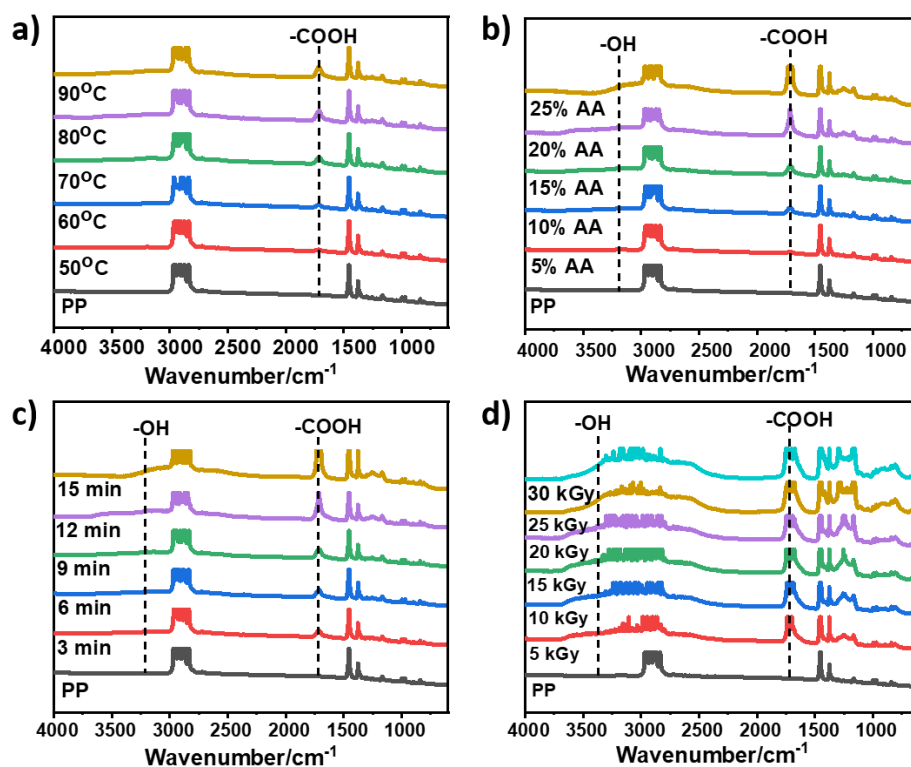


Figure 2.4: FTIR spectra for a) Effect of temperature, b) Effect of concentration, c) Effect of grafting heating time, and d) Effect of electron beam dose.

Compared to the unmodified PP, a novel adsorption peak is shown at 1710 cm^{-1} for all the modified membranes, mainly attributed to the carboxyl group (-COOH) of AA. A broad absorption peak from $3000\text{-}3500\text{ cm}^{-1}$ is also observed for the higher grafted

samples associated with the hydroxyl group (-OH). The increasing peak intensity is noticed with the increasing trend of grafting ratio value ^[179].

2.3.3. PVA graft polymerized PP membrane

The main objective of the AA grafting reaction is to immobilize the AA monomers on the unmodified membrane to initiate enhancing surface hydrophilicity. As for confirming the suitable AA-g-PP membrane for the second step PVA grafting reaction, a linear relationship between different grafting ratios, water contact angles, and membrane pore sizes is built up, which is represented in **Figure 2.5a**. Considering the WCA value and the pore size, 15-20% grafting ratio is maintained for the second step PVA grafting reaction. As the second step of the chemical grafting process, PVA is grafted on the AA-g-PP membranes with different PVA concentrations (1-5%). An increasing grafting ratio is observed by loading a high PVA monomer concentration. However, besides increasing the grafting ratio, the main objective is to final enhancement of surface wettability. **Figure 2.5b** shows that increasing the grafting ratio (5% PVA loading) shows a higher underwater contact angle (161°). A similar observation (**Figure 2.5c-d**) is also observed for enhancing surface hydrophilicity, measured through water contact angle. Worth-noting hydrophilicity is observed for the PVA/AA-g-PP-5 membrane due to the higher concentration of PVA grafting, which provides an abandoned number of hydroxyl functional groups. However, according to obtained UWOCA (161°) and WCA (35°) values, it is assumed that PVA/AA-g-PP membrane can show excellent anti-oil fouling properties.

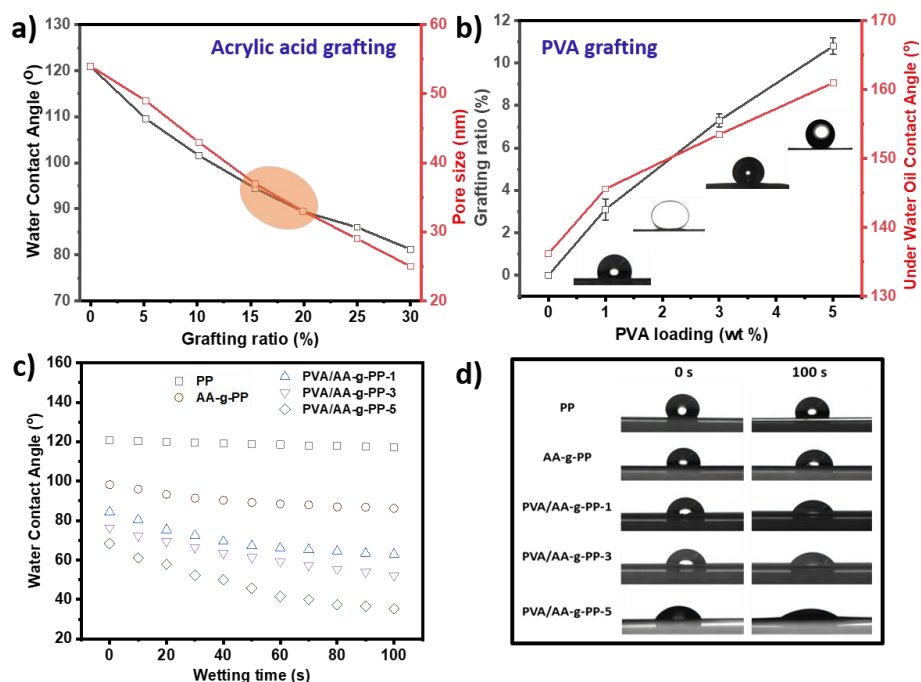


Figure 2.5: a) A linear relation between WCA and pore sizes of different AA-g-PP membranes; b) a linear relation between grafting ratio and UWOCA of different PVA loaded membranes; c) WCA measurement at 100 s wetting time, d) corresponding dynamic photographs at 0 s and 100.

2.3.4. Surface microstructure

The separation and antifouling abilities of modified membranes are greatly influenced by their surface profile. **Figure 2.6a1-a5** illustrates the SEM micrographs of membranes that have been changed by grafting reactions at various PVA concentrations. However, SEM micrographs of unmodified PP membrane show highly and randomly oriented porous surfaces, whereas, AA-g-PP membrane shows some acrylic acid layer in the porous surface. In contrast, PVA/AA-g-PP membrane surface is observed with overlaid and denser surfaces. After modification, the surface of all PVA/AA-g-PP membranes shows some blockage of inner micropores. The reason for the inner pore

CHAPTER 2

blockage issue can be described specially for the PVA/AA-g-PP-5 membrane by containing newly formed hydrophilic functional groups, which are densely grafted in the inner micropore walls. The PVA monomer's polar hydroxyl groups provide strong Van der Waals forces and hydrogen bonds, which can interact strongly with water molecules and operate as a capillary force to draw water droplets up to the inner membrane surface ^{[180][181]}.

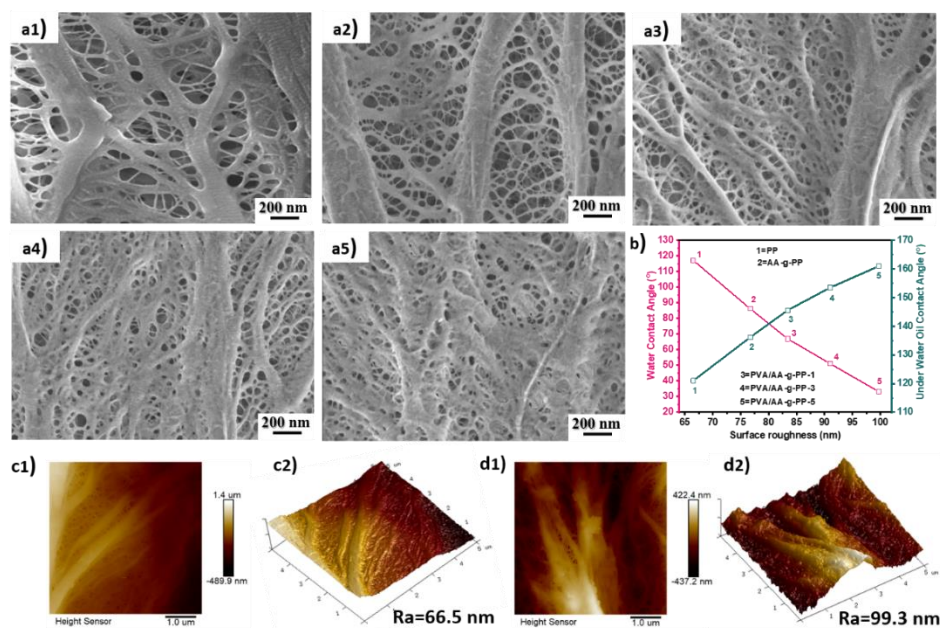


Figure 2.6: SEM micrographs of a1) unmodified PP, a2) AA-g-PP, a3) PVA/AA-g-PP-1, a4) PVA/AA-g-PP-3, and a5) PVA/AA-g-PP-5 membrane; b) a relation graph of membrane wettability and surface roughness; AFM 2D and 3D images of the (c1-c2) unmodified PP, and (d1-d2) PVA/AA-g-PP-5 membrane.

The variations in surface roughness after graft polymerization are also investigated using the AFM analysis. One of the key elements to improving membrane wettability is thought to be increasing the membrane surface roughness ^{[134][182]}. **Figure 2.6b** represents the linear relation between WCA, UWCA, and surface roughness values of different membranes. It is observed that the higher roughness of the PVA/AA-g-PP-5 membrane

CHAPTER 2

shows hydrophilicity and underwater superoleophobicity properties. **Figure 2.6c1-d2** represents the 2D and 3D AFM images with surface roughness (Ra) values of the unmodified PP and PVA/AA-g-PP-5 membrane. The increased surface roughness indicates the grafted AA and PVA on the membrane surface could construct some nano or microstructure, which corresponds with SEM results following the improvement of membrane wettability.

2.3.5. Chemical structure

ATR-FTIR spectra are performed to investigate the successful formation of new functional groups and measure the grafting mechanism of AA and PVA on the PP membrane, which is shown in **Figure 2.7a**. The absorption peak at 1500-1800 cm⁻¹ significantly shows a clear difference for PP, AA-g-PP, and PVA/AA-g-PP membranes. AA-g-PP shows the absorption peak of the –COOH group at 1714 cm⁻¹, while also observed for the PVA/AA-g-PP membranes with the increasing of PVA concentrations ^[183]. It can be assumed that, during the PVA grafting reaction at high temperatures, PVA strongly bonded on the AA-g-PP membrane surface. Furthermore, a broad absorption peak from 3000-3600 cm⁻¹ is observed for AA-g-PP and different PVA-loaded PVA/AA-g-PP membranes, which assisted with the –OH group ^[184]. Moreover, strong intensity of the –OH stretching band is also observed for the PVA/AA-g-PP-5 sample due to the higher concentration of PVA. Importantly, –OH, and –COOH absorption peaks are not found in unmodified membranes, which arises from the grafting process using acrylic acid and polyvinyl alcohol grafting.

CHAPTER 2

Table 2.1: Chemical composition of unmodified PP, modified AA-g-PP, and PVA/AA-g-PP-5 membrane

Sample	Composition (%)	
	C	O
PP	99.43	0.57
AA-g-PP	95.85	4.15
PVA/AA-g-PP-5	85.61	11.54

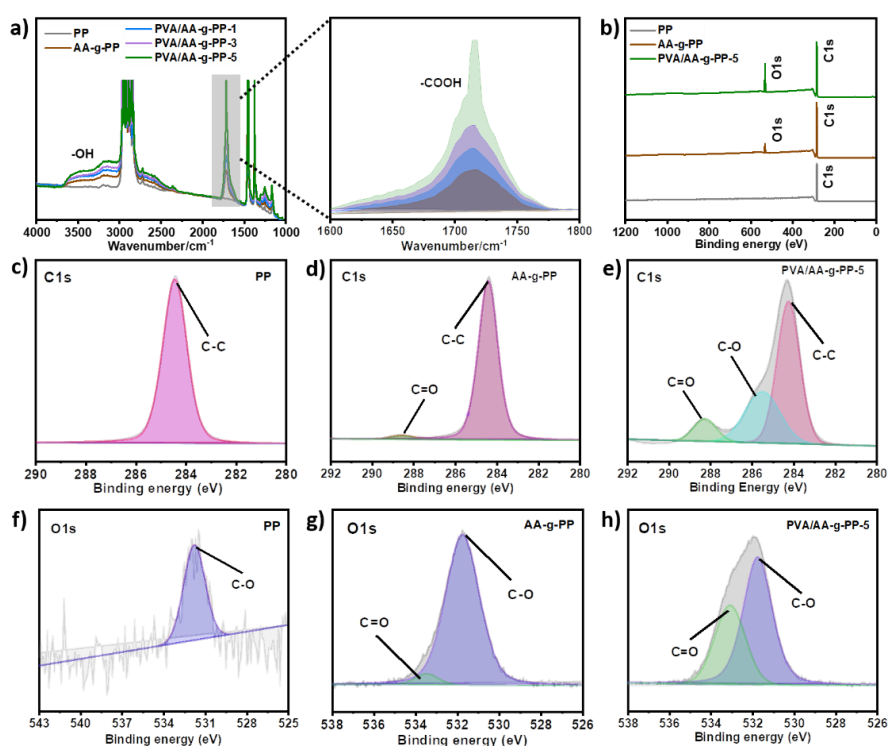


Figure 2.7: Surface chemical compositions of PP, AA-g-PP, and PVA/AA-g-PP membrane. a) ATR-FTIR spectra; b) Wide scan XPS spectra; High-resolution C1s fitting curve of, c) unmodified PP membrane, d) AA-g-PP membrane and e) PVA/AA-g-PP-5 membrane; and High-resolution O1s fitting curve of, c) unmodified PP membrane, d) AA-g-PP membrane and e) PVA/AA-g-PP-5 membrane.

CHAPTER 2

XPS experiment is performed to analyze the samples' functional groups and elemental composition after a successful grafting reaction^[185]. **Figure 2.7b** shows the XPS survey spectra, and **Figure 2.7c-h** shows the C1s and O1s high-resolution XPS spectra of the PP, AA-g-PP, and PVA/AA-g-PP membranes. The change of fitting peaks of C1s spectra gives clear evidence for the modification. The C1s fitting peaks of unmodified PP membrane belong to only C-C (284.4 eV), whereas AA-g-PP membrane belongs to C-C (284.4 eV) and O-C=O (288.2 eV), and PVA/AA-g-PP-5 membrane belongs to three distinct curves of C-C (284.4 eV), O-C=O (288.2 eV), and C-O (285.8 eV). Furthermore, the appearance of the O1s peak in XPS survey spectra is indicated the successful AA and PVA grafting reaction. However, the unmodified PP membrane shows no O elements in high-resolution O1s spectra, whereas AA-g-PP and PVA/AA-g-PP-5 membrane shows two distinct C-O and C=O bonds at around 531.4 eV and 533.1 eV. Furthermore, the strong C=O peak of the PVA/AA-g-PP-5 membrane represents the increased oxygen content due to the successful PVA grafting on the AA-g-PP membrane^[186].

2.3.6. Mechanical and thermal properties

The mechanical and thermal properties are the two main aspects to determine the membrane service life. The mechanical behavior of the unmodified PP membrane, 5 kGy -PP, AA-g-PP, and PVA/AA-g-PP-5 membranes are presented in **Figure 2.8a-b**. It is observed that the mechanical performance of unmodified PP membrane decreases in both MD and TD directions after applying a 5 kGy electron beam dose. The reason might be the sample goes through the heating process during electron beam irradiation, which weakens the inner membrane structure and causes some degradation. However, after grafting by AA and PVA, tensile stress and strain increase in the MD direction compared to the TD

CHAPTER 2

direction. In the TD direction, a decrease in elongation at break is observed in AA-g-PP and PVA/AA-g-PP-5 membranes, where tensile stress shows an increasing trend. Moreover, AA and PVA grafting enhances the mechanical strength in all without destroying the inner pores of the modified membranes ^[179].

TGA results of unmodified PP, AA-g-PP, and PVA/AA-g-PP-5 membranes are shown in **Figure 2.8c**. The analysis results show better thermal behavior of the grafted membranes than the unmodified membrane. The thermal degradation behavior of the membranes shows a few discrete steps to mass loss as the first dehydration step occurs up to 240°C. A slight mass loss of both the AA-g-PP and PVA/AA-g-PP-5 membrane is observed in the dehydration step, which is noted as initial weight loss by evaporating the water molecules of the sample due to the hydrophilicity nature. However, no dehydration is observed for unmodified membranes due to the strong hydrophobic nature of the PP membrane. The intense linear weight loss for all of the modified and unmodified membranes is visible during the second step due to the polymer chain degradation. The unmodified membrane shows maximum weight loss around the temperature reaches 360 °C with a residual percentage of 5%. In contrast, the AA-g-PP membrane shows weight loss around the temperature of 390 °C with a residual percentage of 6%. In addition, the PVA/AA-g-PP-5 membrane shows more stability as compared with the PP and AA-g-PP membrane, which shows weight loss around the temperature of 420°C with a residual percentage of 6.4%. However, up to 600°C, another weight loss step is observed, which can be stated as a reason for removing hydroxyl and carboxyl groups. Almost no residual percentage is observed for PP and AA-g-PP samples around 600°C, where 3.8 % residual remains for the PVA/AA-g-PP-5 membrane, proving the good thermal stability of

CHAPTER 2

hydrophilic modified PVA/AA-g-PP-5 membrane. **Figure 2.8d** shows typical DSC heating thermographs of unmodified PP, AA-g-PP, and PVA/AA-g-PP-5 membranes. A slight increase in melting temperature is observed for AA-g-PP and PVA/AA-g-PP-5 membranes compared with unmodified PP membranes. The melting temperature for unmodified PP membrane is 164°C, whereas AA-g-PP and PVA/AA-g-PP-5 membranes show melting temperatures of 167.2°C and 167.5°C, respectively. The enhancement of melting temperature further proves thermal stability, where AA and PVA grafting monomers act as good nucleating agents.

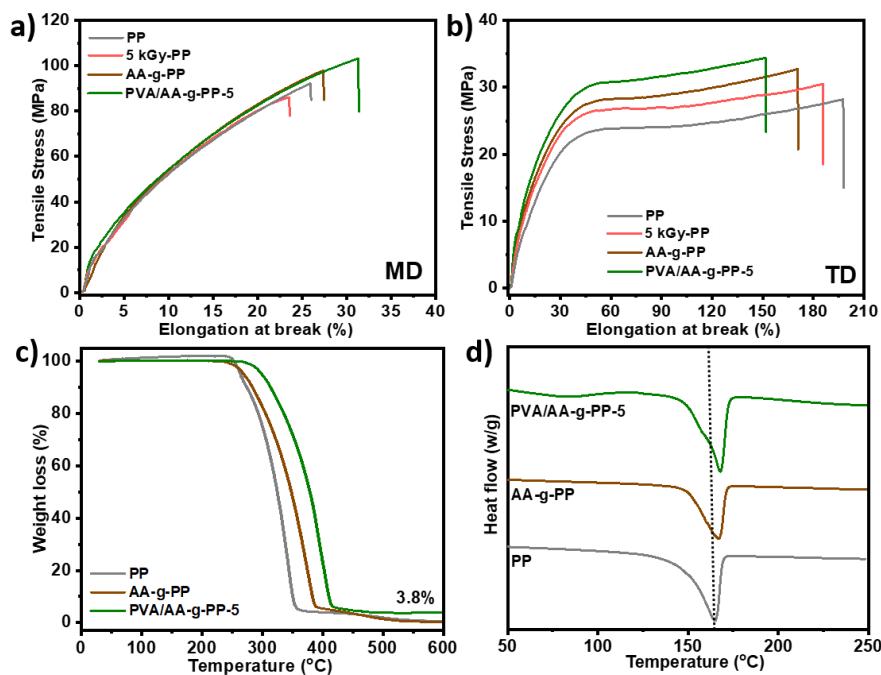


Figure 2.8: Mechanical and thermal properties of PP, AA-g-PP, and PVA/AA-g-PP membranes; a) stress-strain curve at MD direction, b) stress-strain curve at TD direction, c) TGA thermographs, and d) DSC heating curve.

2.3.7. Anti-oil fouling behavior

To assess the impact of graft polymerization modification on the relationship between membrane wetting behavior and dynamic oil fouling properties, the permeability of emulsion (p.e/water) experiment is performed using PP, AA-g-PP, and PVA/AA-g-PP-5 membranes. The effectiveness of surface grafting modification shows excellent enhancement of permeability and rejection ratio of PVA/AA-g-PP membrane as compared with unmodified PP and AA-g-PP membranes (**Figure 2.9a**). As a mechanism responsible for such excellent antifouling properties, PVA polymers have a great propensity to hydrate through carboxylate groups with water molecules, which could provide a steric barrier between the foulants and the membrane surface. Furthermore, to evaluate the long-term stability with oil fouling effectiveness of PVA/AA-g-PP membrane, different oil concentrations (1000, 3000, and 5000 ppm) in emulsion are permeated through the membrane for up to 160 min. According to the findings obtained (**Figure 2.9b**), the permeability decreases with an increase in oil concentration, which is an evident result. However, the water cleaning can recover the initial permeability without much decrease further proving the excellent anti-oil fouling properties of the PVA/AA-g-PP-5 membrane. Additionally, shown in **Figure 2.9c** are the FRR values following the cleaning procedure and the FDR values during the fouling phase. The moderate reduction in the flow profile of the modified PVA/AA-g-PP-5 membrane shows that the potency of membrane fouling is effectively reduced following the PVA grafting reaction. On the other hand, unmodified PP cannot be applied to calculate FRR and FDR, whereas the water flux of the AA-g-PP membrane exhibits a 40% loss in its initial flux and can only be recovered to about ~25%.

CHAPTER 2

As evidenced by a flux drop of just 10% and a flux recovery of more than 99%, the modified membrane, in contrast, demonstrates the best antifouling capabilities.

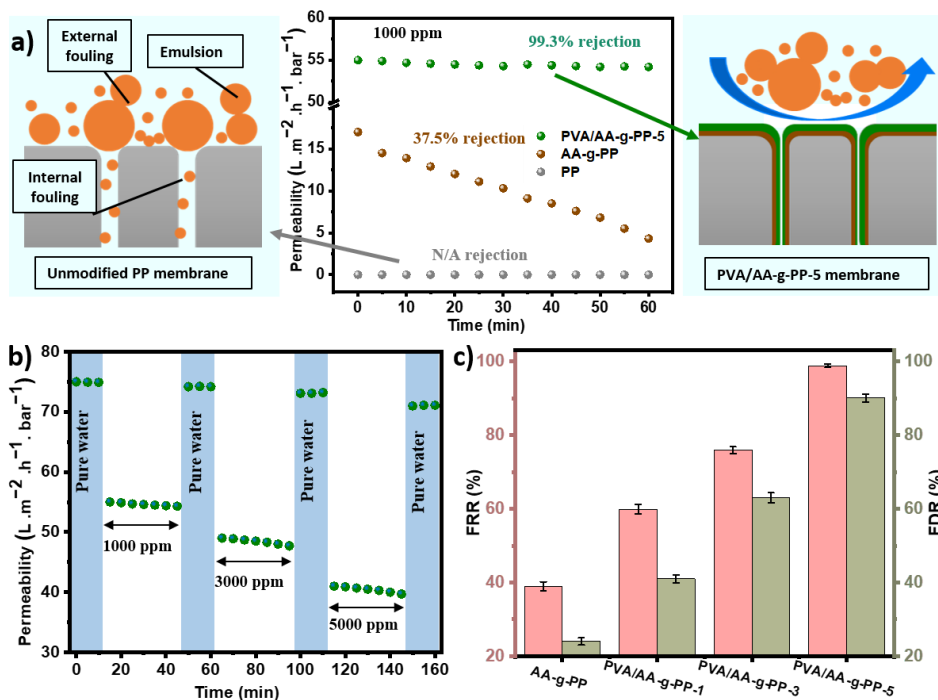


Figure 2.9: a) Permeability and rejections of PP, AA-g-PP, and PVA/AA-g-PP membranes; b) long-term permeability with anti-oil fouling properties of PVA/AA-g-PP membrane, c) FRR and FDR value of different membranes.

2.4. Conclusions

This research work demonstrated the successful anti-oil fouling surface modification process of biaxially oriented PP membrane by pre-irradiation-induced graft polymerization method, where electron beam as irradiation method and acrylic acid and polyvinyl alcohol as the grafting monomer is introduced. However, the successful grafting reaction was confirmed by generating strong $-OH$ and $-COOH$ functional groups in the modified membrane. Additionally, the surface roughness of the PVA/AA-g-PP-5

CHAPTER 2

membrane enhanced from 66.5 nm to 99.3 nm, which constructs micro/nano surface structure, responsible to enhance the wetting properties. More importantly, both thermal and mechanical properties are improved after a successful modification process, proving the excellent chelating agent properties of grafting monomers. In conclusion, this study proposed an effective and facile surface modification method with the enhancement of interfacial properties with excellent anti-oil fouling properties.

CHAPTER 3. Robust super-wetting multi-scale rough biaxial polypropylene membrane for pressure driven separation

The severe toxicity of oily wastewater is considered extremely detrimental to both human health and the environment. Despite previous enormous efforts, it is still challenging to efficiently separate extremely stable micron-sized oils from wastewater emulsion. This study reports a highly mechanically stable biaxial polypropylene membrane with uniform nano-porous structures for excellent separation of tiny oil droplets from the emulsion. A facile and scalable two-step surface modification method has been developed by employing acrylic acid and sodium hydrogen carbonate. This modification method ensures excellent hydrophilicity and underwater superoleophobicity by constructing multiscale micro/nano rough surfaces with separation performances.

3.1. Introduction

The continued expansion of contemporary manufacturing industries has led to a global concern regarding the contamination of water resources by frequent oil spills [187][115][188][189][190]. The existence of numerous surfactants stabilized by tiny micro/nano-sized oil droplets (<20 μm) makes oily wastewater emulsions separation difficult [191][33][192][193]. Compared to widely used conventional methods, membrane-based separation technology has conquered enormous growth and efficient applications in oil/water emulsion separation due to their cost-effectiveness, manufacturing scalability, adjustable pore size, high permeability, and ability to regulate their properties in response to demand [194][195][196][197]. Still, improving high separation efficiency is a continuing

CHAPTER 3

struggle for membrane separation technology ^[198]. In order to achieve highly effective emulsion separation performances, three important parameters- i) membrane hydrophilicity, ii) surface roughness, and iii), membrane pore diameters, should be adjusted ^{[199][200]}.

Membrane hydrophilicity is considered the most required parameter in terms of separating water from wastewater emulsion ^[201]. Hydrophilic modification groups prevent to exposure the hydrophobic parts of membrane materials thus ensuring water permeance ^[13]. However, simply increasing hydrophilicity can boost permeability, but this doesn't always lead to high oil rejection. Therefore, it is imperative to find a solution to the oil-fouling dilemma with the superhydrophilicity feature, which has been extensively studied recently. Remarkably, constructing a supreme multi-scale micro/nano-rough structure is a highly intriguing solution from both a theoretical and practical approach for creating surfaces with great hydrophilicity and underwater super oleophobic properties ^{[56][57]}. As a mechanism, rough surfaces minimize the contact area between oil and membrane surfaces underwater by creating a hydration layer ^{[58][59]}. Wenzel's theory ($\cos\theta^* = r\cos\theta_{ow}$) shows a complementing linear correlation between rough surface (roughness ratio= r) and membrane wetting (underwater oil contact angle= $\cos\theta^*, \cos\theta_{ow}$) ^{[47][48]}. From an explanatory point of view, excellent membrane wettability, especially underwater oleophobicity, is achieved through a higher surface roughness. In contrast, rough surfaces are further thought to be an excellent way to alter the membrane's pore diameters to considerably smaller than emulsified oil droplet sizes. As a result, separation materials having smaller pore sizes can further achieve high separation efficiency based on the oil droplet size exclusion principle ^[33]. Even yet, a lot of research has been conducted on ways

CHAPTER 3

to make rough surfaces in order to improve membrane wettability, but relatively few of it has been led to alter the inner pore sizes. Smaller membrane pore sizes may decrease permeability or the need for external pressure, but doing so is highly effective approach to achieve high separation efficiency. Hence, high oil toxicity removal should take precedence over achieving high permeability as a matter of environmental safety. As a result, creating multi-scale rough surfaces offers a two-pronged strategy for high oil removal by producing underwater superoleophobicity and adjusting the inner pore diameters. Choosing the ideal membrane material and forming a reliable modification technique should therefore be priorities to achieve excellent separation performances.

In light of this, biaxially oriented polypropylene microporous membranes (PP) can replace widely used conventional membranes due to their high mechanical strength in both machine and transitional directions, which provides long service life with outstanding reusability. Furthermore, biaxial PP holds a constant inner microstructure that can ensure excellent nano-scale pore sizes of modified membranes smaller than micron-sized oil droplets^[44]. However, the PP membrane's inherent hydrophobicity makes it easily fouled by oil droplets during separation which reduces productivity, efficiency, and reusability and minimizes its wide applicability^[202]. Considering the abovementioned advantages and limitations, we have previously reported a super hydrophilic surface modification on a commercial biaxial PP membrane via acrylamide grafting with the help of corona-discharge treatment^[44]. Therefore, we develop a facile modification strategy employing a two-step grafting reaction using acrylic acid and NaHCO_3 to acquire a constant multi-scale rough surface with robust super-wetting nature on the biaxial PP membrane (**Figure 3.1**). The PP membrane was exposed to electron beam radiation before the grafting reaction to

CHAPTER 3

generate free radicals. Herein, electron beam irradiation acts as an initiator and initiates the grafting reaction by forming strong covalent bonds with the polar functional groups of acrylic acid and NaHCO_3 [203]. Hence, a unique formation of super hydrophilic $-\text{COONa}$ functional groups are covalently attached and evenly distributed on smooth biaxial PP surfaces, thus creating a multi-scale stable rough surface through the grafting process. Such achieved rough surface assured oil droplets' aggregation upon contact and permitted straightforward water separation from oil/water emulsion. The improved properties of the multi-scale rough biaxial PP membrane surface are anticipated to be a substantial and prospective mass-scale industrial application for long-term emulsion separation.

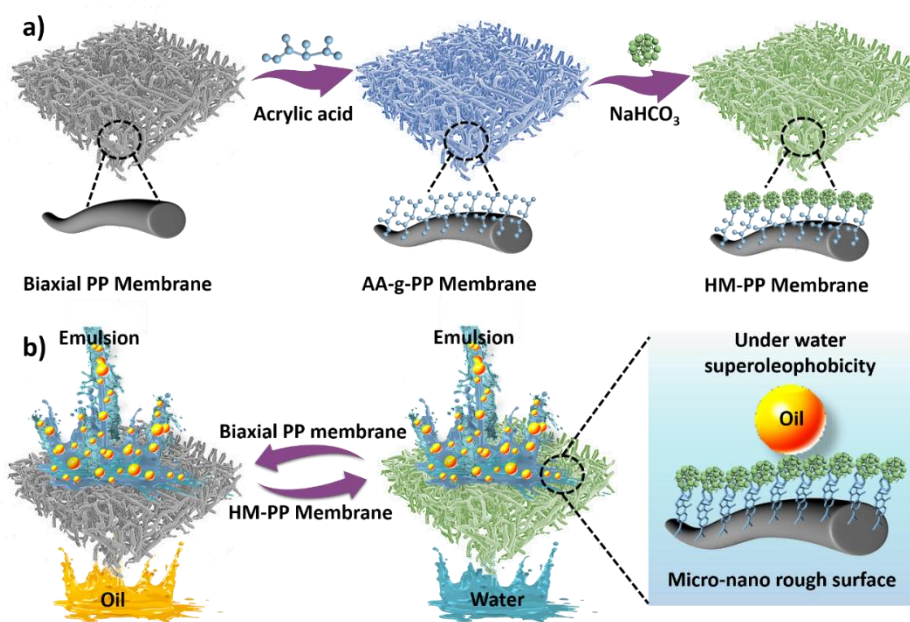


Figure 3.1: Schematic illustration of the a) conversion process of hydrophobic biaxial PP membrane to super-wetted HM-PP membrane and b) emulsion separation method through unmodified and rough surface structured modified PP membrane.

CHAPTER 3

3.2. Experimental

3.2.1. Materials

Sodium hydrogen carbonate, n-butanol (0.808-0.811 g/cm³), Toluene, Hexane, Hydrochloric acid, Sodium hydroxide, and Sodium chloride were supplied from Sinopharm chemical reagent Co., Ltd. (Shanghai, China). The soybean oil used in the separation experiment was bought from the supermarket. Other used chemicals are listed in the 2.2 section.

3.2.2. Membrane characterization

Wide-scale surface roughness was evaluated using XP-1 Stylus Profilometer (Ambios, CA, USA) using 0.5 mm × 0.5 mm surface area. Measurements were taken using both X and Y directions and each direction was measured 5 times in different places.

3.2.3. Calculation of water adsorption energy

To understand the reason for the strong hydration ability of the HM-PP membrane, the structure was optimized by density functional theory (DFT) using the B3LYP method with 6-311+G (d, p) basis sets at the Gaussian 09 package programs. The adsorption energy and equilibrium distance corresponding to each interaction were calculated using the following equation ^[204]:

$$\Delta E_{ads} = E_{(H_2O/HM-PP-x)} - E_{(HM-PP-x)} - E_{(H_2O)} \quad (3.1)$$

Where, $E_{(H_2O/HM-PP-x)}$, $E_{(HM-PP-x)}$, and $E_{(H_2O)}$ represent the optimized total energy of represented functional groups adsorbed by a water molecule, the optimized potential energy of the modified HM-PP membrane, and a free water molecule, respectively, and x represents the different functional groups.

CHAPTER 3

3.2.4. HM-PP membrane fabrication

Biaxial stretched PP membrane was first cut into 5×5 cm in size and washed with ethanol for 30 min and dried in the oven at $60\text{ }^{\circ}\text{C}$ overnight. The dried PP membranes were irradiated by electron beam irradiation (10 MeV, 5 kGy) at Anhui Times Innovation Technology Investment Development Co. Ltd., (Hefei, China). Irradiated PP membranes were immersed into a closed glass tube containing a mixed solution of acrylic acid and deionized water with 10 % (v/v) AA concentration. Nitrogen gas was purged followed by above-mentioned process. Electron beam irradiated unmodified biaxial PP membrane is firstly grafted by acrylic acid (AA-g-PP) by maintaining a 20% grafting ratio. After the grafting reaction, the membranes were instantly washed and dried in the oven. Therefore, the AA-g-PP membrane further went through NaHCO_3 treatment.

3.2.5. Surfactant-stabilized oil/water emulsion preparation

Surfactant stabilized oil/water emulsions of various oils (petroleum ether, toluene, hexane, and soybean oil) are prepared by using a 1:100 v/v ratio, and different soybean oil content using (0.5, 1.00, 3.00, 5.00, and 10.00)/100 v/v ratio. 0.04 wt% Tween 20 surfactant was added into 100 ml water with continuous stirring for 30 min. Various oils with different concentrations were dropped into the mixed solution using a dropper and magnetically stirred for 24 h.

3.3. Results and discussion

3.3.1. Hydrophilic modified (HM-PP) membrane

Three variable parameters have been applied for NaHCO_3 treatment on the AA-g-PP membrane, noted as concentration (5, 10, 15 wt %), temperature (30, 50, 70, and $90\text{ }^{\circ}\text{C}$),

CHAPTER 3

and time (1-10 h). After successful NaHCO_3 treatment, all the samples have been observed by performing a WCA test. As shown in **Figure 3.2a-c**, all the HM-PP membranes display a tremendous decrease in WCA value with the increase in monomer concentration and reaction temperature due to reacting more hydrophilic groups in the membrane surface. The lowest WCA ($15.5 \pm 2.9^\circ$) value is observed until a certain period of heating time (5 h). Moreover, the reverse decreasing trend of hydrophilicity is observed with a further increase in heating time with reported WCA values for 6 h, 7 h, and 10 h treatment time is $24.4 \pm 2.4^\circ$, $29.8 \pm 3^\circ$, and $45.7 \pm 3.1^\circ$, respectively. Such increasing the heating time leads to amalgamating more NaHCO_3 into the membrane surface, might start blocking the inner pores, and can be the main reason for the barrier of absorbing the water. Therefore, 90 °C temperature, 15 % concentration, and 5 h heating time are selected as required parameters to prepare the final HM-PP membrane.

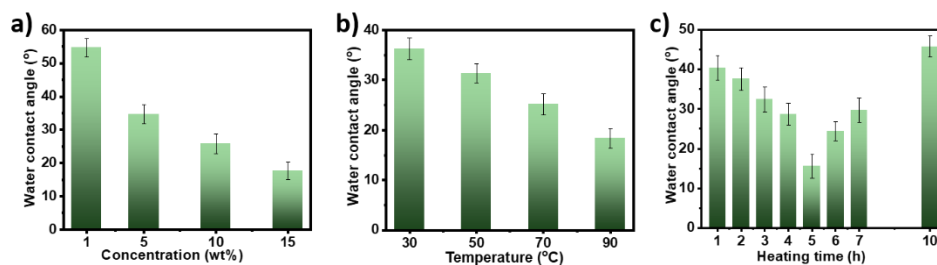


Figure 3.2: WCA data of NaHCO_3 treatment in different variable parameters a) temperature, b) concentration, and c) heating time.

3.3.2. Surface microstructure and chemical compositions

The surface microstructure of unmodified PP membrane is observed with randomly oriented porous surfaces, whereas HM-PP membrane surfaces show denser grafted rough surfaces with less pore volume (**Figure 3.3a-c**). The reason for the rough surface is the newly formed hydrophilic functional groups are densely grafted on the surface and inner

CHAPTER 3

pore walls. The EDS micrographs of the HM-PP membrane are shown in **Figure 3.3d**. It is observed that the HM-PP membrane is rich in O, and Na elements, which are distributed uniformly throughout the membrane surface. Furthermore, it is observed that with the modification, the pore volume decreases along with the average pore diameter decrease respectively (**Figure 3.3e**).

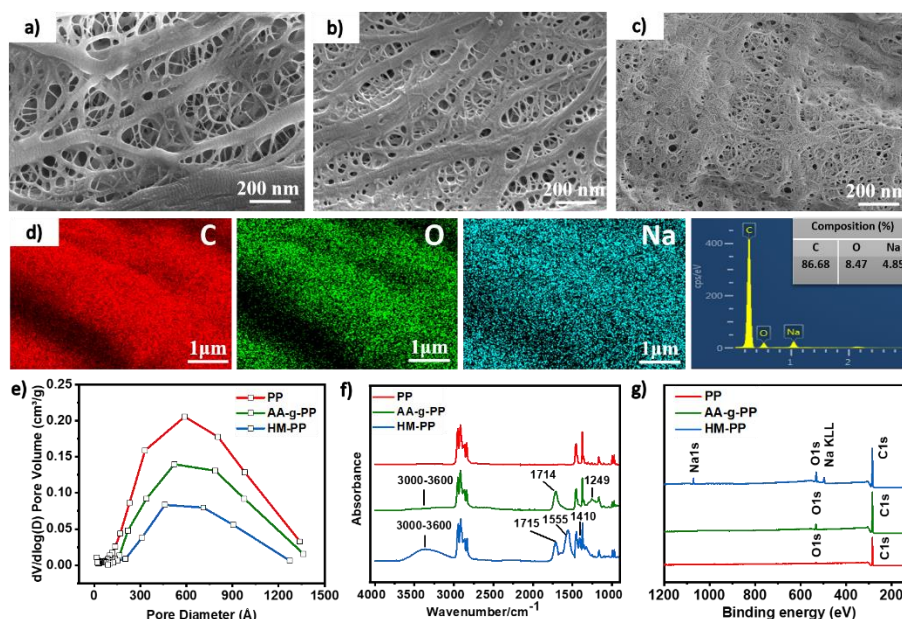


Figure 3.3: (a-c) Surface microstructure of PP, AA-g-PP, and HM-PP membranes, d) EDS mapping images of HM-PP membrane with elemental percentile, e) average pore diameter, f) ATR-FTIR, and g) Survey XPS spectra

The thickness and density increase observed in the cross-sectional images also demonstrate the successful grafting on the inner wall of the pore. The membrane thickness is 83 μm , 86 μm , and 90 μm for PP, AA-g-PP, and HM-PP samples, respectively.

CHAPTER 3

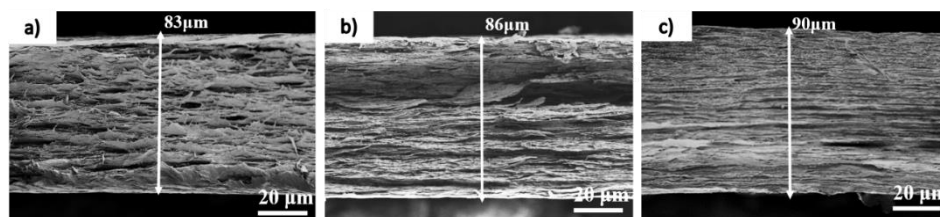


Figure 3.4: Cross-sectional micrographs of a) unmodified PP, b) AA-g-PP, and c) HM-PP membrane

Nitrogen adsorption/desorption isotherms data matches with the type II Nitrogen adsorption/desorption isotherms curve along with an H3 hysteresis loop (**Figure 3.4a**). The corresponding surface area of PP, AA-g-PP, and HM-PP was 17.4, 10.5, and 6.9 m²/g, respectively. In contrast, decreasing in porosity value is also observed. The porosity value of unmodified PP, AA-g-PP, and HM-PP membrane is 54 ± 3.2 %, 45 ± 3.9 %, and 33 ± 4.9 % respectively (**Figure 3.5b**).

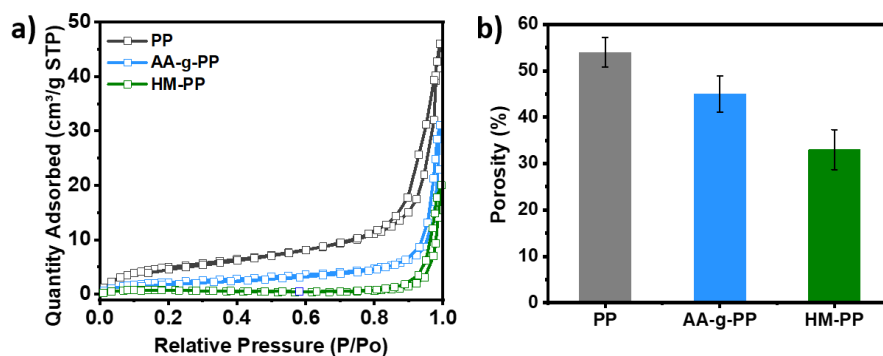


Figure 3.5: a) N₂ adsorption/desorption curves and b) porosity value of PP, AA-g-PP and HM-PP membrane.

CHAPTER 3

Table 3.1: BET surface area of PP, AA-g-PP, and HM-PP membrane

Sample	BET surface area (m ² /g)
PP	17.373
AA-g-PP	10.468
HM-PP	6.863

ATR-FTIR spectra are performed to investigate the successful formation of new functional groups and measure the grafting mechanism of acrylic acid and sodium hydrogen carbonate on the PP membrane **Figure 3.3f**. The absorption peak at 1249 cm⁻¹ is attributed to the –C-O stretching band for the AA-g-PP sample, where –COO-Na symmetrical stretching vibration absorption peak is found around 1410 cm⁻¹ for the HM-PP sample. As shown in the data, the absorption peak at 1500-1800 cm⁻¹ significantly shows a difference for PP, AA-g-PP, and HM-PP. AA-g-PP showed the absorption peak of the –COOH group at 1714 cm⁻¹, while the strong peaks of –COOH groups and –COO-Na groups are observed for the HM-PP sample at 1715 cm⁻¹ and 1555 cm⁻¹ respectively [205]. It can be assumed that, during the grafting reaction at high temperatures, acrylic acid strongly bonded on the PP membrane surface. Moreover, the –COOH groups partly transformed into –COO-Na groups after sodium hydrogen carbonate treatment. Furthermore, a broad absorption peak from 3000-3600 cm⁻¹ is observed for AA-g-PP and HM-PP samples, which is assisted by the –OH group [184]. However, strong intensity of the –OH stretching band is observed for the HM-PP sample which is affiliated with the super hydrophilic nature of the HM-PP sample. Importantly, –OH, –COOH, and –COO-Na

CHAPTER 3

absorption peaks are not found in an unmodified PP membrane, which is arising from the grafting process using acrylic acid and sodium hydrogen carbonate treatment.

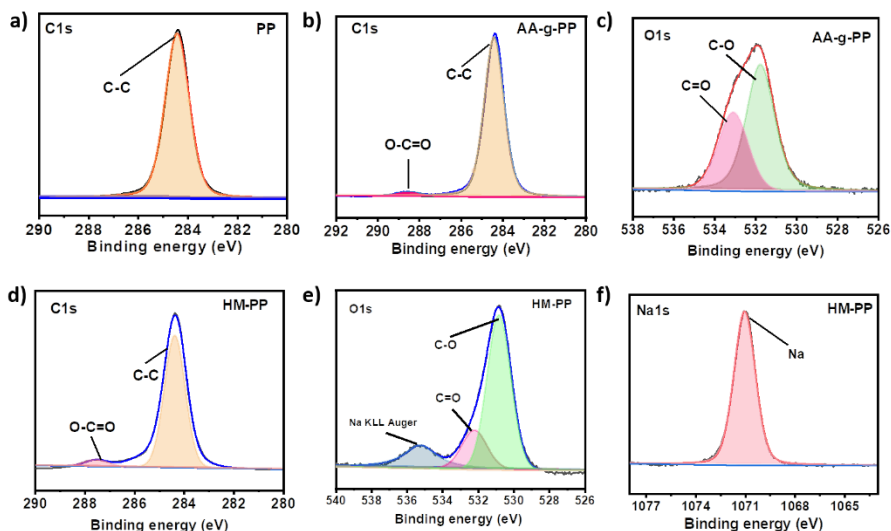


Figure 3.6: (a-f) High-resolution C 1s, O 1s, and Na 1s, XPS spectra of PP, AA-g-PP, and HM-PP membranes.

XPS experiment is performed to analyze the functional groups and elemental composition of the samples after successful grafting by acrylic acid and sodium hydrogen carbonate treatment [185]. **Figure 3.3g** shows the survey XPS spectra, and **Figure 3.6a-f** shows the C, O, and Na high-resolution XPS spectra of the unmodified PP, AA-g-PP, and HM-PP samples. The appearance of O 1s and Na 1s peaks in survey spectra indicates the successful AA grafting and NaHCO_3 treatment. Furthermore, the change of fitting peaks of C 1s and O 1s spectra gives more clear evidence for the modification. The C 1s fitting peaks of AA-g-PP and HM-PP samples both belong to C-C (284.4 eV) and O-C=O (288 eV). The O 1s fitting peaks for all samples are considered as C-O and C=O bonds at around 531.4 eV and 533.1 eV. In addition, a higher Na KLL Auger is observed at 535.5 eV only in the O 1s spectrum of the HM-PP sample, which demonstrates oxygen content increasing

CHAPTER 3

in the HM-PP sample due to the successful sodium hydrogen carbonate treatment ^[206]. Only Na 1s peak is obtained in the HM-PP sample at 1071.1 eV binding energy because of the existence of sodium.

3.3.3. Multi-scale surface roughness

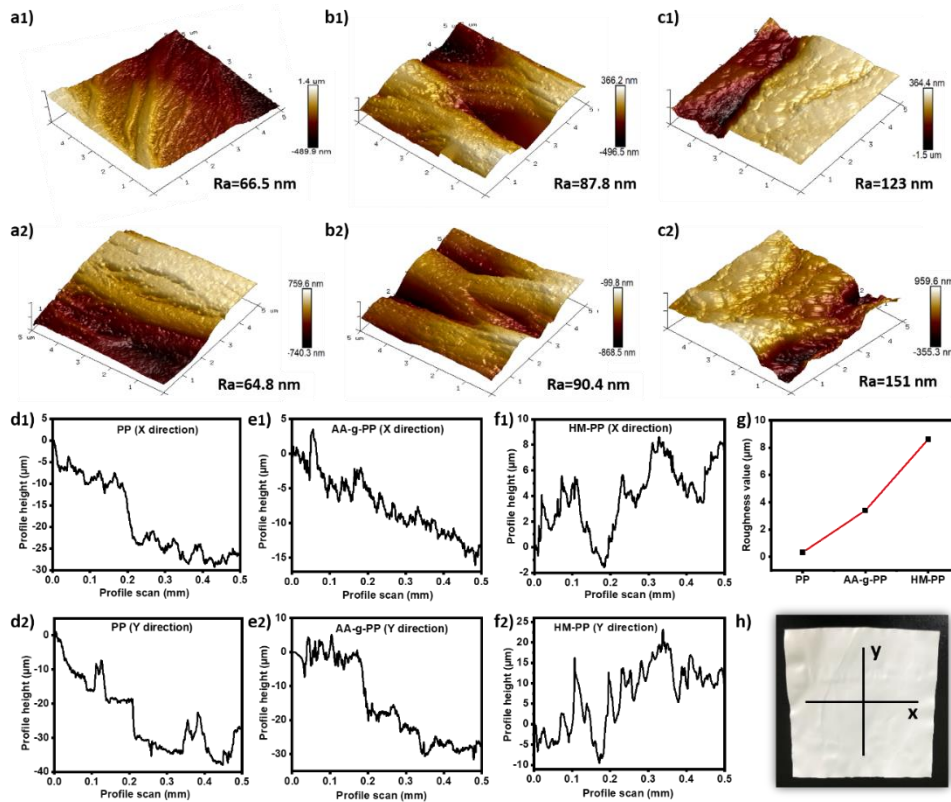
Multi-scale roughness defines the roughness modeling at multiple length scales ^[207]. Herein, the developed multiscale rough surface is deeply analyzed and confirmed by SEM, AFM, and profilometer experiments. SEM micrographs confirm the rough surface microstructure in a small nanometer area, whereas AFM represents the surface roughness in a micrometer (5 μ m) area, and profilometer data shows the surface roughness in more large millimeters (0.5 mm) area. In addition, AFM surface roughness of unmodified and modified membranes is more intensely investigated in the air, and underwater conditions (**Figure 3.7a1-c2**). The results show that the unmodified PP membrane surface is relatively smooth in both air and underwater conditions with reported roughness values of 66.5 and 64.8 nm, respectively. The introduction of AA to the PP membrane enhances hydrophilicity along with surface roughness. A larger increase in roughness is spotted after NaHCO₃ treatment. The reaction between NaHCO₃ and AA on the membrane surface largely affects the increase of surface roughness, and this phenomenon is consistent with the above SEM results. However, the HM-PP membrane exhibits a higher roughness value underwater (151 nm) than it does in the air (123 nm). This is because when the nanoscale heterogeneous hydrophilic substrates emerge in water, numerous water molecules are attracted to the hydrophilic functional groups of a rough surface and formed a hydration layer thus creating a more roughed surface underwater. Hence, such properties are thought to be an efficient barrier for oil droplets from wetting substrates underwater. Furthermore,

CHAPTER 3

a large-scale (0.5 mm) surface area is analyzed to evaluate the multi-scale roughness value of unmodified and modified membranes, as shown in **Figure 3.7d1-h**. The average arithmetic roughness value is calculated using the following formula [208].

$$\text{Arithmetic average roughness, } R_a = \frac{1}{S} \int_S^0 |z| ds \quad (3.2)$$

Where S represents the measured area and z represents the relative profile height. The average roughness value is calculated using both the x and y directions of the membranes. The obtained roughness value using a wide scan area still shows higher roughness of the HM-PP membrane (8.6 μm) than the unmodified PP membrane (0.32 μm). Uniformity and increasing roughness of HM-PP membrane further prove the successful modification and hence can be utilized as an efficient oil barrier in underwater conditions.



CHAPTER 3

Figure 3.7: 3D AFM values measured in the (a1-c1) air condition, (a2-c2) underwater condition; Multiscale roughness value in X and Y direction; (d1-d2) unmodified PP membrane, (e1-e2) AA-g-PP membrane, (f1-f2) HM-PP membrane; g) linear graph of average roughness value, and h) digital images of a membrane with marking X and Y directions.

3.3.4. Membrane wettability

The modified HM-PP membrane shows excellent super hydrophilicity (0°) as compared with the unmodified PP (118.4°), and the AA-g-PP membrane (79.1°), as shown in **Figure 3.8a**. Worth-noting super hydrophilicity of HM-PP membrane is reported due to the abandoned number of carboxyl, sodium carboxylate, and hydroxyl functional groups. This decreasing trend in WCA can be described as the enhancement interaction among the inner surface and water droplets because of the presence of hydrophilic functional groups by arising strong Van der Waals force and hydrogen bonds ^[181]. The DFT simulation (**Figure 3.8d-g**) also further discusses such super hydrophilicity behavior of different functional groups. Corresponding obtained water adsorption energy results for the CH₃, COOH, and COONa groups of PP, AA-g-PP, and HM-PP membranes are 18.831, -21.807, and -68.293 kJ/mol, respectively. Such the highest negative and lower binding energy of the COONa functional group with the shortest hydrogen bond distance (2.24 Å) with water molecules signifies an incredibly strong hydration ability with a more stable complex of HM-PP membrane ^{[204][209][210]}. Additionally, UWOCA of the HM-PP membrane is performed to observe the membranes' superoleophobicity behavior in water, as shown in **Figure 3.8c**. The HM-PP membrane shows excellent underwater superoleophobicity with

CHAPTER 3

a reported oil contact angle value of 161.8° for petroleum ether, 162.1° for hexane, 162.9° for toluene, and 164.3° for soybean oil, respectively.

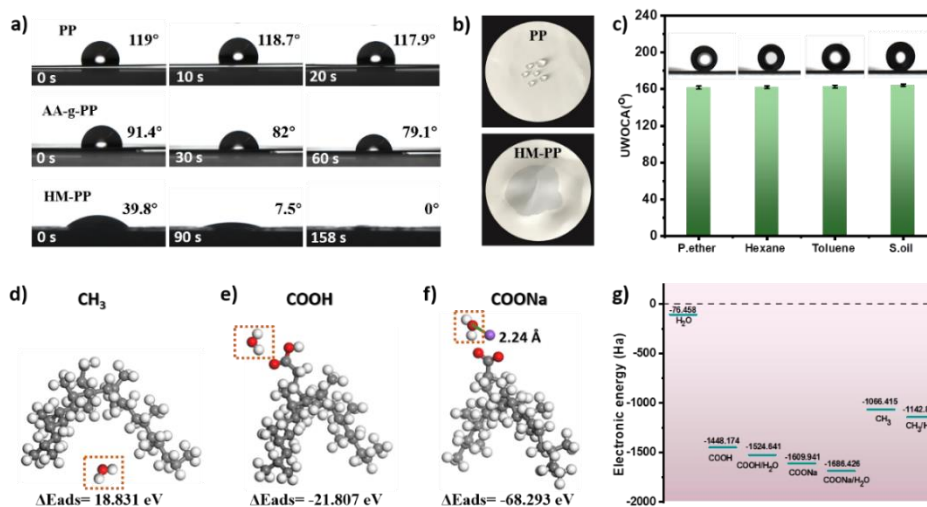


Figure 3.8: a) Dynamic WCA images and values, b) membrane wetting images; c) UWOCA of HM-PP membrane; (d-f) DFT optimized geometries of water adsorbed by CH₃, COOH, and COONa group of PP, AA-g-PP, and HM-PP membrane respectively (an orange dashed frame marks the water molecule and grey, white, red, and purple represents C, H, O, and Na respectively), and i) corresponding electrical energy values in Hartree unit ($1\text{Ha}=2565.5$ kJ/mol= 627.5094 kcal/mol) to calculate the water-binding energy.

3.3.5. Membrane stability performance

Thermal and mechanical stability is considered a very important parameter for practical applications. The analysis results (**Figure 3.9a**) show better thermal behavior of the HM-PP membrane as compared with PP and AA-g-PP membranes. The thermal degradation behavior of all the membranes shows three discrete steps of mass loss- the dehydration step, the polymeric chain degradation step, and the final weight loss step. At

CHAPTER 3

the final weight loss step from 400 °C to around 800 °C, almost no residual percentage is observed for PP and AA-g-PP membranes, where 15 % residual is remaining for the HM-PP sample. In addition, **Figure 3.9b-c**) illustrates the mechanical behavior of PP, AA-g-PP, and HM-PP membranes in both machine and transverse directions. After grafting with acrylic acid and sodium hydrogen carbonate, tensile stress and strain both increased in MD direction as compared to TD direction. It can be said that the acrylic acid and sodium hydrogen carbonate treatment enhances both thermal and mechanical strength without destroying the inner pores of the modified membranes ^[179]. Membrane stability in a different complex environment can be destroyed under different extreme conditions. The stability of the HM-PP membrane is analyzed by emerging in 1M HCl, 1M NaOH, 1M NaCl, and saturated NaCl (20%) water solution for 12 h (**Figure 3.9d**). No significant changes are observed in UWOCA values and represent robust superoleophobicity behavior with more than 160° UWOCA values.

CHAPTER 3

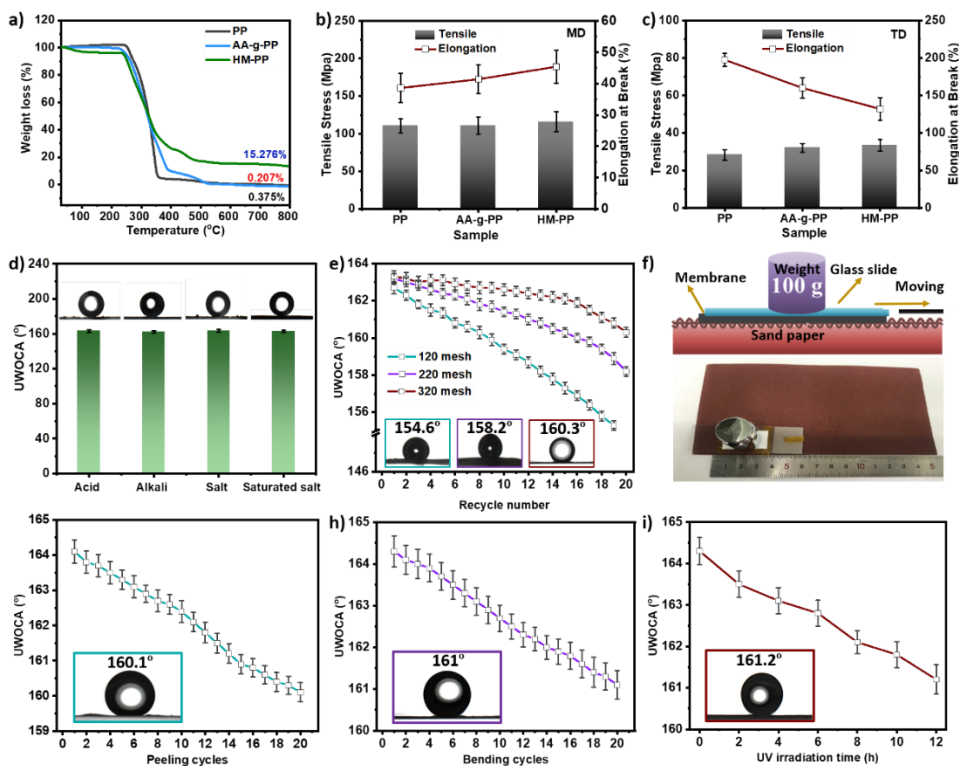


Figure 3.9: a) Thermal stability; (b-c) mechanical stability in MD and TD directions; d) UWOCA at harsh environments with corresponding dynamic UWOCA images; e) variation of UWOCA of the HM-PP membrane after being abraded by different sandpapers; f) the schematic illustration of sand abrasion test; g) scotch tape peeling, h) membrane bending and i) UV irradiation time.

Additionally, the HM-PP membrane is abraded using different mesh (grit no 120, 220, and 320) sandpaper ^[211]. The enormous decrease in UWOCA value after 20 cyclic performances are observed in **Figure 3.9e**). More decreases in UWOCA value (154°) are observed for using 120 mesh, which contains high coarse grit that can easily destruct surface structure. Further, the membrane stability is tested using a scotch tape peeling and bending process of up to 20 cycles (**Figure 3.9g-h**). The reason behind the decrease in

CHAPTER 3

UWOCA value is due to the loss of some micro/nano structure of membrane followed by the abrasion process (**Figure 3.10**).

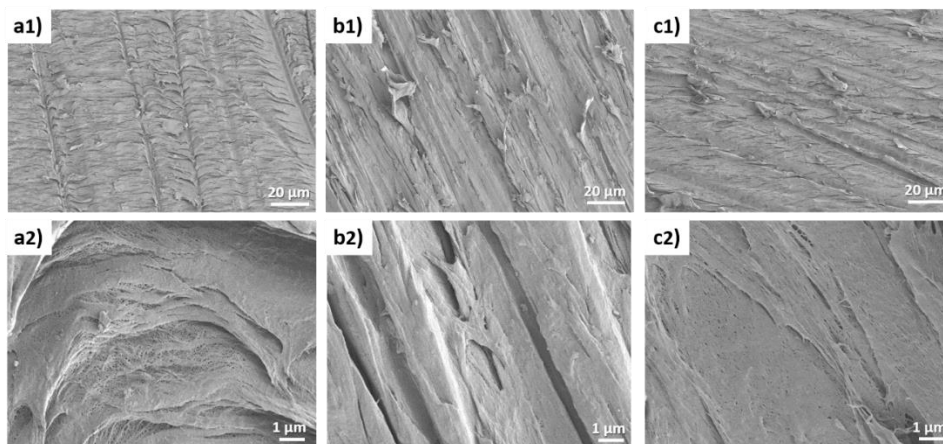


Figure 3.10: SEM images of sand paper abraded HM-PP membrane using (a1-a2) 120 mesh, (b1-b2) 220 mesh, and (c1-c2) 320 mesh sandpaper.

Additionally, the UV stability of the membrane was analyzed using a UV lamp under different (UV) irradiation times. As shown in **Figure 3.9i**, the underwater superoleophobicity (161.2°) of the HM-PP membrane shows a slight decrease after 12 h UV irradiation time (**Figure 3.11**).

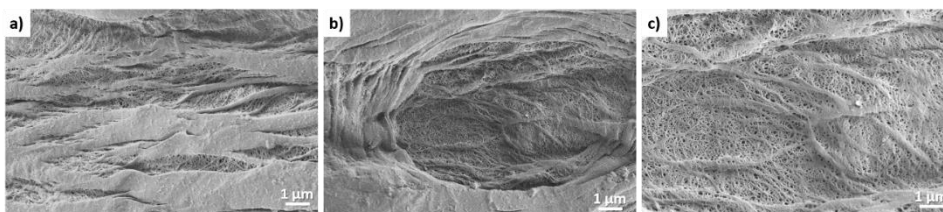


Figure 3.11: SEM images of HM-PP membrane after a) scotch tape peeling, h) bending and i) UV irradiation.

CHAPTER 3

3.3.6. Anti-oil fouling properties

The subaqueous adhesion of the oil experiment to the modified membrane is performed by the approach-compress-detach method. The dynamic images of **Figure 3.12a** represent that the soybean oil droplets are forced to touch the modified membrane surface by the micro syringe, which forms the compressed oil droplet shape and lately is entirely and easily detached the oil droplets from the membrane surface. Repeatedly lifting the oil droplet without any obvious deformation in droplet size exhibits excellent oil resistance behavior with the low oil adhesion properties of the modified HM-PP membrane ^[102].

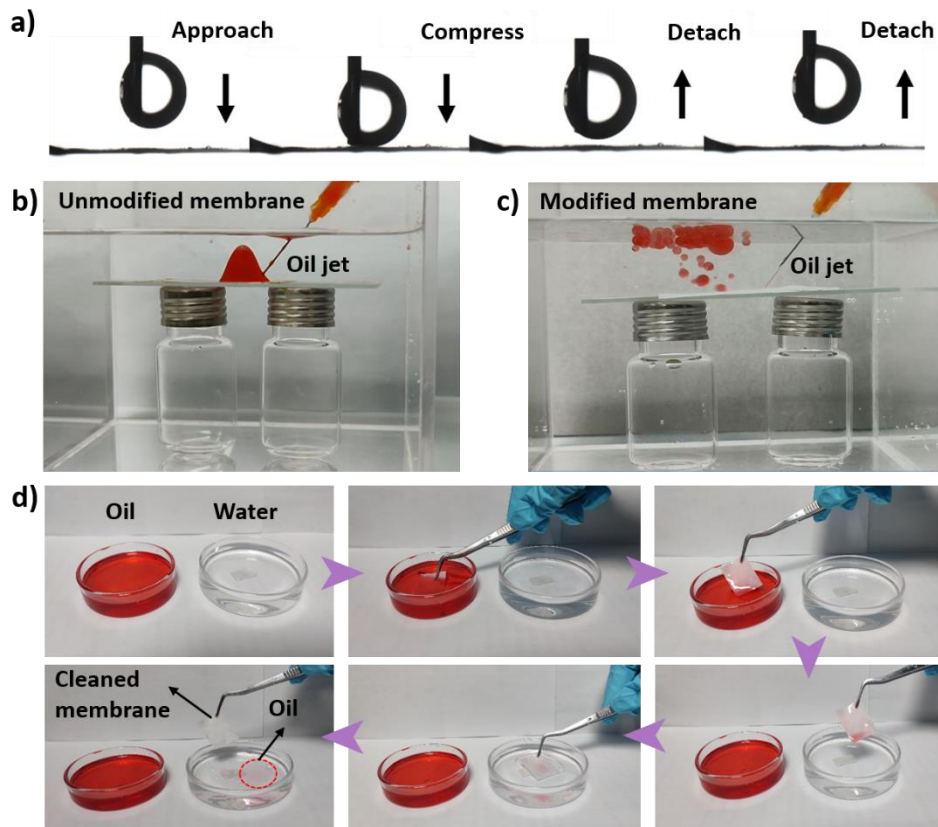


Figure 3.12: a) Anti-oil adhesion properties by the approach-compress-detach method; dynamic photographs of underwater soybean oil contamination by b)

CHAPTER 3

unmodified PP membrane, c) modified HM-PP membrane; d) excellent self-oil cleaning properties of HM-PP membrane.

Further, to test the anti-oil fouling properties, a dyed soybean oil jet is sprayed to the unmodified PP and modified HM-PP membrane by using a syringe in underwater conditions. The soybean oil jet makes a contact with the unmodified membrane and gathers on the surface where the oil jet swiftly bounces and floats to the water's surface after making a contact with the modified HM-PP membrane surface, as shown in **Figure 3.12b-c**. To represent the excellent self-oil cleaning properties, the pre-wetted HM-PP membrane is initially submerged in dyed soybean oil. After that, the oil-containing membrane is immersed in water where the oil layer is easily separated from the membrane surface as marked in the red circle in **Figure 3.12d**.

3.3.7. Emulsion separation performances

A domestic ultrafiltration cup is used for the emulsion separation process, where the prewetted membrane is placed between the feed chamber and the separated channel. The separation experiments were carried out using 0.6 MPa operation pressure. **Figure 3.13a-b** illustrates the digital images of the experiment setup with the optical microscope images of feed and permeate water. Before separation, the milky emulsion contains numerous microscopic oil droplets whereas, after separation, a clear and transparent water solution with no oil droplets is obtained. The acquired DLS particle size range for feed emulsion (0-3000) nm and separated water (0-15) nm is shown in **Figure 3.13c-d**. The optical microscope and the DLS data confirm that the oil droplets once discovered in the emulsion cannot be found anymore after the separation process, which indicates successful oil removal from the emulsion.

CHAPTER 3

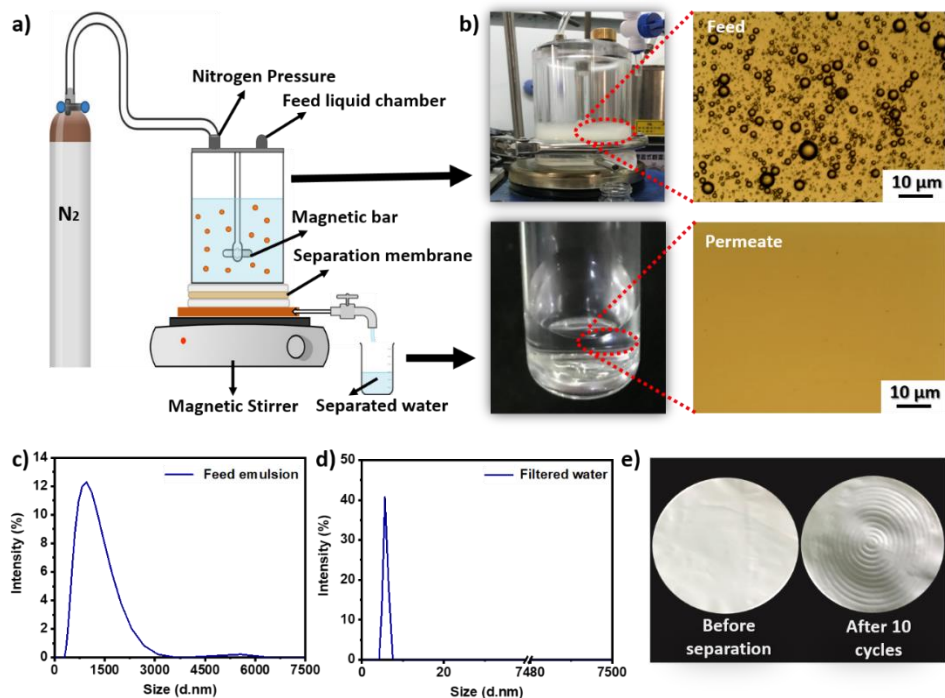


Figure 3.13: Schematic illustration of the emulsion separation device, b) optical microscope and digital images of feed and filtered water, (c-d) oil droplet sizes of feed and filtered water measured by DLS, e) digital photographs of HM-PP membrane before and after 10 cycles emulsion separation.

Figure 3.13e shows the digital photographs of the HM-PP membrane before and after 10-cycle emulsion separation. There is no crack or broken structure observed by visual of the membrane even after 10 cycles of separation at high pressure. Some circle wrinkles appear in the membrane after separation, which arises from the separated channel of the ultrafiltration cup device. There is no crack or broken structure observed by visual and inner SEM microstructure of the membrane even after 10 cycles of separation at high pressure (Figure 3.14).

CHAPTER 3

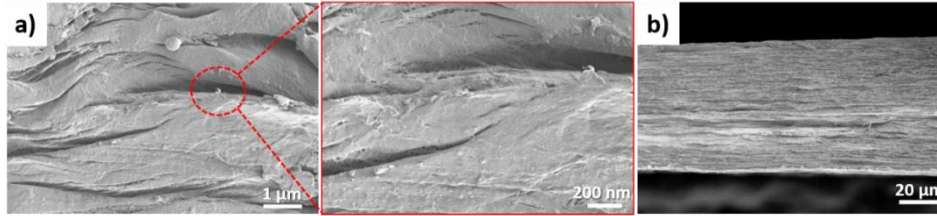


Figure 3.14: a) Surface microstructure and b) cross-sectional micrographs of HM-PP membrane after 10 cyclic separations.

The obtained data (**Figure 3.15a-c**) shows excellent permeation flux and efficiency for petroleum ether ($444.3 \pm 7.8 \text{ L m}^{-2} \text{ h}^{-1}$, 99.53 %), Toluene ($419.5 \pm 9.3 \text{ L m}^{-2} \text{ h}^{-1}$, 99.7 %), Hexane ($437.1 \pm 8.19 \text{ L m}^{-2} \text{ h}^{-1}$, 99.55 %) and soybean oil ($394.2 \pm 8.5 \text{ L m}^{-2} \text{ h}^{-1}$, 99.85 %) respectively. Therefore, due to the high viscosity of soybean oil, the permeation flux decreased compared to other light oils used in this work.

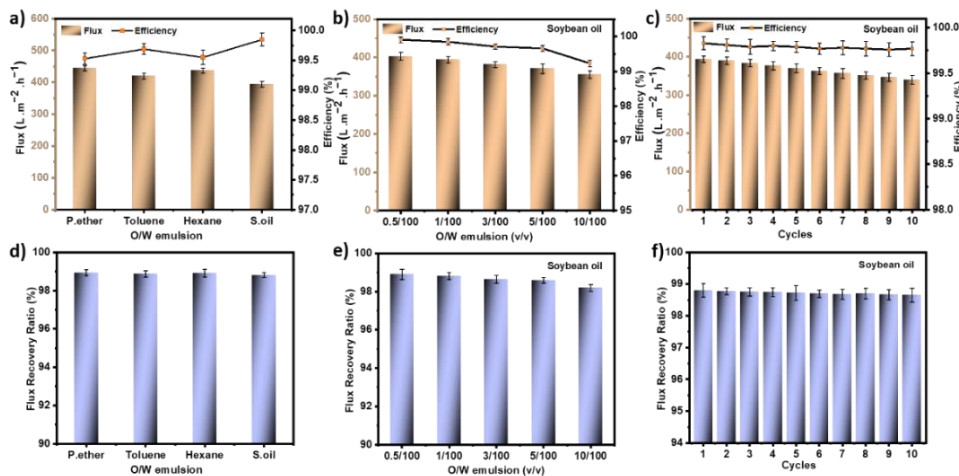


Figure 3.15: Separation performances of HM-PP membrane - a) various oil/water emulsions, b) different soybean oil content emulsion, c) cyclic performances; FRR value using d) various oil/water emulsions, e) different soybean oil content emulsion, f) cyclic performances.

CHAPTER 3

Further, to evaluate the HM-PP membrane's separation performances, soybean oil in low to high-concentration emulsion is separated. It is observed that with the increasing concentration of soybean oil in emulsion, the permeate flux is decreased correspondingly. Followed by the same concentration of different oils used for O/W emulsion, (1/100 (v/v)) soybean oil emulsion is analyzed for cyclic performance. Therefore, outstanding performances are observed for 1/100 (v/v) O/W emulsion without significant changes in flux and efficiency value. Still, separation efficiency data (> 99 %) is maintained even after 10 times separation, proving the better service life and reusability of the modified HM-PP membrane. Furthermore, the FRR (%) is calculated for various oils and different soybean oil-content emulsion-separated membranes, as shown in **Figure 3.15d-f**.

All the obtained FRR data shows excellent values with more than 98 %. However, the simultaneous decrease in FRR values for the high soybean oil content (10/100 (v/v)) emulsified emulsion can be due to its numerous micron-sized emulsified oil droplets thus blocking the water passageways ^[212], still maintaining more than 98 % after each cycle at 10 times recycled performance. In addition, a comparison of our excellent separation performances between our work and other reported literature is summarized in the following table.

.

CHAPTER 3

Table 3.2: A comparison of various membrane separations of emulsified oil/water emulsion.

Material	Oil	Surfactant	Flux (L/m ² h)	Eff. (%)	Pressure	Ref.
TA modified PVDF	Hexane	Tween 80	56	98.0	0.8 bar	[213]
CS- TPP@PDA@nylon	Colza oil	SDS	220.9	99.0	Vacuum pressure	[214]
Polyacrylonitrile- electrospun membrane	Toluene	Tween 80	39.6	98.8	Gravity- driven	[215]
TA-Cu ²⁺ /PVDF membrane	Lubrica nt oil	CATB	43.20	97.65	0.9 bar	[216]
Zirconia Hollow fiber membrane	Soybean oil	Span-80: Tween-80	300.55	99.7	1 bar	[217]
PPS-50 membrane	Chlorob enzene	SDS	12.51	98.72	Gravity- driven	[218]
HM-PP membrane	Soybean oil	Tween 20	394.2	99.85	0.6 MPa	Our work

3.4. Conclusions

In summery, this significant research work illustrates simple and effective surface modification techniques using acrylic acid and sodium hydrogen carbonate monomer to modify the surface of a biaxial PP membrane. The modified membrane exhibits noteworthy super-wetting properties with outstanding thermal, mechanical, and chemical stability in different harsh environments. These excellent results are caused by the surface-modifying

CHAPTER 3

monomers used in this work to develop a multiscale micro/nano rough surface, which results in a significant selective barrier to prevent the penetration of oil droplets. By virtue of super-wetting properties, outstanding separation performances (>99 %) with impressive recycling properties are achieved. Therefore, enhanced properties of the modified membrane apprise that the modified HM-PP membrane can be applied in large quantities industrial scale as emulsified emulsion separation application to mitigate our daily life emulsion toxicity.

CHAPTER 4. Super hydrophilic modified biaxial polypropylene membrane for gravity-driven separation

Considering the protection of our natural environment from oily wastewater toxicity, the biaxially orientated polypropylene (PP) microporous membrane is taken as a suitable substrate to prepare a super hydrophilic and underwater superoleophobic membrane for oily wastewater separation. It is designed as a large-scale, cost-effective, and stable technology with the minimum possible environmental pollution to prepare the membrane for oily wastewater emulsion separation. The hydrophobic PP membrane is initially treated via corona discharge treatment followed by a grafting reaction with hydrophilic acrylamide monomer to generate rough micro-nano structures and polar functional groups. Due to its excellent mechanical properties with a uniformly modified micro-nano porous structure, significant separation flux with high efficiency is achieved for layered mixtures, surfactant-free, and surfactant-stabilized emulsions. Consequently, all separation processes are handled by the energy-saving gravity-driven separation method.

4.1. Introduction

The acceleration of modernization causes huge demand for industrial production, which generates an enormous amount of oily wastewater annually ^{[219][220][221]}. For environment protection and sustainable development, it is desirable to separate oil from this oily wastewater before discharging it into the environment, which, however, is still a challenge for some kinds of wastewater. Compared with other existing forms of oil in wastewater, surfactant stabilized emulsion is noted as extremely challenging and complex

CHAPTER 4

one to separate due to their stable and macro-nano-sized (0.1 μm to 20 μm) oil droplets in water ^{[222][223][53]}. To target emulsified oil/water separation, much effort has been devoted to designing membrane separation materials, which should meet the following requirements such as- nanometer pore size, super hydrophilic surface, low cost, and reusability.

Polymeric membrane-based separation technologies are considered an advanced and promising approach since of their abundant significant advantages such as high separation efficiency, uniform nano/micropore size distribution ($< 0.3 \mu\text{m}$), low cost, and reliability, especially can apply the surfactant stabilized emulsion separation ^{[11][224][225]}. Historically, various common attempts were attempted to separate stabilized emulsions by using specifically designed mesh (0.25 mm to 0.038 mm) ^[49], porous sponge (100 μm to 200 μm) ^[50], fabric (6.64 μm to 18.9 μm) ^[51] materials. Therefore, materials with pore sizes in several micros and/or millimeters are not appropriate for tiny nano-sized emulsion separation ^[54]. To separate these emulsions, the most effective approach is to select the separation materials with pore sizes in micro/nanometer less than oil droplet sizes.

Surface properties are another concern affecting oil-water separation. Utmost basis hydrophobic polymer membrane causes severe membrane fouling, which endures plaguing the ideal performances due to absorbing the oil droplets during the emulsion separation ^[226]. Therefore to enhance the membrane surface wettability, the membrane pore structure along with the surface properties are considered the foremost factors, which affect the permeation flux and oil rejection rate of the membrane by enhancing the anti-oil fouling properties ^{[59][211][63]}. Considering the oil droplets as the “soft particles” with strong deformation ability, the oil rejection rate is mainly influenced by oil droplet size exclusion,

CHAPTER 4

where the membrane surface properties especially membrane pore sizes play a critical role in the effect of the separation mechanism ^{[33][6]}. Membranes with super hydrophilic and underwater superoleophobic surfaces have been demonstrated to have high permeation flux in separating emulsified and stable oil droplets from water ^{[131][100]}.

Based on the above-discussed principle in developing a high-performance membrane for surfactant stabilized oily wastewater, in the current work we take the biaxially stretched PP microporous membrane as the basis membrane, which has the advantage of nanometer pore size, low cost, good mechanical properties ensuring reusability. Commercially available mostly polymeric membranes are reported poor mechanical strength, which causes lower self-life and reliability in the separation application area ^[148]. The technology of biaxially stretched PP microporous membrane was first invented by *Xu et al.* ^[227] and nowadays commercially and widely produced for lithium-ion battery separators, which has a nanoporous structure with average pore sizes normally smaller than 40 nm ^{[145][228]}. Compared to other polymeric membranes prepared through thermal-induced phase separation, uniaxial stretch and electrospinning such as polyacrylonitrile (PAN) nanofibrous membrane ^[229], polyvinylidene fluoride (PVDF) membrane ^[115], due to large drawing ratios induced chain and crystal orientation, the biaxially stretched PP microporous membrane possesses high mechanical strength both in the machine and transitional direction. Therefore, higher mechanical stability can provide long membrane service life with outstanding reusability.

Despite their above-mentioned remarkable features, unfortunately biaxially stretched PP microporous membranes are hydrophobic by nature. To meet the requirement for separating surfactant-stabilized oily wastewater, modification of the surface to super

CHAPTER 4

hydrophilicity is highly demanded. Various surface modification methods such as chemical methods (coating, grafting, crosslinking), irradiation methods (corona, electron beam, gamma, UV), etc. are widely studied ^{[127][230][18][19][159]}. The assigned drawbacks of chemical surface modification methods are time-consuming, can not achieve permanent hydrophilicity, and importantly decreased the modified membrane pore size, which causes a huge decline in permeation flux. For example, *Qu et al.* ^[231] modified the PVDF membrane by three steps crosslinking method, wherein the first step PVDF was modified by hydrophilic modifier N-vinyl-2-pyrrolidone and Vinyl-triethoxysilane, second step modification was done by immersing in PDA/PEI solution, and third step modification was performed by crosslinking reaction with FeCl₃ water solution. The obtained results showed the decrease in modified membrane pore sizes with increasing the crosslinking steps, which later affects the membrane flux performances. Far along, FeCl₃ cross-linked PVDF membrane exhibited huge declining in pure water flux as compared with the first and second step modified PVDF membrane.

In contrast, the achievement of super hydrophilicity is still not possible just by applying irradiation technology on the membrane surface. Furthermore, the membrane went through heat treatment during the irradiation process to generate free radicals on the surface, which can tremendously affect the membranes' mechanical stability and service life. Thus, the combination of irradiation and grafting methods can elucidatorily solve all of these above-mentioned shortcomings. Among all the irradiation technology, corona treatment is considered a cost-effective, stable, and large-scale process not only by generating different hydrophilic (-OH, -COOH, -C=O) functional groups in the membrane surface, but also by increasing the membrane pores by maintaining a certain period of

CHAPTER 4

treatment time and power ^{[112][6]}. Therefore, the chemical grafting reaction after corona treatment less damage to the membrane bulk and pore structure than other methods, which makes the membrane thermally and mechanically stable, where the grafting monomer works as a nucleating agent and forms a stable hydrophilic chemical structure with the corona treated membrane ^{[112][232]}. For example, *Sadeghi et al.* ^[233] used corona treatment to change the surface properties of PES membranes and evaluated the influence of corona treatment time and power along with different solvents. Whereas, *Adib et al.* ^[134] modified the PES membrane by using corona treatment and grafting reaction with hyperbranched polyethylene glycol to improve the anti-oil fouling properties of the membrane. Therefore, this facial modification strategy provides more distinct advantages involving membrane stability in different harsh conditions and bestows permanent super hydrophilicity with desirable underwater super oleophobicity.

Herein, we developed a large-scale, cost-effective, and stable technology with minimum possible environmental pollution to construct a super hydrophilic and underwater superoleophobic PP membrane. Modifying the surface of the biaxially stretched PP membrane using corona treatment is the first step, followed by a grafting reaction with acrylamide (AM) on the corona-treated membrane surface (**Figure 4.1**). Different AM parameters (such as concentration, reaction temperature, and grafting duration) were studied comprehensively to find acceptable conditions for AM monomer grafting reaction to produce surface nanostructures with permanent super hydrophilicity and underwater super oleophobicity. The obtained separation results revealed excellent gravity-driven permeation flux and high separation efficiency as compared with other studies.

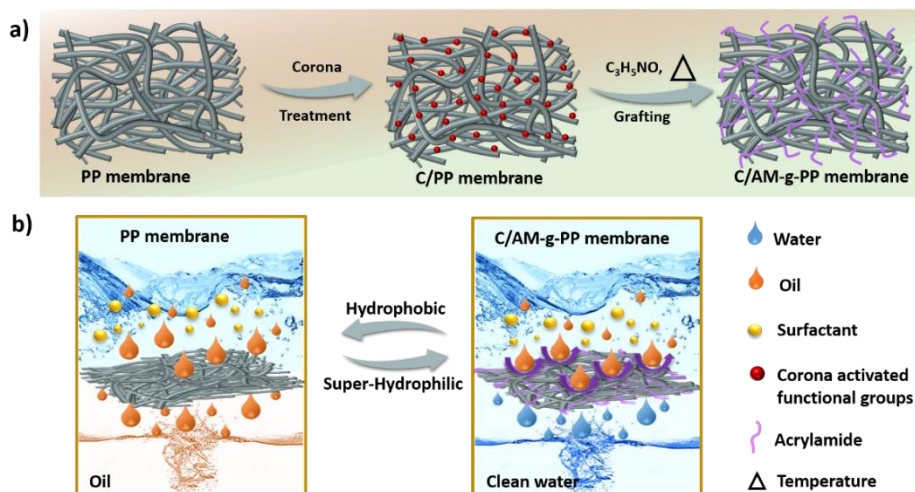


Figure 4.1: Schematic illustration of the (a) preparation of commercial biaxially oriented PP membrane and the transformation process of hydrophobic PP membrane to super hydrophilic C/AM-g-PP membrane, (b) emulsion separation mechanism through unmodified hydrophobic and modified super hydrophilic PP membrane.

4.2. Experimental

4.2.1. Materials and chemicals

Acrylamide, Methylene blue were purchased from Sinopharm chemical reagent Co., Ltd. (Shanghai, China). Other used chemicals are listed in the 2.2 and 3.2 sections.

4.2.2. Modification process of C/AM-g-PP membrane

The polypropylene membrane (5 cm × 5 cm in size) was washed twice with ethanol and deionized water for 30 min for removing all the contamination. Finally, the washed membranes were dried overnight at 60 °C in the oven. The dried PP membranes were treated by a corona discharge machine (Ruian Zhi Lin Technology Co, Ltd., China). Corona treatment power was maintained from 300 W to 500 W. Each power was applied

CHAPTER 4

for different treatment times from 10 s to 300 s. Immediately WCA and SEM experiments were performed to analyze the membrane wettability and inner surface structure. Later on, the selected corona-treated membrane was immersed in a closed glass tube containing a mixed solution of AM and deionized water with different AM concentrations (5-20) % (v/v). Nitrogen gas was purged into the reaction mixture for 30 min in a glass tube and then the glass tube was immersed in the water bath for (15-60) min as heating time at different temperatures (30 - 90) °C. After the grafting reaction, the samples were instantly rinsed three times with acetone and distilled water to remove the homopolymer. Finally, the membranes were placed in a vacuum oven for drying at 60 °C overnight.

4.2.3. Calculation of water adsorption energy

To understand the reason for the super hydrophilicity and strong hydration ability of the C/AM-g-PP membrane, the structure was optimized by density functional theory (DFT) using the B3LYP method with 6-311+G (d, p) basis sets at the Gaussian 09 package programs. The adsorption energy and equilibrium distance corresponding to each interaction were calculated using the following equation ^[234]:

$$\Delta E_{ads} = E_{(H_2O/C/AM-g-PP-x)} - E_{(C/AM-g-PP)} - E_{(H_2O)} \quad (4.1)$$

Where, $E_{(H_2O/C/AM-g-PP-x)}$, $E_{(C/AM-g-PP)}$, and $E_{(H_2O)}$ represent the optimized total energy of different functional groups of modified C/AM-g-PP membrane.

4.2.4. Preparation of different oil/water emulsion and separation performances

For the oil/water layered mixture, a series of oil (petroleum ether, hexane, toluene, and soybean oil) were mixed with pure distilled water (colored with methylene blue for better comparison) at a volume ratio of 1:4 (v/v). Therefore, two types of surfactant-free

CHAPTER 4

and surfactant-stabilized emulsions were prepared using a 1:99 (v/v) ratio of different oils and distilled water. Water flux, flux rejection recovery, and separation efficiency are calculated using the above equation described in section 2.2.6.

4.3. Results and discussion

4.3.1. Fabrication of super hydrophilic C/AM-g-PP membrane

The corona treatment is the first step to generating hydrophilicity of the PP membrane by utilizing different power (300-500 W) and treatment time (10-300 s). The corresponding hydrophilicity and surface morphology of the C/PP membrane is analyzed through the WCA and SEM experiment.

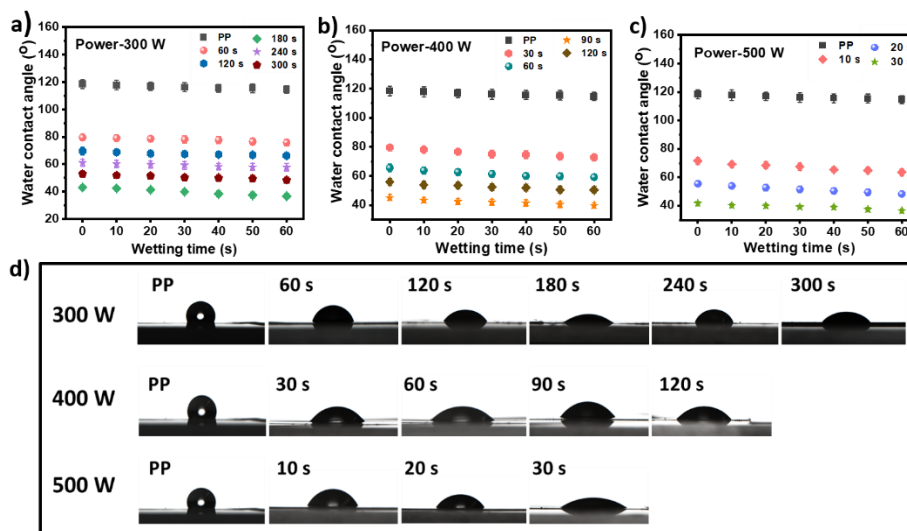


Figure 4.2: Wettability behavior of C/PP membrane by dynamic water contact angle experiment at different power over the different treatment times. a) power-300 W (treatment time-60 s, 120 s, 180 s, 240 s, and 300 s; b) power-400 W (treatment time-30 s, 60 s, 90 s, and 120 s); c) power-500 W (treatment time- 10 s, 20 s, and 30 s); d) optical images of water contact angle of C/PP membrane at different power and treatment time.

CHAPTER 4

All the corona-treated membranes using different power resulted in improved hydrophilicity by generating different polar groups (**Figure 4.2**). Based on the principle of avoiding irradiated macro surface destruction (shrinking and/or melting spot) of PP membrane after corona treatment, high power and longer treatment time are avoided (**Figure 4.3**). Considering the membrane morphology and the wettability behavior for the further grafting experiment, 300 W power and 120 s treatment time are finalized for the hydrophilic modification process with a reported WCA value of 66.2°, and the modified membrane is labeled as C/PP membrane. The grafting method is the second step of improving the hydrophilicity, and acrylamide is applied to enhance the surface and inner pore hydrophilicity. A detailed AM grafting experiment is performed by controlling three important parameters: monomer concentration (5-20 % in volume), temperature (30-90 °C), and grafting time (15-60 min).

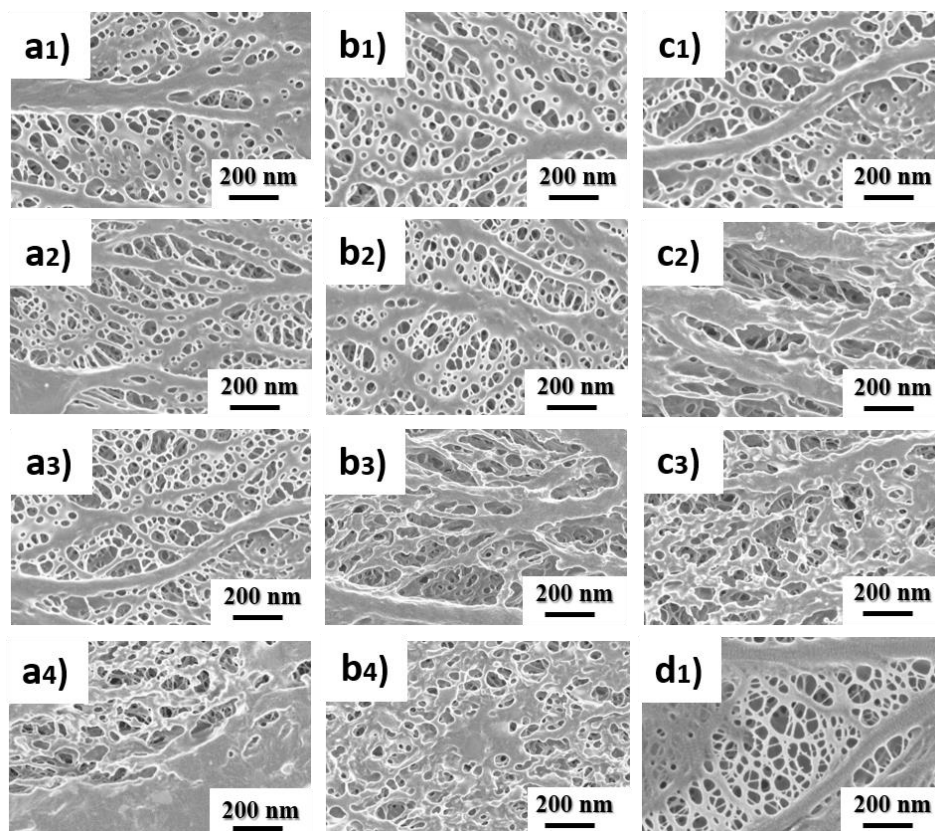


Figure 4.3: SEM micrographs of C/PP membrane using different treatment power and time, 300 power (a1-a4)- 60s, 120s, 180s, 240s treatment time; 400 power (b1-b4)- 30s, 60s, 120s, and 180s treatment time; 500 power (c1-c3)- 10s, 20s, and 30s treatment time; and d) unmodified PP membrane.

A significant increasing trend is observed in the grafting ratio value with increasing all the parameters (**Figure 4.4**). The higher monomer concentration and longer grafting time cause more AM monomer amalgamation on the membrane surface, whereas the higher temperature accelerates the reaction.

CHAPTER 4

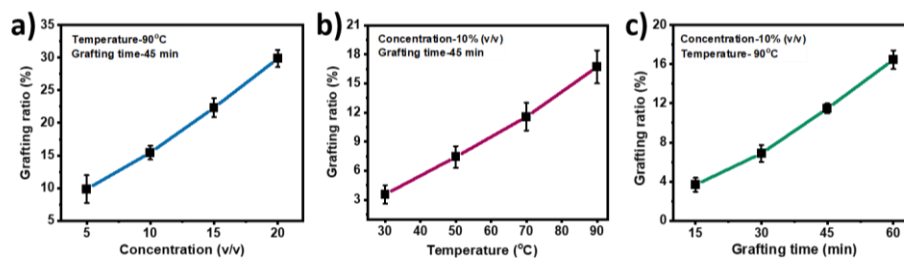


Figure 4.4: The grafting ratio value of a) monomer concentration at 90 °C temperature and 45 min grafting time, b) temperature using 10 % (v/v) monomer concentration and 45 min grafting, c) monomer grafting time using 10 % (v/v) monomer concentration at 90 °C temperature.

The final hydrophilicity of all the different parameter grafted membranes is shown in **Figure 4.5a-c**. Excellent decreases in WCA values are obtained for all the AM grafted membranes compared with the C/PP membrane. After confirming the optimum concentration (10 % (v/v)) and temperature (90 °C), it is observed that both 45 and 60 min grafting time modified membranes show super hydrophilicity at 60 s wetting time. To select the best membrane for separation application, a more exact wetting time is analyzed for 45 min and 60 min grafted membrane, as shown in **Figure 4.5d-e**. The 45 min grafted membrane shows $\sim 0^\circ$ WCA value within 30 s wetting time while the 60 min grafted membrane does within 60 s wetting time. The reason may be the longer grafting time made the membrane surface much more compact and homogeneous that hindering the wetting speed of the water droplets. Typically, the 45 min grafted membrane is selected as the C/AM-g-PP membrane to test structure, chemical composition, and separation performances.

CHAPTER 4

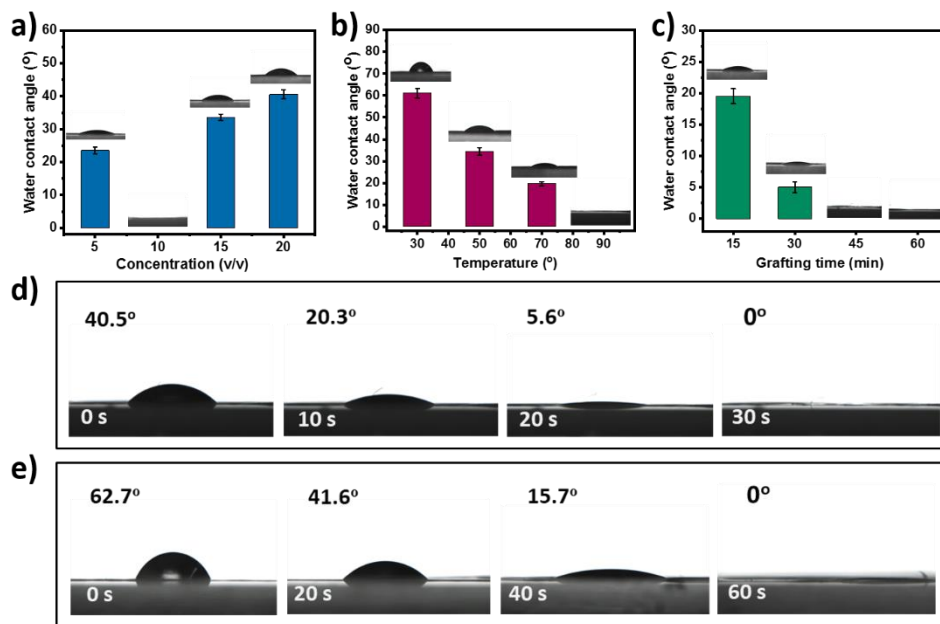


Figure 4.5: Water contact angle values of using different a) monomer concentration, b) temperature, c) grafting time; WCA images of different wetting times represent the wetting behavior of C/AM-g-PP membrane for d) 45 min and e) 60 min grafting time.

4.3.2. Chemical structure and compositions

Surface wettability and corresponding emulsion separation performances largely depend on the chemical composition and the membrane structure [235]. **Figure 4.6a** represents the possible chemical structure of the modified membrane and its corresponding functional groups confirmed by ATR-FTIR and XPS experiments. **Figure 4.6b** illustrates the difference in absorbance peak of PP, C/PP, and C/AM-g-PP membranes according to the chemical structure. The characteristic absorbance peaks of the PP membrane at 2960-2800, 1450, and 1376 cm^{-1} can be observed in all the membranes. The corona treatment-induced chemical composition change is verified by the appearance of $-\text{C}-\text{O}$ at 1278 cm^{-1} , $-\text{C}=\text{O}$ at 1733 cm^{-1} and 1639 cm^{-1} , and $-\text{O}-\text{H}$ at 3000-3600 cm^{-1} in the C/PP membrane. In

CHAPTER 4

addition, the successful grafting of AM is proved by the increased peak intensity of $-C=O$, $-C-N$, and $-C-O$, and the appearance of $-N-H$ at $3000-3600\text{ cm}^{-1}$ in $C/AM-g-PP$ [236]. Furthermore, the XPS results in **Figure 4.6c-f** identify the chemical elements and compositions to affirm the grafting monomers. XPS survey spectra in **Figure 4.6c** show the presence of $O1s$ emission peak for the C/PP membrane due to the corona treatment, and the presence of $O1s$ and $N1s$ emission peak for $C/AM-g-PP$ membrane because of AM grafting. Moreover, the successful modification is also proved via the fitting peaks change of the $C1s$ high-resolution XPS spectra (**Figure 4.6d-f**). The four fitting peaks in $C1s$ of the $C/AM-g-PP$ membrane belong to $C-C$ (284.88 eV), $C-O$ (285.48 eV), $C-N$ (286.38 eV), and $C=O$ (288.68 eV) respectively.

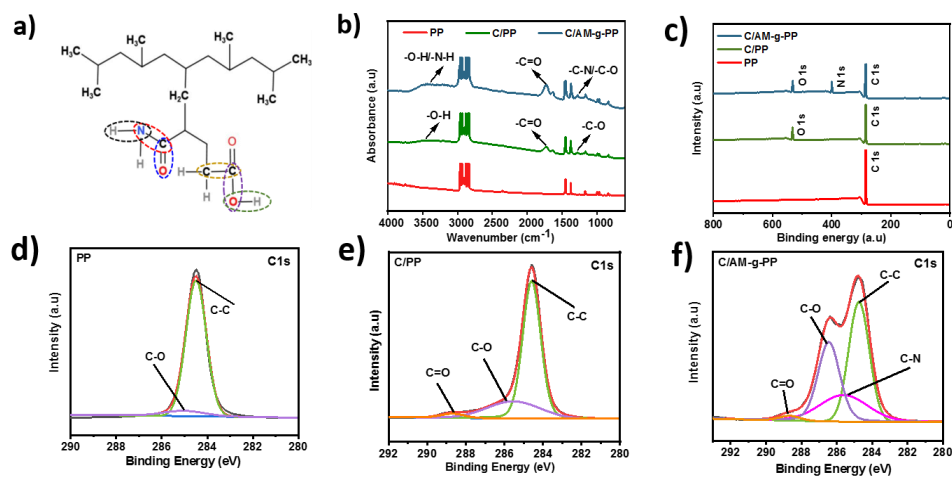


Figure 4.6: Surface chemical compositions of PP, C/PP, and super hydrophilic C/AM-g-PP membrane. a) Possible chemical structure with new functional groups of C/AM-g-PP membrane, b) ATR-FTIR spectra, c) wide scan XPS spectra; High-resolution $C1s$ fitting curve of d) unmodified PP membrane, e) C/PP membrane, and f) C/AM-g-PP membrane.

CHAPTER 4

4.3.3. Surface morphology & macroscopic properties

Surface microstructure and cross-sectional micrographs of unmodified PP, C/PP, and C/AM-g-PP membranes are performed for a better understanding of the membrane structure variation after corona treatment and acrylamide grafting. In **Figure 4.7a1-b1**, it can be seen that the randomly oriented porous structure of the PP membrane becomes a much wider and smooth porous structure after corona treatment. In addition, in **Figure 4.7c1**, the densely compact surface with obviously smaller pores is observed for the C/AM-g-PP membrane after the successfully grafted AM monomers covering the porous structure of the C/PP membrane by forming distinct micro-nano structures.

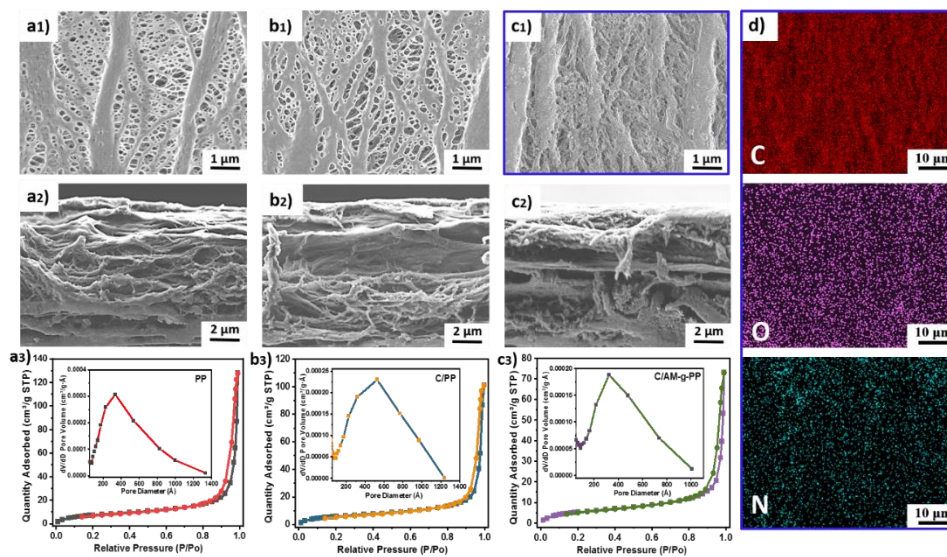


Figure 4.7: (a1-c1) SEM surface microstructure, (a2-c2) cross-sectional micrographs, (a3-c3) nitrogen adsorption/desorption properties of unmodified PP membrane, C/PP membrane, and C/AM-g-PP membrane, respectively and d) EDS scanning images of C, O, and N elements of C/AM-g-PP membrane.

The grafted acrylamide inside the membrane pores can be considered as another fundamental parameter for high-efficiency oil/water separation due to the pore diameter decrease. As shown in **Figure 4.7a3-c3**, the nitrogen adsorption-desorption isotherms of all the membranes displayed high absorption at a high relative pressure ($0.8 < P/P_0 < 1$) [237]. Furthermore, from EDS **Figure 4.7d**, it is also observed that the C/AM-g-PP membrane is rich in O, and N elements, which are distributed uniformly throughout the membrane surface. However, compared with the PP membrane, the pore diameter increase of the C/PP and decrease of the C/AM-g-PP membrane are observed and match the surface morphology.

4.3.4. Membrane wettability behavior and stability performances

To discover the suitable membrane for separation application, the pure water flux of unmodified PP, C/PP, and C/AM-g-PP membranes with different acrylamide grafting times (15-60 min) is tested by applying gravity-driven force. Before testing the pure water flux, all the membranes are wetted in pure distilled water. Unmodified PP, C/PP, C/AM-g-PP#15min membranes show poor pure water flux of about $0 \text{ L m}^{-2} \text{ h}^{-1}$ due to their extreme hydrophobicity and less hydrophilicity behavior, whereas C/AM-g-PP#30 min membrane represents the pure water flux of $179.54 \text{ L m}^{-2} \text{ h}^{-1}$. This obtained pure water flux is matched with the good hydrophilicity (WCA, $5 \pm 0.9^\circ$) of the C/AM-g-PP#30 min membrane. Subsequently, a significant increase in pure water flux value is observed for both C/AM-g-PP#45 min and C/AM-g-PP#60 min membranes. The reported fluxes are 4329 and 2565 $\text{L m}^{-2} \text{ h}^{-1}$, respectively, which can correlate with their super hydrophilicity behavior (WCA, $\sim 0^\circ$) as well. Therefore, the highest pure water flux membrane (C/AM-g-PP#45 min) is selected as the best membrane for further separation application, which is simply named as

CHAPTER 4

C/AM-*g*-PP membrane like above. Before the separation, as another important property, the underwater oleophobicity behavior of the C/AM-*g*-PP membrane is measured by UWOCA and shown in **Figure 4.8a**.

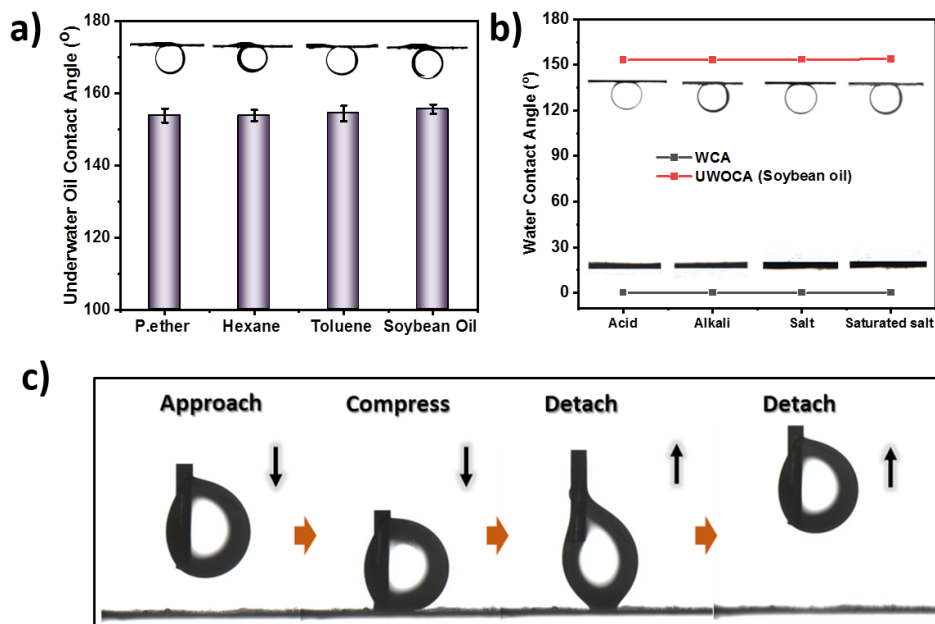


Figure 4.8: a) Under water-oil contact angle value with optical images of oil droplets (Petroleum ether, Hexane, Toluene, and Soybean oil), b) WCA and UWOCA values of C/AM-*g*-PP membrane at different complex conditions, c) dynamic oil (Soybean oil) adhesion properties of C/AM-*g*-PP membrane by the approach-compress-detach method.

Besides the super hydrophilicity behavior, the C/AM-*g*-PP membrane offers excellent underwater super-oleophobicity, where UWOCA values $>150^\circ$ for petroleum ether, hexane, toluene, and soybean oil. The highest UWOCA value (155.6°) is obtained for soybean oil. Typically, using soybean oil, the subaqueous oil adhesion experiment of the C/AM-*g*-PP membrane is performed by the approach-compress-detach method, as

CHAPTER 4

shown in **Figure 4.8c**. It is observed that soybean oil droplets are forced to touch the membrane surface, which formed the compressed oil droplet shape and lately is entirely detached from the membrane surface. The low oil adhesion property of the C/AM-g-PP membrane indicates high separation efficiency for oil/water emulsion separation [238].

Figure 4.8b shows that the C/AM-g-PP membrane still possesses very stable super hydrophilicity and oleophobicity in different complex environments. The C/AM-g-PP membrane maintains 0° WCA and more than 150° UWOCA values by dipping into acid (1M HCl), alkali (1M NaOH), salt (1M NaCl), and saturated salt (30% NaCl) conditions for 10 h, which proves the practical application under different harsh conditions.

4.3.5. Theoretical mechanism of underwater oleophobicity and super hydrophilicity

The mechanism of membrane surface wettability could be further explained theoretically by following Young's equation [239],

$$\cos \theta_e = \frac{\gamma_{SV} - \gamma_{SL}}{\gamma_{LV}} \quad (4.2)$$

Where θ_e represents the contact angle value and γ_{SV} (solid-vapor) γ_{SL} (solid-liquid) and γ_{LV} (liquid-vapor) are the corresponding interfacial energy. However, to explain the membrane underwater super oleophobicity behavior, it is reasonable to apply the equation with the oil droplet on a solid surface in the presence of both water and air interfaces. Thus, the following equation can be generated [240],

$$\cos \theta_3 = \frac{(\gamma_{o-g} \cos \theta_1) - (\gamma_{w-g} \cos \theta_2)}{\gamma_{o-w}} \quad (4.3)$$

Where γ_{o-g} , θ_1 , γ_{w-g} , θ_2 , γ_{o-w} , and θ_3 represent the oil-gas interface tension, oil contact angle in the air, water-gas interface tension, water contact angle in the air, oil-water interface and

CHAPTER 4

the oil contact angle in the water. Herein, due to the excellent underwater oleophobicity behavior, if we consider soybean oil as a reference, then the interfacial tension of soybean oil/water is 30.26 mN/m^[241]. Whereas water/air surface tension is 73 mN/m^[242], and measured soybean oil/air surface tension is 28.4 mN/m. Now in the air interface, the initial water contact angle is 40.5°, and the soybean oil contact angle is 15°. Therefore, according to the above equation, the obtained value for $\cos \theta_3$ is -0.927, where θ_3 equals 158°, representing the superoleophobic behavior in underwater conditions, which theoretically aligns with our experimental value.

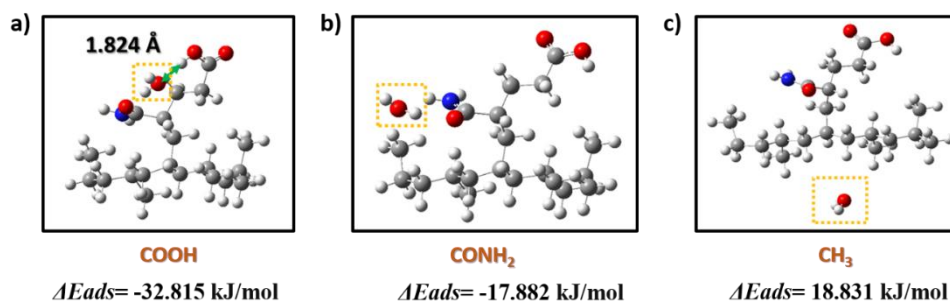


Figure 4.9: Water adsorption energy calculation, (a-c) DFT optimized geometries of water adsorbed by COOH, CONH₂, and CH₃ groups respectively, and corresponding calculated water adsorption energy. The water molecule is marked by a yellow dashed frame and grey, white, red, and blue represent C, H, O, and N respectively.

The super hydrophilicity behavior is also further discussed by simulation. **Figure 4.9a-c** represents the DFT-optimized geometries of COOH, CONH₂, and CH₃ group of modified C/AM-g-PP membrane with corresponding water molecule adsorption. Obtained water adsorption energy results revealed that the COOH group contains the lowest value (-32.815 kJ/mol), whereas the water adsorption energies for CONH₂ and CH₃ groups are -17.882 kJ/mol and 18.831 kJ/mol, respectively. Decreasing energy represents the negative

CHAPTER 4

water adsorption value which formed a very stable complex and the lowest value indicates an extremely strong hydration ability ^[234]. According to the water adsorption energy, the predicted stabilities and hydration abilities groups are $\text{COOH} > \text{CONH}_2 > \text{CH}_3$. Moreover, *Chen et al.* stated that a shorter distance is responsible for the stronger hydrogen bond interaction which yields a more stable complex ^[209]. Inspired by this statement, (COOH) represents the shortest hydrogen bond distance 1.824 Å, which means the most stable complex. Hence, the relation between the water adsorption energy and the surface wettability can be explained as well. Unmodified PP membrane contains only CH_3 groups in chemical structure as it proves less stable complex with water molecules, and its positive water adsorption energy shows hydrophobic behavior. The modified C/AM-g-PP membrane contains COOH and CONH_2 groups after modification and the CH_3 group in the backbone. The newly formed COOH and CONH_2 groups show lower and negative water adsorption energy with a stable complex form, which is the reason behind the achievement of super hydrophilicity.

4.3.6. Emulsion separation performances

The C/AM-g-PP membrane possesses super hydrophilicity and underwater super-oleophobicity, making it promising for oil/water separation applications. The membrane separation performance is investigated by three types of oily wastewater, where each contains various oil (petroleum ether, hexane, toluene, and soybean oil). All the separation experiments are performed by the gravity-driven method, which is a highly energy-saving separation mode ^[243]. A modified C/AM-g-PP membrane is inserted between the two-glass tubes. A series of the 500 mL oil-water layered mixture, surfactant-free, and surfactant stabilized emulsion are poured into the upper glass tube and permeate water was collected

CHAPTER 4

from the bellow glass beaker. Due to the mechanism of super hydrophilicity and underwater super oleophobicity of the C/AM-g-PP membrane, water penetrates the membrane immediately whereas the oil is repelled off on the upper glass tube. **Figure 4.10** shows the image of the petroleum ether/water layered mixture and surfactant stabilized emulsion separation process as a reference, where water was colored with methylene blue for clear observation during layered mixture separation.

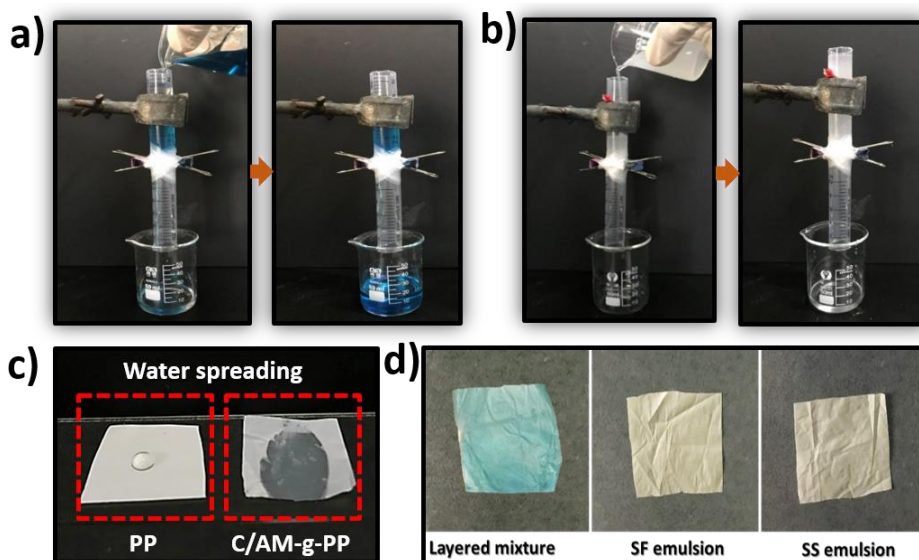


Figure 4.10: Digital photographs of the oil and water separation process a) layered mixture separation, b) surfactant stabilized emulsion separation, c) digital image of the water spreading over unmodified PP and modified C/AM-g-PP membrane, and d) photographs of the different emulsion separated membrane.

The membrane shows excellent permeate flux and separation efficiency of petroleum ether ($3715 \text{ L m}^{-2} \text{ h}^{-1}$ and 99.7 %), hexane ($3536 \text{ L m}^{-2} \text{ h}^{-1}$ and 99.8 %), toluene ($3417 \text{ L m}^{-2} \text{ h}^{-1}$ and 99.9 %), and soybean oil ($3178 \text{ L m}^{-2} \text{ h}^{-1}$ and 99.9 %) for the oil-water layered mixtures. The layered mixture can be separated easily due to the underwater super

CHAPTER 4

oleophobicity of the membrane strongly supports preventing the oil from passing through with water molecules. For the surfactant-free emulsion, the membrane shows a much lower permeate flux (compare to the layered mixture) but still possesses outstanding permeate flux and higher separation efficiency of petroleum ether ($1385 \text{ L m}^{-2} \text{ h}^{-1}$ and 99.3 %), hexane ($1196 \text{ L m}^{-2} \text{ h}^{-1}$ and 99.45 %), toluene ($1057 \text{ L m}^{-2} \text{ h}^{-1}$ and 99.45 %), and soybean oil ($918 \text{ L m}^{-2} \text{ h}^{-1}$ and 99.5 %). Moreover, for the surfactant stabilized emulsion, the membrane shows more decrease in permeate flux and separation efficiency of petroleum ether ($985 \text{ L m}^{-2} \text{ h}^{-1}$ and 98.16 %), hexane ($796 \text{ L m}^{-2} \text{ h}^{-1}$ and 98.35 %), toluene ($717 \text{ L m}^{-2} \text{ h}^{-1}$ and 98.52 %), and soybean oil ($598 \text{ L m}^{-2} \text{ h}^{-1}$ and 98.59 %) (**Figure 4.11a-c**). The difference between layered mixtures and surfactant-stabilized emulsions in permeate flux and separation efficiency can be attributed to the fact that oil droplets float as an oil cake layer on top of the water in layered mixtures due to the lower density of oil than water. As a result of the extremely hydrophilic membrane surface, water is transported quickly through the membrane, and the oil cake layer is readily repelled off and resulting in a higher permeate flux and efficiency ^[244]. The surfactant-free emulsion is mechanically stirred and results in small oil droplets ranging in size from 20 to 150 microns ^[222]. Following that, the coalescence action significantly leads to coalesced oil droplets generating a free continuous oil layer for a surfactant-free emulsion ^[245] ^[246]. This action cause causes a reduction in permeate flux while maintaining a high separation efficiency. The function of surfactant in a surfactant-stabilized emulsion is to break down the oil droplets into very stable tiny sizes below 20 microns ^[222]. Whereas some oil droplets are smaller than membrane pore sizes and thus easier to pass through the porous membrane with water molecules, eventually blocking the water passageways ^[247]^[44]^[45]. As a result, the permeate flux is greatly reduced,

CHAPTER 4

and some absorbed microscopic oil droplets pass through with permeate water during continuous separation, lowering the efficiency value. However, even considering the concerns mentioned above during emulsion separation, the C/AM-g-PP membrane retains good permeate flux and separation efficiency for surfactant-stabilized emulsions.

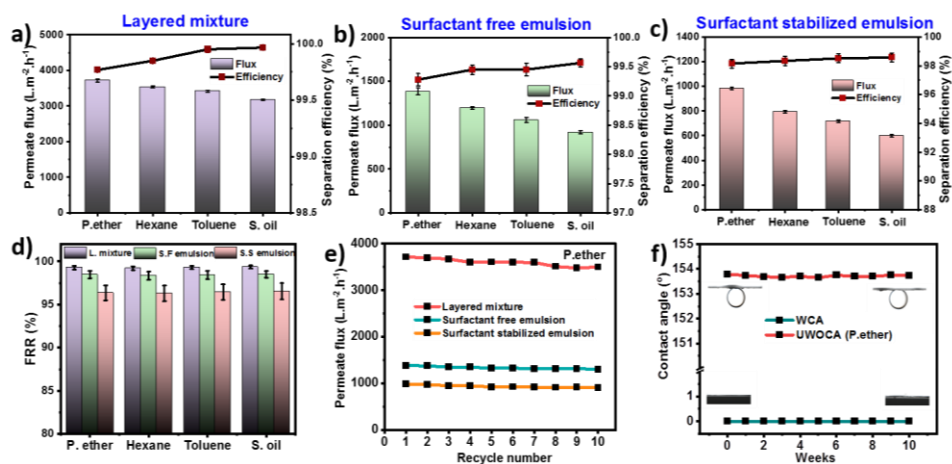


Figure 4.11: Permeate flux and separation efficiency of C/AM-g-PP membrane for the separation of various oil (Petroleum ether, Hexane, Toluene, and Soybean oil) from water; a) oil/water layered mixture, b) surfactant-free emulsion, c) surfactant stabilized emulsion, d) flux recovery ratio values, d) changes of the permeate fluxes of the layered mixture, surfactant-free emulsion, and surfactant stabilized emulsion for Petroleum ether over 10 recycle numbers, and f) permanent hydrophilicity and underwater oleophobicity (P. ether) behavior of C/AM-g-PP membrane measured over 10 weeks.

The Hagen-Poiseuille equation can be used to analyze the reason why the permeate flux of C/AM-g-PP membrane for various emulsions shows discrepancy behavior. The permeate flux is defined by the following equation [50]:

CHAPTER 4

$$\text{Permeate flux, } J = \frac{p\pi r^2 P}{8\eta L\tau} \quad (4.4)$$

Where p , r , L , and τ are the porosity, pore size, membrane thickness, and pore tortuosity of the C/AM-g-PP membrane, respectively. η is the viscosity of each emulsion, and P is the pressure. During the gravity-driven separation process, the feed emulsion column height was kept conformably to ensure constant separation pressure. As for using the same C/AM-g-PP membrane for emulsion separation, parameters such as p , r , L , and τ can be neglected due to merely minor changes. The viscosity of emulsion (η) remains the key parameter, which would lead to the increasing and decreasing of permeate flux. The viscosity of petroleum ether, hexane, toluene, and soybean oil is 0.219, 0.283, 0.517, and 40.5 mPa·s, respectively ^[250–253]. *Al-Wahaibi et al.* stated that the increasing oil content in water could increase the viscosity of emulsions ^[254], whereas in our experiment oil/water ratio was maintained at 1:99 (v/v) for both surfactant-free and surfactant-stabilized emulsion using different oils. So according to the viscosity value of different oils, the permeate flux of the C/AM-g-PP membrane is petroleum ether > hexane > toluene > soybean oil. In addition, **Figure 4.11d** shows that the FRR values of the C/AM-g-PP membrane maintain more than 99 % for layered mixture, whereas > 98 % for surfactant-free emulsion and > 96 % for surfactant stabilized emulsion. The lowest FRR values for surfactant stabilized emulsion are caused by the surfactant absorbed on the membrane surface, which makes it more difficult to remove the adhered oil by backwashing ^[212].

Besides the excellent permeate flux and efficiency, cyclic performance and durability are the other two important properties, which are observed over 10 recycle separations. **Figure 4.12** shows that layered mixture separation of different oils over 10-

CHAPTER 4

recycle separation still maintains high permeate flux and efficiency. Increasing the recycle numbers results in a modest decrease in permeate flux while raising the associated efficiency values.

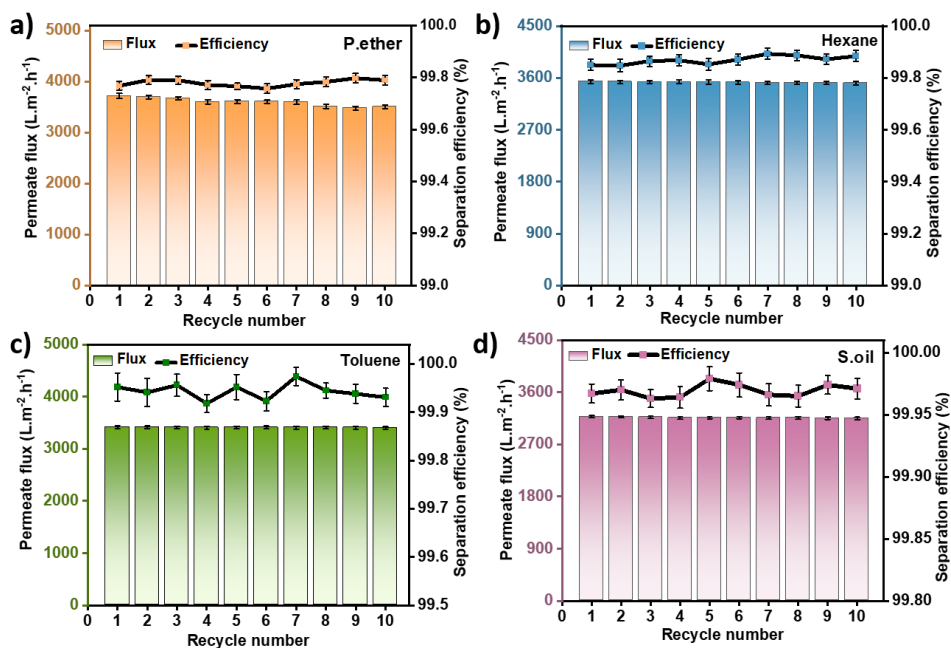


Figure 4.12: Permeate flux and corresponding separation efficiency performance of C/AM-g-PP membrane of different oil/water layered mixture, a) petroleum ether; b) hexane, c) toluene, and d) soybean oil over 10 recycle number.

A similar trend is observed for surfactant-free emulsion. Typically, the permeate flux comparison of petroleum ether in the layered mixture, surfactant-free emulsion, and surfactant stabilized emulsion was analyzed over 10 recycle numbers and shown in **Figure 4.11e**. The measured data shown in **Figure 4.11f** indicate the C/AM-g-PP membrane has permanent hydrophilicity and underwater oleophobicity over 10 weeks. Moreover, no membrane breakage is observed in the membrane surface after recycling performances. **Figure 4.10d** shows the digital photographs of the membrane after separating petroleum

CHAPTER 4

ether in different types of oily wastewater. The microstructure of the membrane after surfactant stabilized emulsion separation is shown in **Figure 4.13**. No inner membrane breakage is observed, while a little porous and fine surface is noticed for all separated membranes.

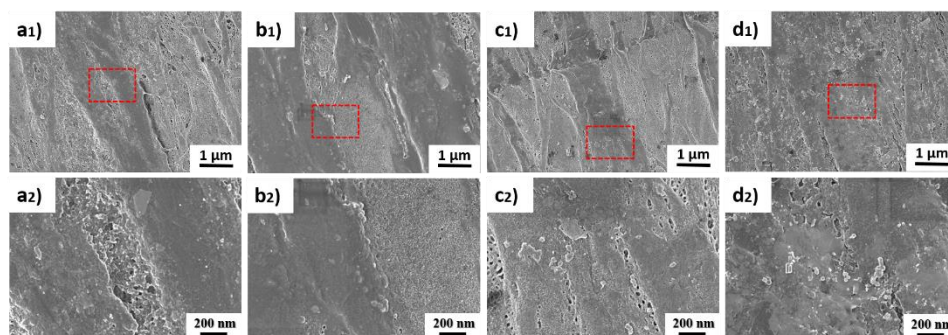


Figure 4.13: Surface morphology in low and wide resolutions of C/AM-g-PP membrane after surfactant stabilized oil-in-water emulsion separation, (a1-a2) Petroleum ether, (b1-b2) hexane, (c1-c2) toluene, and (d1-d2) soybean oil.

These excellent results confirm the stable separation ability, durability, and good reusability of the C/AM-g-PP membrane, which is a great and favorable property to minimize the cost of reusing the material ^[255]. Such excellent performances of the C/AM-g-PP membrane are mostly due to the following two factors: (i) the C/AM-g-PP membrane possesses excellent hydrophilicity and underwater super-oleophobicity, and (ii) the emulsified liquid droplets were effectively intercepted due to the powerful sieving action of the selective barrier caused by the uniformly dense porous surface of the modified membrane. An optical microscopy experiment is further performed to qualitatively evaluate the permeate water, as shown in **Figure 4.14a-b**. There are plenty of micron-nano-sized oil droplets in the optical images of the original milky feed emulsions of both

CHAPTER 4

surfactant-free and surfactant-stabilized emulsions. After filtration, the corresponding permeates water becomes transparent and colorless, and no oil droplets are detected over the entire microscopic image.

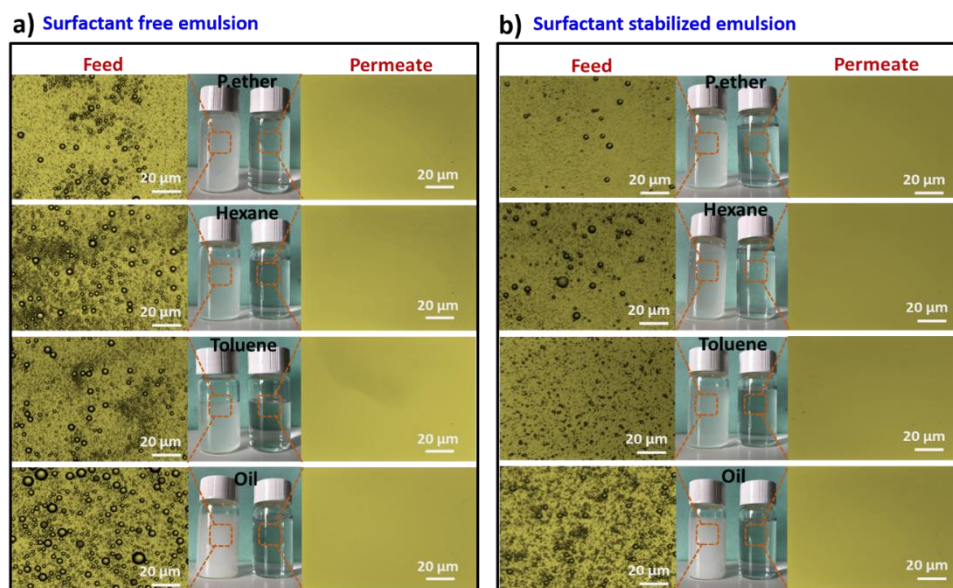


Figure 4.14: Optical microscopy and digital photographs of a) surfactant-free and b) surfactant-stabilized feed emulsion and permeate water of Petroleum ether, Hexane, Toluene, and Soybean oil.

The above results demonstrate that the C/AM-g-PP membrane has favorable reusability and excellent stability for macro and nano-sized emulsion separation with great permeate flux and high separation efficiency. Furthermore, a comparison between the other reported work and the C/AM-g-PP membrane in this study is made to evaluate the separation performances, as shown in **Figure 4.15** [256][131][257][258][259][236][260][261][262][236][263][264][265][88]. The separation performances of the C/AM-g-PP membrane in this work exceed that of other results presented here. Analyzing the comparison data, it is obvious that the modification process via corona-induced acrylamide

CHAPTER 4

grafting exhibited excellent super hydrophilicity with high water permeability than that of the other modified membranes. The reason might be due to the corona-induced grafting process, which can significantly reduce the WCA value just by maintaining treatment time and power. Therefore, the C/AM-g-PP membrane is expected to become a potentially effective material in oil/water emulsion treatment, prepared by a time-consuming and promising method.

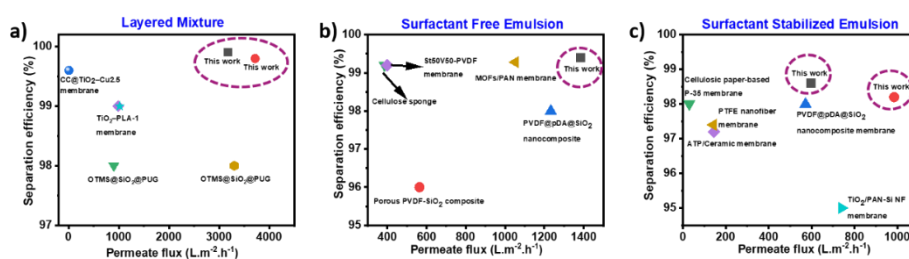


Figure 4.15: Comparison of separation efficiency and permeate flux of various membranes with our work, a) layered mixture, b) surfactant-free emulsion, and c) surfactant stabilized emulsion.

4.4. Conclusions

In conclusion, an efficient, facial, and scalable surface modification method is developed to convert the commercial biaxial hydrophobic PP membrane to super hydrophilic. The corona treatment is applied to generate the hydrophilic carbonyl and carboxyl functional groups and the acrylamide monomers are grafted on the membrane to possess permanent hydrophilicity and underwater oleophobicity. The modified C/AM-g-PP membrane shows excellent permanent super hydrophilicity (WCA ~ 0°) and underwater oleophobicity behavior (UWOCA >150°) over 10 weeks. These comprehensive and outstanding properties are responsible for achieving high permeation flux and separation

CHAPTER 4

efficiency in the gravity-driven separation method for all categories of oil/water mixture and emulsion. Notable high permeation flux ($3715 \text{ L m}^{-2} \text{ h}^{-1}$ for P.ether) and separation efficiency (99.9 % for Soybean oil) are obtained for the layered mixture. Although decreasing flux and efficiency are obtained both for surfactant-free and surfactant-stabilized emulsion, the C/AM-g-PP membrane still maintains high separation performances ($985 \text{ L m}^{-2} \text{ h}^{-1}$ and 98.16 % for petroleum ether in surfactant-stabilized emulsion) with excellent durability (10-recycle numbers) as compared with many previous works. Overall, the fascinating performances of the C/AM-g-PP membrane are expected to have a tremendous prospective application in a commercial area, which can largely mitigate all kinds of emulsion separation challenges.

CHAPTER 5. Advanced super-wetting multipollutant removal biaxial polypropylene membrane for gravity driven separation

The hazardous toxicity of oily wastewater creates a negative impact on the environment and ecosystem that has made water separation an open challenge on a global scale. A promising and workable tactic to prevent contaminations and effective water separation from oily wastewater has been proved using cutting-edge advanced polymeric membrane-based separation technology. Excessive hydrophobicity, contamination vulnerability, and membrane fouling are recurring and crippling problems for the treatment of oily wastewater. To overcome these problems, we design a facile, scalable, and highly efficient layer-by-layer modification technique using a polyethylene imine and levo-3,4 dihydroxyphenylalanine crosslinked multi-layer assembled super-wetting hierarchical rough membrane surface. The synergistic development of the rough surfaces causes the embeddedness of wetting properties of the modified membrane with excellent separation performances by removing multi pollutants (oil particles and bacteria) from oily wastewater in a more energy-efficient way.

5.1. Introduction

The deterioration of water quality due to oily wastewater has emerged as a major barrier to the growth of contemporary society and become a global issue for sustainable environmental development ^{[266][267][268]}. Additionally, various organisms are adversely obstructed by oily wastewater, which frequently carriage a threat to the entire ecosystem

CHAPTER 5

^[269]. The present water treatment research is now centered on the construction of extremely cost-effective, energy-saving, organic pollutants removal and multifunctional advanced purification technologies ^{[61][270]}. Such advanced technology helps to separate water and oil with high separation efficiency thus cleansing oily wastewater, eliminating various pollutants and hazardous toxicity, and providing both economic and environmental benefits. As the key to purification technologies, developing an advanced multifunctional super-wetting material has attracted growing attention in the highly efficient emulsion separation area with the capability of removing multi-pollutants.

Polymeric membrane-based separation technology is regarded as an effective technique due to its uniform pores, high mechanical durability, easily scalable and excellent reusability as compared with other traditional separation materials ^{[199][271][272]}. Widely used traditional materials are only suitable for separating immiscible oil/water mixtures, but not for separating oil/water emulsions, due to the large pore size of the substrates thus causing severe oil fouling ^{[33][115]}. Oil droplets are typically on the micro- to nanoscale in surfactant-stabilized emulsion systems ^[273]. Therefore, based on the oil droplet size exclusion principle, membrane materials containing uniform nanopores can accomplish high separation efficiency in terms of emulsion separation ^{[274][275]}. This makes polymeric membranes an ideal substrate for emulsion separation. However, the inherent hydrophobicity nature limits their wide application area and thus needs to solve to get excellent separation performances. To achieve super hydrophilicity and underwater superoleophobicity properties, creating hierarchical rough structures is widely used for emulsion separation from both theoretical and practical standpoints ^[58]. Thus, hierarchical rough surfaces not only enhance the membrane wetting but are also considered a great

CHAPTER 5

solution for adjusting the membrane's pore sizes to much smaller than emulsified oil droplet sizes.

Assembling multiple hydrophilic layers on the membrane surface can produce a hierarchical super-wettable rough surface, which can be achieved by the layer-by-layer (LBL) modification method. The usual LBL assembly procedure includes immersing a membrane substrate alternately and repeatedly in two polyelectrolyte solutions with opposite charges to create a multilayered membrane by electrostatic forces ^[276]. Numerous tunable features can be adjusted such as membrane thickness, and inner pore sizes according to demand through this method ^[114]. However, to get homogeneous monomer distribution to create a rough surface, selecting appropriate monomers is highly important. Therein, the branching polymer polyethylene imine (PEI) and levo-3,4 dihydroxyphenylalanine (L-dopa) layer offer more stability and can operate as a super-wetting functional layer for membrane modification. The amino-rich hyper-branched structured PEI is highly water-soluble and can easily be adsorbed onto the membrane and pore surfaces, further hydrophilizing the membrane, increasing its water permeability and possibly making it more resistant to fouling by oil and other non-polar solvents ^{[277][278][279]}. Additionally, L-dopa is a cost-effective zwitterionic amino acid, widely found in *mucuna pruriens* beans ^[280]. L-dopa is a carboxylation form of dopamine and thus contains an additional carboxylic acid group in its structure which provides abundant surface modification possibilities as compared with widely used dopamine ^[281]. Although L-dopa is broadly used as a neurotransmitter medication for Parkinson's disorder but is also being investigated recently for other wide applications ^[282]. L-dopa can also easily create a crosslinking reaction between catechol groups through oxidation, which results in the

CHAPTER 5

structural stability that is provided by the polymerization process [281]. Even though a lot of research has already been done on surface modification using PEI/Dopamine monomer, L-dopa is still not extensively researched for emulsion separation. *Ding et al.* applied a one-step L-dopa/3-amino-propyltriethoxysilane reaction on the PP membrane for hydrophilic modification and a lower permeate flux around $100 \text{ L m}^{-2} \text{ h}^{-1}$ is achieved [283]. On the contrary, *Zhang et al.* used L-dopa/poly(diallyl dimethyl-ammonium) LBL modification method but still much lower flux around $16 \text{ L m}^{-2} \text{ h}^{-1}$ is obtained [284]. It is important to find a significant solution to enhance the separation performances for oil/water emulsion separation using this excellent environment-friendly and green L-dopa monomer.

Herein, in our study mechanically robust biaxially oriented polypropylene (PP) membrane has been chosen as a fundamental substrate due to its less application in the emulsion separation area. PP membrane has excellent mechanical strength in both machine and transitional directions, resulting in a long service life and remarkable reusability [148]. Since PP is chemically inert, it is challenging to attach hydrophilic compounds to the membrane surfaces through any modification processes. Therefore, PP membrane was first activated by corona discharge treatment to generate a large number of hydrophilic functional groups. Therefore, PEI/L-dopa layers have been deposited to the corona-discharged PP membrane (**Figure 5.1**). Such an efficient modification method shows great enhancement in a rough surface and membrane wettability by increasing the modification layers. Finally, the desired properties are achieved at 15 PEI/L-dopa layered membranes such as 1. Superhydrophilicity and underwater superoleophobicity properties guarantee high separation performances 2. Nano-sized membrane pores thus ensure high separation efficiency for surfactant stabilized emulsion, and 3. Excellent anti-bacterial properties of

CHAPTER 5

the modified membrane act as various micro-organisms' removal. The obtained results suggested that our excellent modified advanced anti-bacterial and anti-oil fouling membrane holds great practical potential for the removal of multi contaminants from oily wastewater.

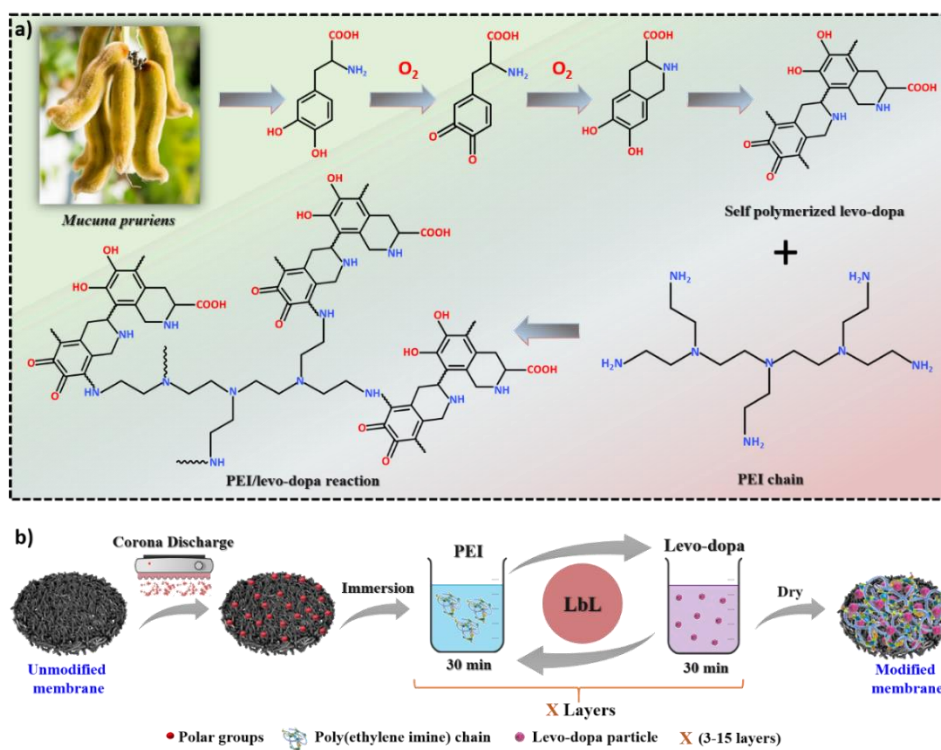


Figure 5.1: Schematic illustration of the a) possible chemical reaction mechanism and, b) modification process of the super-wetting membrane.

5.2. Experimental

5.2.1. Materials

Polyethyleneimine (PEI), Levo-3,4 dihydroxyphenylalanine, was supplied from Sinopharm chemical reagent Co., Ltd. (Shanghai, China). Kerosene oil (viscosity=10 mPa.s) was obtained from Sigma-Aldrich Co., LLC. (Shanghai, China). Vegetable oil was

CHAPTER 5

bought from the local super shop. Other used chemicals are listed in the 2.2, 3.2, and 4.2 sections.

5.2.2. Preparation of monomer solutions

In terms of preparing a monomer solution, PEI (0.2 g) was dissolved in a Tris-buffer solution (100mL, pH =8.5, 100 mM) by continuous magnetic stirring for 12 h at room temperature. Whereas, L-dopa (0.2 g) was added into a Tris-buffer solution (100mL, pH =8.5, 100 mM) by continuous magnetic stirring for 12 h at 80 °C. Afterward, the L-dopa solution was stored for three days in a dark place for self-polymerization to obtain the black L-Dopa solution (**Figure 5.2**). Therefore, directly incorporating the necessary quantity of NaCl into the L-Dopa solutions to prepare 1M NaCl containing 0.2 g/L L-Dopa solutions, which is further stored for membrane modifications.

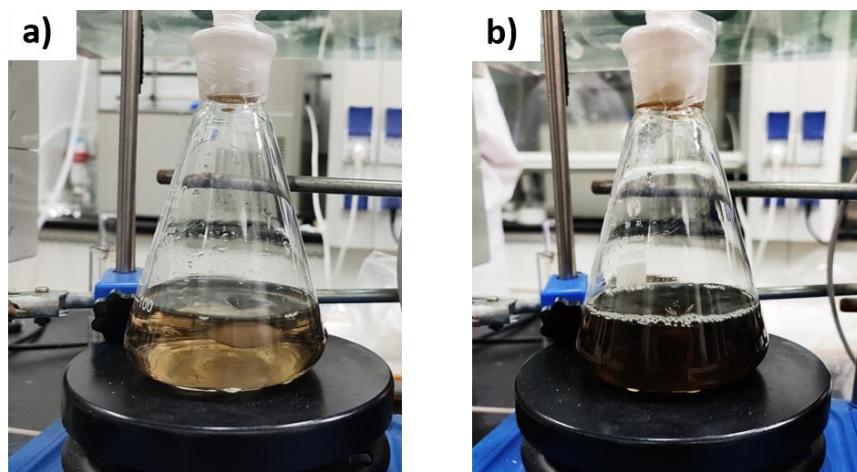


Figure 5.2: L-dopa solution a) before and b) after self-polymerization.

5.2.3. Layer-by-Layer assembling modification process

PP membrane (3 cm × 3 cm in size) was cleaned twice in ethanol for 30 minutes to remove all impurities. The membranes were then dried overnight at 60 °C in the oven after being thoroughly cleaned. Following that, the dried PP membranes have treated on both

CHAPTER 5

sides using a corona discharge machine to increase the chemical interaction between the membrane and monomers by producing different polar groups. Before the LBL self-assembled modification process, corona treated PP membrane was first wetted with ethanol for 30 s as a membrane pretreatment. The PP membrane was therefore alternately immersed first in PEI solutions for 30 minutes, and then for another 30 minutes in L-Dopa solutions, which was regarded as 1 layer. This cycling modification was repeated for up to 15 layers, with the membrane being thoroughly cleansed with deionized water and dried at 60 °C. Different layered membrane's successful deposition is evaluated by calculating polymerization yield by using the grafting ratio formula.

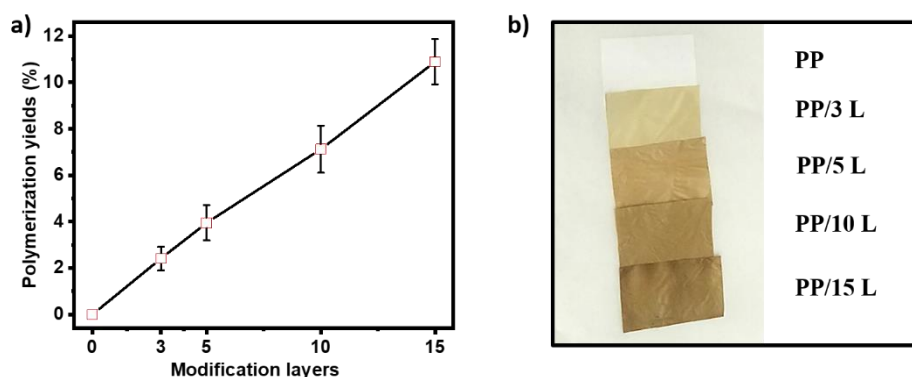


Figure 5.3: a) Polymerization yields, b) Digital photographs of unmodified and different layer assembled PP membranes.

5.2.4. Oil/water emulsions preparation and separation experiments

Two types of oily wastewater (free oil layer mixture and surfactant stabilized emulsion) are prepared to evaluate the membrane's effective separation efficiency by using four various oils (petroleum ether, hexane, kerosene oil, and vegetable oil) using the previously discussed formula.

5.3. Results and discussion

5.3.1. Micro-morphology and chemical compositions

The surface microstructure of unmodified and different LBL-assembled PP membranes is analyzed using SEM (Figure 5.4a1-a5). LBL-constructed membrane surfaces exhibit denser growth of PEI and L-Dopa monomers on surfaces with decreasing pore volumes along with surface area as compared to randomly oriented porous unmodified PP membrane surfaces. The modified PP surfaces become rougher with increasing modification cycles due to dense polymerization.

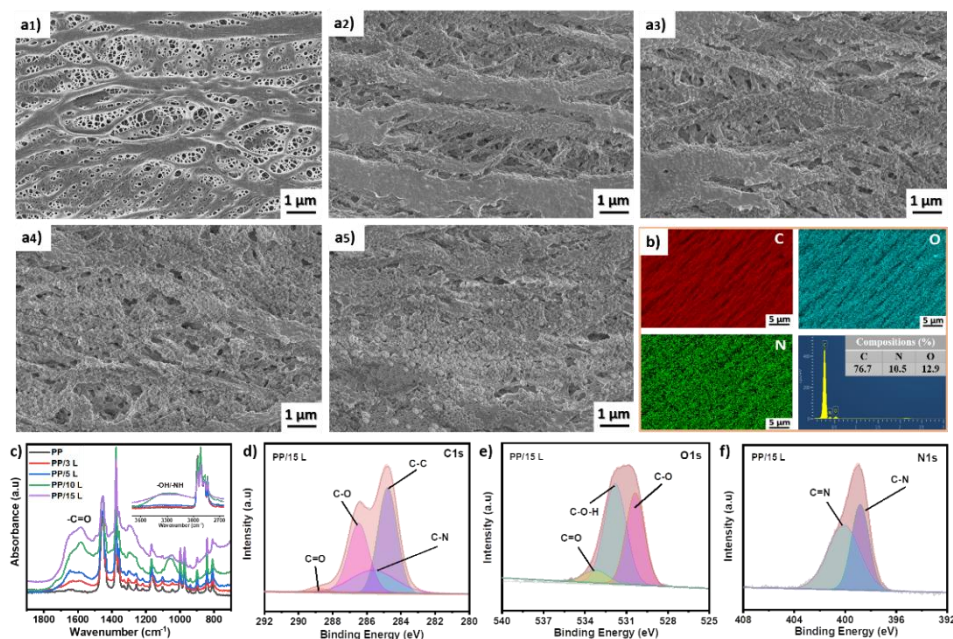


Figure 5.4: Surface microstructure of (a1-a5) unmodified PP membrane, PP/3 L, PP/5 L, PP/10 L, and PP/15 L membrane; (b) EDS mapping images of PP/15 L membrane with elemental percentile; (c) ATR-FTIR spectra; (d-f) high-resolution C1s, O1s, and N1s XPS spectra of PP/15 L membrane.

CHAPTER 5

The newly formed hydrophilic functional groups from crosslinked PEI and L-dopa reactions are compactly integrated into the inner micropore walls. Thus, assumptions are confirmed by EDS elemental mapping of the PP/15 L membrane, as shown in **Figure 5.4b**. It is observed that the PP/15 L membrane is highly rich in C, O, and N elements and is distributed uniformly throughout the membrane surface. The modified membrane's proposed chemical structure and associated functional groups are confirmed by ATR-FTIR and XPS spectroscopy ^[285]. ATR-FTIR spectroscopy (**Figure 5.4c**) reveals that the chemical composition appearance of -C=O at $(1520\text{-}1760\text{ cm}^{-1})$, and -O-H/-N-H at $3000\text{-}3600\text{ cm}^{-1}$ is observed for all LBL assembled membranes except unmodified PP membrane thus proves the successful modification. The peak intensity of -C=O , and -O-H/-N-H functional groups enhanced correspondingly with increasing LBL assembling layers. Moreover, the successful modification is also proved via the fitting peaks change of the C1s, O1s, and N1s high-resolution XPS spectra of unmodified PP and modified PP/15 L membrane (**Figure 5.4d-f**). The different layered modified membranes demonstrate another successful variation by decreasing carbon proportion and increasing oxygen and nitrogen percentages, respectively.

5.3.2. Relation between surface roughness and membrane wettability

The membrane's wettability is an essential factor to achieve optimum separation performances ^[286]. Therefore, the super-wetting performance of the membrane can be improved by creating a micro-nano hierarchical structure on the membrane surface. Additionally, these hierarchical rough microstructures improved wettability, enhanced anti-oil-fouling, and reusability performances by reducing the oil attachment to the membrane surface ^[287]. Therefore, a linear correlation between surface roughness and

CHAPTER 5

membrane wettability is deeply analyzed, as shown in **Figure 5.5a-b**. Decreasing WCA and increasing UWOCA are observed by enhancing the surface roughness. Such results clearly show a strong linear correlation between membranes' wetting properties along with surface roughness. **Figure 5.5c1-c2** and **Figure 5.5d1-d2** represent the unmodified PP and modified PP/15 L membrane's surface roughness value with 2D AFM images and their surface topography profile, respectively. The outcomes demonstrate the comparatively smooth surface of the PP membrane with reported roughness values of 66.4 nm, where the introduction of PEI and L-Dopa monomers to the PP membrane enhances surface roughness up to 159 nm.

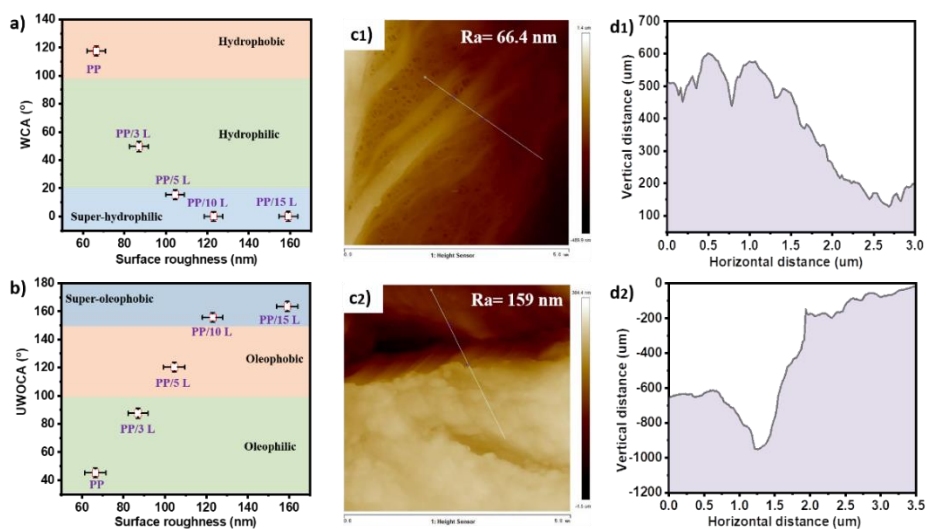


Figure 5.5: (a-b) A relation graph of surface roughness with WCA and UWOCA values, respectively; (c1-c2) 2D AFM images and (d1-d2) surface topography profiles of PP and PP/15 L membrane.

The obtained linear relation shows PP/5 L, PP/10 L, and PP/15 L membranes show hydrophilicity and super hydrophilicity properties. Therefore, to choose the best super-wetting membrane from different layered membranes, a detailed WCA with specific

CHAPTER 5

wetting time and UWOCA using different oils is investigated (**Figure 5.6a-b**). It is observed that PP/15 L membrane shows excellent super hydrophilicity and underwater superoleophobicity, which further supports the linear relation of membranes' roughness and wetting properties. The following Cassie-Baxter model can be further applied to theoretically explain such a relation ^{[48][288]}.

$$\cos\theta^* = r\varphi\cos\theta_t + \varphi - 1 \quad (5.1)$$

Here, θ_t , θ^* , φ and r represents theoretical and obtained UWOCA values, measured fractional area and the roughness factor ratio, respectively. It is significant to state that only $r \geq 1$ state in terms of the θ_t and θ^* ratio can enhance the wetting, which successfully proves that the obtained high roughness of the PP/15 L membrane is responsible for excellent superhydrophilicity and underwater superoleophobicity. Therefore, the obtained excellent UWOCA is compared with different reported literature (**Figure 5.6c**) ^{[289][290][291][229][292][293]}. As a more thorough explanation, such growing roughness combined with different hydrophilic layers can provide a strong hydration layer underwater and adjust the modified membranes' pore to be less than emulsified oil droplets (**Figure 5.6d**). These features aid in achieving high underwater superoleophobicity and anti-oil fouling, which pertains to achieving high separation efficiency during emulsion separation.

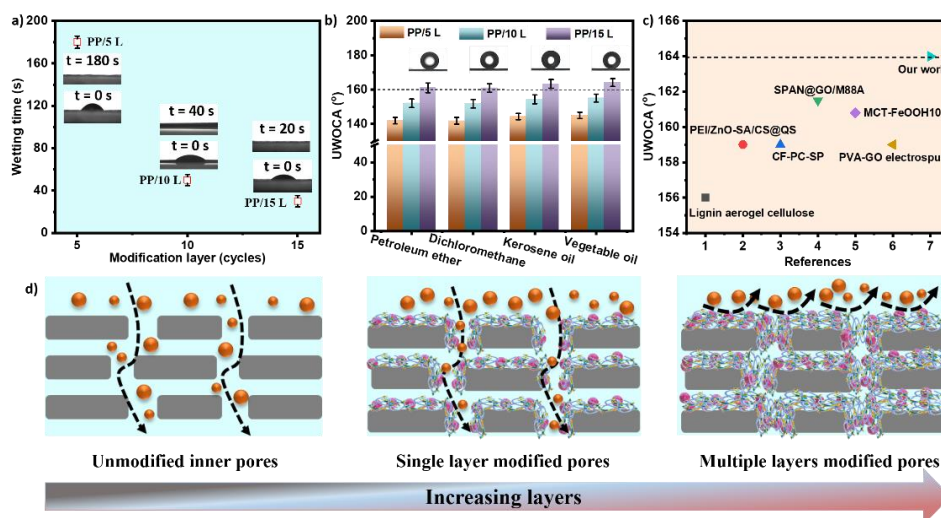


Figure 5.6: a) Differences of wetting time with different modification layers, b) underwater oil contact angle of PP/15 L membrane using different oils, c) a comparison of underwater oil contact angle value with our work and other reported literature, d) a schematic illustration of the inner pore structure of unmodified and different layered modified membranes with anti-oil fouling performances.

5.3.3. Environmental stability of the membrane

Hydrophilic substances could quickly lose their wettability under various extreme circumstances. As a result, membrane stability in many complicated environments a crucial factor in many practical applications [294]. The PP/15 L membrane is tested under various erosion circumstances to examine the membrane stability by conducting WCA and UWOCA experiments. **Figure 5.7a–c)** describes the sandpaper abrasion, bending, and scotch tape peeling experimental values, respectively with inserted digital experimental images. For sandpaper abrasion experiments, 500 grit sandpaper is used to abrade the modified membrane up to 10 times. A cycle is defined as 15 cm of movement of the membrane along the ruler while it is face-down on sandpaper, followed by 15 cm of

CHAPTER 5

movement and a 90° counterclockwise rotation of the membrane [18]. After 10 cyclic performances, a slight decline in membrane wetting is observed. It is assumed that the loss of the membrane's modification structure through the above erosion processes is what caused the wettability value to drop. To examine the membrane's UV resilience, the membrane is placed under a UV lamp (325 nm) using different exposure durations (15-90 min), as shown in **Figure 5.7d**. The chemical stability of the PP/15 L membrane (**Figure 5.7e**) is evaluated by immersing in the different pH solutions for 12 h and the WCA and UWOCA tests are carried out using the immersed membrane.

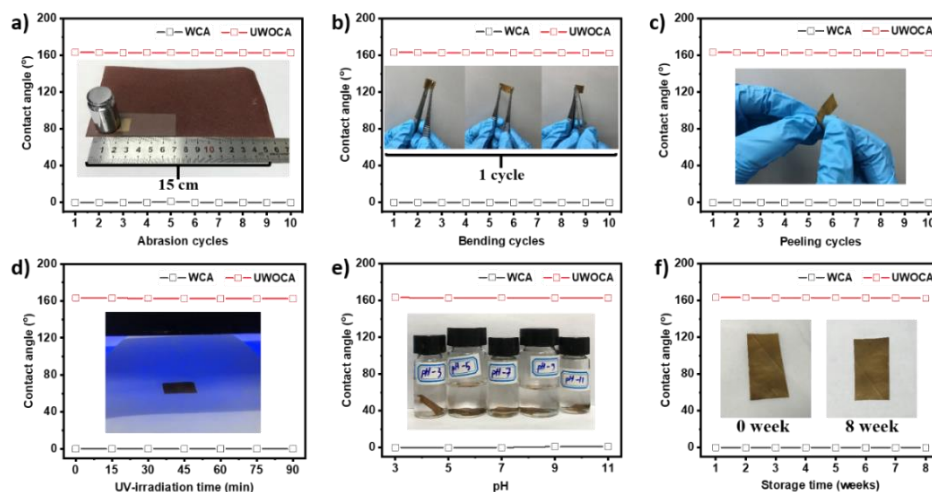


Figure 5.7: Water contact angle and underwater oil contact angle value of PP/15 L membrane in various complex conditions; a) sandpaper abrasion, b) membrane bending, c) scotch tape peeling, d) UV radiation exposure; e) different pH values, f) membrane storage over 8 weeks. All UWOCA experiments were carried out using vegetable oil.

Furthermore, the quantified unchanged values displayed in **Figure 5.7f**) represent the long-term super hydrophilicity and underwater super oleophobicity of the PP/15 L

membrane that has been measured over 8 weeks. No significant changes in values are observed, which represents robust wettability behavior of PP/15 L membrane in different harsh conditions. Therefore, all of the aforementioned findings recommend that the modified membrane has high stability features, which can ensure the emulsion separation feasible in various harsh environments.

5.3.4. Separation performances of oily wastewater

The membrane's wettability behavior is considered a fundamental aspect regarding oil/water emulsions separation as the hydrophilicity feature allows water droplets to spread out fast and pass through, while the underwater oleophobicity feature repels oil droplets. Therefore, PP/15 L membrane is promising for oil/water separation applications due to its super hydrophilicity and underwater super-oleophobicity properties. In accordance to testify to the practical effectiveness of the membrane separation process, the free oil layer mixture and surfactant stabilized emulsion of different oils are separated using a super-wetting PP/15 L membrane. Every separation experiment is carried out using gravity-driven separation mode. The obtained permeation flux and efficiency values of the free oil layer mixture are shown in **Figure 5.9a** for petroleum ether ($2325.3 \text{ L m}^{-2} \text{ h}^{-1}$, 99.82 %), dichloromethane ($2113.1 \text{ L m}^{-2} \text{ h}^{-1}$, 99.85 %), kerosene oil ($1891.5 \text{ L m}^{-2} \text{ h}^{-1}$, 99.88 %), and vegetable oil ($1584.2 \text{ L m}^{-2} \text{ h}^{-1}$, 99.91 %) respectively. Contrarily, **Figure 5.9b** displays the permeation flux and efficiency values of the surfactant-stabilized emulsion for petroleum ether ($529.3 \text{ L m}^{-2} \text{ h}^{-1}$, 99.62 %), dichloromethane ($493.1 \text{ L m}^{-2} \text{ h}^{-1}$, 99.69 %), kerosene oil ($453.5 \text{ L m}^{-2} \text{ h}^{-1}$, 99.78 %), and vegetable oil ($419.2 \text{ L m}^{-2} \text{ h}^{-1}$, 99.83 %) respectively.

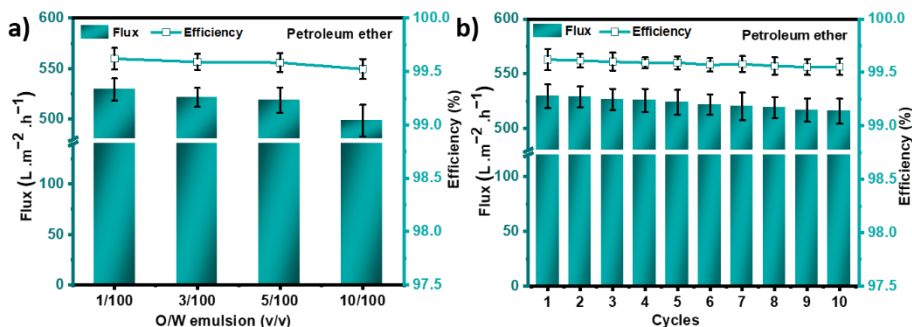


Figure 5.8: a) Permeate flux and corresponding separation efficiency, b) membrane cycling performances of PP/15 L membrane using petroleum ether/water emulsion.

To further access the PP/15 L membrane's cyclic and flux recovery ratio performances, petroleum ether/water emulsion using different concentrations is evaluated (Figure 5.8). It has been noticed that the permeate flux is decreased in direct proportion by using different kinds of oils for both free oil layer mixture and emulsified emulsion. The following Hagen-Poiseuille equation can be used to comprehend why the permeate flux of the PP/15 L membrane is decreasing for different emulsions [50]:

$$\text{Permeate flux, } J = \frac{p\pi r^2 P}{8\eta L\tau} \quad (5.2)$$

Where the pore size, membrane thickness, porosity, and tortuosity are denoted by the letters p , r , L , and τ respectively. P stands for pressure, and η denotes each emulsion's viscosity. When employing the same PP/15 L membrane for emulsion separation, parameters like p , r , L , and τ can be abandoned due to only minimal changes. The fundamental factor that determines how much permeate flux changes is the emulsion's viscosity (Table 5.1).

CHAPTER 5

Table 5.1: The viscosity of different oils that are used in this work.

Oil	Viscosity (mPa·s)	Ref.
Petroleum ether	0.219	[250]
Dichloromethane	0.395	[295]
Kerosene oil	0.517	obtained
vegetable oil	40.5	[253]

To maintain the same oil concentration, the predicted permeate flux of the PP/15 L membrane is therefore as follows petroleum ether > dichloromethane > kerosene oil > vegetable oil following the viscosity value of various oils **Figure 5.9c**. Furthermore, to execute the separation experiment for a long period, the stability performance of the membrane is also examined. Up to 300 minutes of gravity-driven pressure is used to feed a vegetable oil/water-free layer mixture and emulsion through the membrane (**Figure 5.9d**). The membrane was cleaned with deionized water for 15 minutes after every 50 minutes of filtering to efficiently remove the oil cake layer at the membrane surface, which allowed the flux to return to its initial level ^[296]. Therefore, the FRR is also calculated for various emulsions using different oils as shown in **Figure 5.9e**. The free oil layer mixture yields higher FRR values, while emulsions exhibit lower FRR values because of their tiny oil droplets, making them easier to flow through PP/15 L membrane ^[247]^[45]. Since some absorbed microscopic oil droplets pass through with permeate water during continuous separation, the permeate flow is significantly reduced, which lowers the flux, efficiency, and reusability characteristics. However, all the obtained FRR data shows excellent values with more than 97 % for surfactant-stabilized emulsion and more than 99% for the layered

CHAPTER 5

mixture. A comparison of the separation performances of our research and other published literature is shown in **Figure 5.9f** [215][217][214][216][297][298][264].

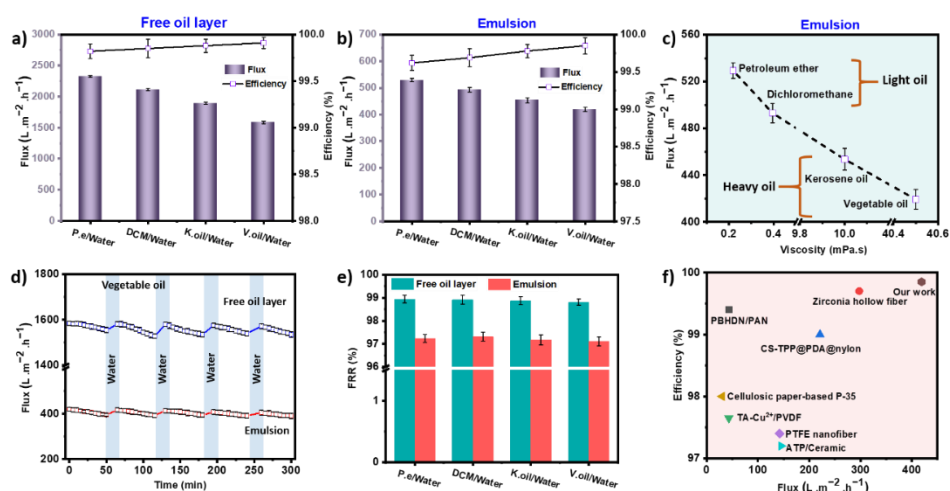


Figure 5.9: Separation fluxes and efficiency of PP/15 L membrane using various oil/water as a) free oil layer mixture, b) surfactant stabilized emulsion, c) a relation curve of flux in regards to different oil viscosity; d) a continuous separation flux, e) flux recovery ratio f) a comparison of surfactant-stabilized emulsion performances of our work with other literature.

Thus, to enlighten the above separation mechanism through the surfactant emulsion, oil demulsification and aggregation properties of emulsified emulsion are shown in **Figure 5.10a**. The PP/15 L membranes were attached to glass slides and wetted with water, and then vegetable oil/water emulsion was spread to the membrane and observed under an optical microscope. It is obvious to see that oil droplets from the emulsion start gathering and accumulating into large oil droplets after 45 s. It is presumed that excellent super wetting behavior of PP/15 L membrane strongly leads to oil droplets accumulation from the emulsion by emulsion flow driving force (\vec{F}_{fd}), which is correlated to oil surface

CHAPTER 5

tension (γ_{oil}), hydrophilicity ($\cos\theta_{water}$) and underwater oleophobicity ($\cos\theta_{oil}$) of PP/15 L membrane and can be well explained by the following equation ^[44],

$$\vec{F}_{fd} = \gamma_{oil} (\cos\theta_{water} - \cos\theta_{oil}) \quad (5.3)$$

The obtained values of hydrophilicity and underwater oleophobicity in our work are $\approx 0^\circ$ and $>160^\circ$, respectively. Therefore, it can be calculated that such outstanding values of our work become the foremost reason for oil droplets' agglomeration. Furthermore, **Figure 5.10b1-b4** and **Figure 5.10c1-c4** provide information on oil droplets of petroleum ether and vegetable oil emulsion before and after separation, respectively. It is observed that both petroleum ether and vegetable oil emulsion show a milky appearance with larger oil particle size, while permeating water shows clear, transparent, and almost no oil particles.

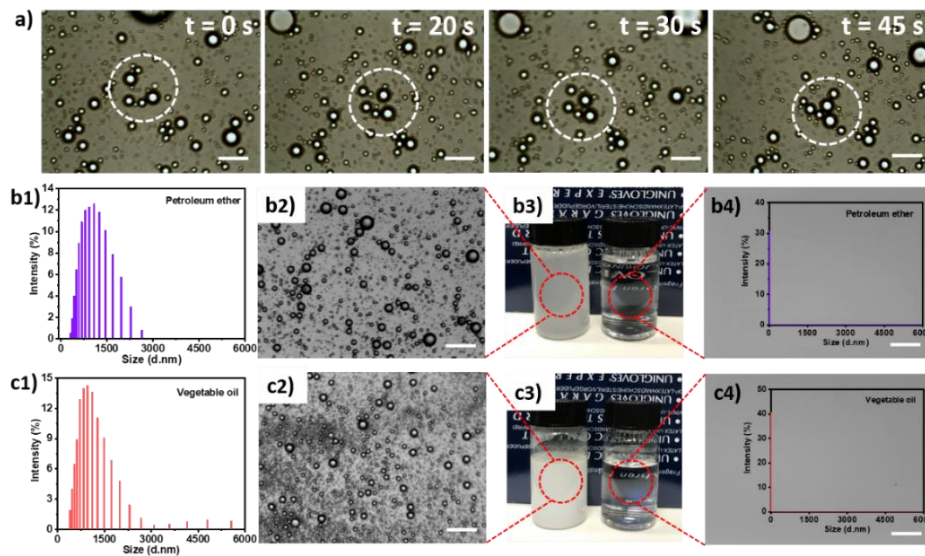


Figure 5.10: a) Oil demulsification and aggregation properties of the surfactant-stabilized emulsion; DLS oil droplet information with digital photographs of surfactant stabilized feed emulsion and permeate water; (b1-b4) petroleum ether and (c1-c4) vegetable oil.

5.3.5. Anti-bacterial performance

Due to the zwitterion features of L-dopa and amino-rich PEI solution, the PP/15 L membrane demonstrates strong anti-bacterial activities against *S. aureus* (Gram-positive) and *E. coli* (Gram-negative) bacteria. According to the findings, PP/15 L membrane reduces *S. aureus* and *E. coli* viability by 92.8 and 88.6%, whereas the unmodified PP membrane has little of an influence **Figure 5.11a-b**. Overall studies suggest that the PP/15 L membrane is excellent at suppressing bacteria growth in challenging wastewater conditions along with the removal of a variety of contaminants.

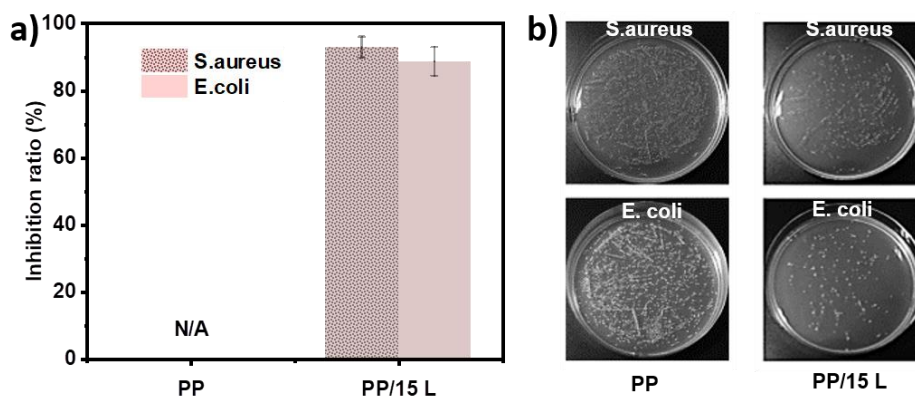


Figure 5.11: Anti-bacterial activities on *S. aureus* and *E. coli* bacteria incubated with PP and PP/15 L membranes, and b) their corresponding digital images.

5.4. Conclusions

We demonstrated the fabrication of advanced rough surface PP/15 L membrane by multilayer assembling of PEI/L-dopa monomers on corona-deposited PP membrane. Benefiting from the hierarchical rough structured membrane surface, excellent membrane wetting properties have been achieved. Additionally, stable membrane-wetting properties are obtained in different complex environments such as-membrane abrasion, bending,

CHAPTER 5

peeling, UV irradiation, pH resistance, long storage time, etc. Such stable wetting properties that have been achieved by constructing rough surface helps to obtain excellent separation performances both for free oil layer mixture and surfactant stabilized emulsion. Additionally, a higher flux recovery ratio can be achieved after separation. More importantly, amino-rich PEI and zwitterionic L-dopa monomers show significant anti-bacterial properties against *S. aureus* and *E. coli* bacteria, respectively. Overall, improved features of the advanced modified membrane inform that this effective surface modification approach can be implemented on a big industrial scale as an oil/water emulsion separation application to reduce multiple pollutant toxicity from our daily lives.

CHAPTER 6. Summary and future perspectives

The development of the modified biaxial polypropylene membrane has been thoroughly examined, including the design principles of functional super-wetting surface with excellent anti-oil-fouling properties. Overall, the findings from this dissertation will enable a better understanding of the modified biaxial PP membrane in the oily wastewater separation area. Specific contributions of this dissertation work are described below:

- **PVA/AA-g-PP-5 membrane** demonstrates the successful anti-oil fouling properties, modified by the pre-irradiation-induced graft polymerization method. The strong –OH and -COOH functional groups in the modified membrane are generated by the successful grafting reaction of AA and PVA monomers. Additionally, the surface roughness of the PVA/AA-g-PP-5 membrane is enhanced, which constructs micro/nano surface structure and is responsible for enhancing the wetting properties. Such enhanced properties show a high oil rejection percentage.
- **HM-PP membrane** exhibits super-wetting properties with outstanding thermal, mechanical, and chemical stability in different harsh environments. These excellent outcomes are caused by the surface-modifying AA and NaHCO₃ monomers used in this work to develop a multiscale micro/nano rough surface, which results in a significant selective barrier to prevent the penetration of oil droplets.
- **C/AM-g-PP membrane** shows excellent permanent super hydrophilicity and underwater oleophobicity behavior over 10 weeks. The applied corona treatment generates the hydrophilic carbonyl and carboxyl functional groups and the acrylamide monomers are grafted on the membrane to possess permanent wetting

CHAPTER 6

properties. These comprehensive and outstanding properties are responsible for achieving high permeation flux and separation efficiency in the gravity-driven separation method for all categories of oil/water mixture and emulsion.

- **PP/15 L membrane** demonstrates the fabrication of advanced rough surface by multilayer assembling of PEI/L-dopa monomers on corona-deposited biaxial PP membrane. Benefiting from the hierarchical rough structured membrane surface, excellent membrane wetting properties are achieved. Additionally, stable membrane-wetting properties are obtained in different complex environments helps to obtain excellent separation performances. Additionally, amino-rich PEI and zwitterionic L-dopa monomers show significant anti-bacterial properties against *S. aureus* and *E. coli* bacteria, respectively.

Notwithstanding the impressive advancements made in oil/water separation research using biaxial PP membranes, several difficulties still, need to be resolved. To encourage the growth of this discipline, the following study directions are specifically suggested.

- Fouling is the primary disadvantage of the separation process. Membrane fouling issues adversely affect the membrane separation process by decaying their life. As the foremost approach, future research should largely focus on the developing of unique material that is extremely resistant to oil and organic solvents.
- Although several research has been noted and addressed in the development of creating the anti-fouling ability of membrane surfaces, the mechanisms or theories underlying this performance are still limited to the microstructure.

CHAPTER 6

- To further understand the quantitative relationship between surface microstructure/composition and anti-fouling features of the membrane surface, fundamental investigations on mechanisms/theories from a molecular scale perspective are highly required.
- Thus to control the membrane fouling, a suitable surface modification approach must be used. Additionally, selecting adequate modification monomers is also one of the most important criteria going forward to generating super wetting properties. On the other hand, lab-scale developed modification methods may suffer complications when moving to industrial applications with huge productions. Therefore, the factor that is needed to consider when using these new methods and materials is their endurance and resistance to damage while in usage, which is still within limits.

To date, a variety of surface modification techniques, including surface grafting, irradiation, coating, crosslinking, and layer-by-layer assembly, have been developed to create super-wetting surfaces on PP membranes. Unfortunately, these widely used modification methods for PP membranes are still challenging, laborious, and time-consuming, making it challenging to accomplish continuous and large-scale production (**Figure 6.1**). Hence, from the standpoint of practical application, there is still a great need for more efficient, facile, universal, and all-encompassing methodologies for modifying PP membrane surfaces. To tackle these insurmountable issues and encourage the rapid advancement of the oily wastewater separation area for use in practical applications, more in-depth study and innovative thinking in the area of surface engineering are required.

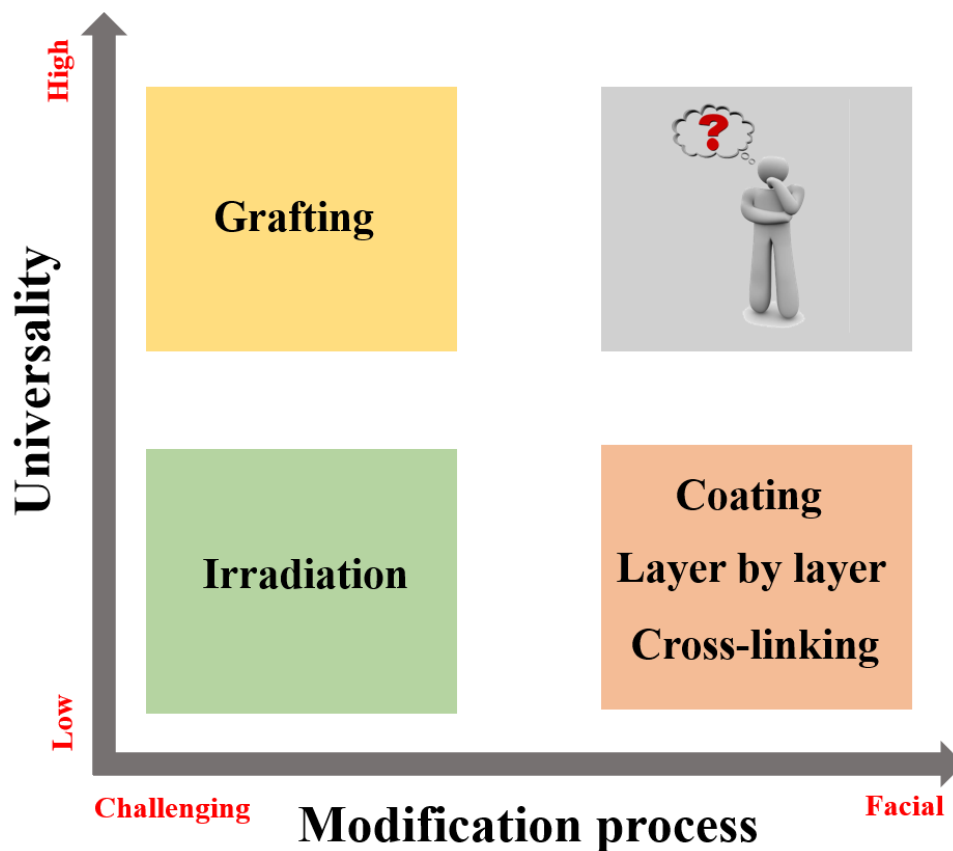


Figure 6.1: Schematic graph of the recent progress of the different modification methods for constructing super wetting biaxial PP membrane surface and the need for more effective and universal strategies.

LIST OF PUBLICATIONS

LIST OF PUBLICATIONS

1. **Z.R.Usha**, *et al.* Robust super-wetting biaxial polypropylene membrane with multi-scale roughness structures for highly efficient oil/water emulsion separation, *Journal of Environmental Chemical Engineering*, 2023, 11, 109670.
2. **Z.R.Usha**, *et al.* Super hydrophilic modified biaxially oriented polypropylene microporous membrane for excellent gravity-driven oil/water emulsion separation, *Journal of Membrane Science*, 2022, 660, 120840.
3. **Z.R.Usha** *et al.* Advanced super-wetting biaxial polypropylene membrane for multipollutant removal from oily wastewater, *Journal of Environmental Chemical Engineering*, 2023 (Under Review).
4. **Z.R.Usha** *et al.* Recent progress of polymeric membranes for efficient oil/water separation, 2023, (Under processing).
5. D.M.D. Babiker, **Z.R.Usha**, *et al.* Recent progress of composite polyethylene separators for lithium/sodium batteries, *Journal of Power Sources*, 2023, 564, 232853.
6. J.C. Habumugisha, **Z.R.Usha**, *et al.* Thermally stable and high electrochemical performance ultra-high molecular weight polyethylene/poly(4-methyl-1-pentene) blend film used as Li-ion battery separator, *Applied Materials Today*, 2021, 24(1), 101136.
7. D.M.D. Babiker, R.Yu, **Z.R.Usha**, *et al.* High performance ultra-high molecular weight polyethylene nanocomposite separators with excellent rate capabilities designed for next-generation lithium-ion batteries, *Materials Today Physics*, 2022, 23, 100626.
8. D.M.D. Babiker, C. Wan, B. Mansoor, **Z.R.Usha**, *et al.* Superior lithium battery separator with extraordinary electrochemical performance and thermal stability based on hybrid UHMWPE/SiO₂ nanocomposites via the scalable biaxial stretching process, *Composites Part B*, 2021, 211, 108658.

REFERENCES

REFERENCES

- [1] ISMAIL N H, SALLEH W N W, ISMAIL A F. Hydrophilic polymer-based membrane for oily wastewater treatment: A review[J/OL]. *Separation and Purification Technology*, 2020, 233(August 2019): 116007.
- [2] SANTORO S, AVCI A H, POLITANO A. The advent of thermoplasmonic membrane distillation[J/OL]. *Chemical Society Reviews*, 2022, 51(14): 6087-6125.
- [3] YAN T, CHEN X, ZHANG T. A magnetic pH-induced textile fabric with switchable wettability for intelligent oil/water separation[J/OL]. *Chemical Engineering Journal*, 2018, 347: 52-63.
- [4] WU M, MU P, LI B. Pine powders-coated PVDF multifunctional membrane for highly efficient switchable oil/water emulsions separation and dyes adsorption[J/OL]. *Separation and Purification Technology*, 2020.
- [5] ABDEL-ATY A A R, AZIZ Y S A, AHMED R M G. High performance isotropic polyethersulfone membranes for heavy oil-in-water emulsion separation[J/OL]. *Separation and Purification Technology*, 2020, 253.
- [6] SALIMI P, AROUJALIAN A, IRANSHAHI D. Graft copolymerization of zwitterionic monomer on the polyethersulfone membrane surface by corona air plasma for separation of oily wastewater[J/OL]. *Separation and Purification Technology*, 2021, 258(117939).
- [7] GUPTA R K, DUNDERDALE G J, ENGLAND M W. Oil/water separation techniques: A review of recent progresses and future directions[J/OL]. *Journal of Materials Chemistry A*, 2017, 5(31): 16025-16058.
- [8] GAO L L, LU Y C, ZHANG J L. Biotreatment of restaurant wastewater with an oily high concentration by newly isolated bacteria from oily sludge[J/OL]. *World Journal of Microbiology and Biotechnology*, 2019, 35(11): 1-11.

REFERENCES

- [9] AL-SHAMRANI A A, JAMES A, XIAO H. Destabilisation of oil-water emulsions and separation by dissolved air flotation[J/OL]. *Water Research*, 2002, 36(6): 1503-1512.
- [10] ZHAO C, ZHOU J, YAN Y. Application of coagulation/flocculation in oily wastewater treatment: A review[J/OL]. *Science of the Total Environment*, 2021, 765: 142795.
- [11] ZARGHAMI S, MOHAMMADI T, SADRZADEH M. Superhydrophilic and underwater superoleophobic membranes - A review of synthesis methods[J/OL]. *Progress in Polymer Science*, 2019, 98: 101166.
- [12] LEE W J, GOH P S, LAU W J. Antifouling zwitterion embedded forward osmosis thin film composite membrane for highly concentrated oily wastewater treatment[J/OL]. *Separation and Purification Technology*, 2019, 214(July 2018): 40-50.
- [13] DONG D, ZHU Y, FANG W. Double-Defense Design of Super-Anti-Fouling Membranes for Oil/Water Emulsion Separation[J/OL]. *Advanced Functional Materials*, 2022, 32(24).
- [14] LIU W, YANG G, HUANG M. Ultrarobust and Biomimetic Hierarchically Macroporous Ceramic Membrane for Oil – Water Separation Templated by Emulsion- Assisted Self-Assembly Method[J/OL]. 2020.
- [15] ZHU Y, CHEN P, NIE W. Greatly Improved Oil-in-Water Emulsion Separation Properties of Graphene Oxide Membrane upon Compositing with Halloysite Nanotubes[J]. 2018.
- [16] WAN IKHSAN S N, YUSOF N, AZIZ F. Efficient separation of oily wastewater using polyethersulfone mixed matrix membrane incorporated with halloysite nanotube-hydrous ferric oxide nanoparticle[J/OL]. *Separation and Purification Technology*, 2018, 199(September 2017): 161-169.
- [17] ZUO J hao, CHENG P, CHEN X fan. Separation and Purification Technology

REFERENCES

- Ultrahigh flux of polydopamine-coated PVDF membranes quenched in air via thermally induced phase separation for oil / water emulsion separation[J/OL]. *Separation and Purification Technology*, 2018, 192(August 2017): 348-359.
- [18] ABUDONIA K S, SAAD G R, NAGUIB H F. Surface modification of polypropylene film by grafting with vinyl monomers for the attachment of chitosan[J/OL]. *Journal of Polymer Research*, 2018, 25: 1-11.
- [19] ZHANG S, WANG W, WANG H. Synthesis and characterisation of starch grafted superabsorbent via 10 MeV electron-beam irradiation[J/OL]. *Carbohydrate Polymers*, 2014, 101: 798-803.
- [20] YU L, HAN M, HE F. A review of treating oily wastewater[J/OL]. *Arabian Journal of Chemistry*, 2017, 10: S1913-S1922.
- [21] MAGGAY I V, CHANG Y, VENAULT A. Functionalized porous filtration media for gravity-driven filtration : Reviewing a new emerging approach for oil and water emulsions separation[J/OL]. *Separation and Purification Technology*, 2021, 259(November 2020): 117983.
- [22] SHALABY M S, SOŁOWSKI G, ABBAS W. Recent Aspects in Membrane Separation for Oil / Water Emulsion[J/OL]. 2021, 2100448: 1-20.
- [23] KANG Z, ZHAO Y, YANG D. Review of oil shale in-situ conversion technology[J/OL]. *Applied Energy*, 2020, 269(April): 115121.
- [24] ZHAO F, FAN Y, ZHANG S. Assessment of efficiency improvement and emission mitigation potentials in China's petroleum refining industry[J/OL]. *Journal of Cleaner Production*, 2021, 280(x).
- [25] KHOR C M, WANG J, LI M. Performance, energy and cost of produced water treatment by chemical and electrochemical coagulation[J/OL]. *Water (Switzerland)*, 2020, 12(12): 1-14.
- [26] MA J, YAO M, YANG Y. Comprehensive review on stability and demulsification

REFERENCES

- of unconventional heavy oil-water emulsions[J/OL]. *Journal of Molecular Liquids*, 2022, 350: 118510.
- [27] ZHU Y, WANG D, JIANG L. Recent progress in developing advanced membranes for emulsified oil/water separation[M/OL]//*NPG Asia Materials*. 2014: e101.
- [28] YOU X, LIAO Y, TIAN M. Engineering highly effective nanofibrous membranes to demulsify surfactant-stabilized oil-in-water emulsions[J/OL]. *Journal of Membrane Science*, 2020, 611(118398).
- [29] BAIG U, FAIZAN M, SAJID M. Multifunctional membranes with super-wetting characteristics for oil-water separation and removal of hazardous environmental pollutants from water: A review[J/OL]. *Advances in Colloid and Interface Science*, 2020, 285: 102276.
- [30] SONG J, LI S, ZHAO C. A superhydrophilic cement-coated mesh: an acid, alkali, and organic reagent-free material for oil/ water separation †[J/OL]. *Nanoscale*, 2018, 10.
- [31] ZHANG Y, CHEN Y, HOU L. Pine-branch-like TiO₂ nanofibrous membrane for high efficiency strong corrosive emulsion separation[J/OL]. *Journal of Materials Chemistry A*, 2017, 5(31): 16134-16138.
- [32] ZHANG J, FANG W, ZHANG F. Ultrathin microporous membrane with high oil intrusion pressure for effective oil/water separation[J/OL]. *Journal of Membrane Science*, 2020, 608(118201).
- [33] LI H, MU P, LI J. Inverse desert beetle-like ZIF-8/PAN composite nanofibrous membrane for highly efficient separation of oil-in-water emulsions[J/OL]. *Journal of Materials Chemistry A*, 2021, 9(7): 4167-4175.
- [34] JIANG X, YANG F, GUO Z. Superwetting surfaces for filtration separation of high-viscosity raw petroleum/water mixtures[J/OL]. *Journal of Materials Chemistry A*, 2022, 10(27): 14273-14292.

REFERENCES

- [35] ZHANG W, LIU N, CAO Y. Superwetting Porous Materials for Wastewater Treatment: from Immiscible Oil/Water Mixture to Emulsion Separation[J/OL]. *Advanced Materials Interfaces*, 2017, 4(10).
- [36] BAIG U, FAIZAN M, WAHEED A. A review on super-wettable porous membranes and materials based on bio-polymeric chitosan for oil-water separation[J/OL]. *Advances in Colloid and Interface Science*, 2022, 303(March): 102635.
- [37] QIU L, SUN Y, GUO Z. Designing novel superwetting surfaces for high-efficiency oil-water separation: Design principles, opportunities, trends and challenges[M/OL]//*Journal of Materials Chemistry A*. (2020).
- [38] MOUSA H M, FAHMY H S, ALI G A M. Membranes for Oil / Water Separation : A Review[J/OL]. 2022, 2200557: 1-36.
- [39] TUMMONS E, HAN Q, TANUDJAJA H J. Membrane fouling by emulsified oil: A review[J/OL]. *Separation and Purification Technology*, 2020, 248(October 2019).
- [40] YANG J, YU T, WANG Z. Substrate-independent multifunctional nanostructured coating for diverse wastewater treatment[J/OL]. *Journal of Membrane Science*, 2022, 654(April): 120562.
- [41] OBAID M, MOHAMED H O, YASIN A S. Under-oil superhydrophilic wetted PVDF electrospun modified membrane for continuous gravitational oil/water separation with outstanding flux[J/OL]. *Water Research*, 2017, 123: 524-535.
- [42] TIAN Q, QIU F, LI Z. Structured sludge derived multifunctional layer for simultaneous separation of oil/water emulsions and anions contaminants[J/OL]. *Journal of Hazardous Materials*, 2022, 432(February): 128651.
- [43] LINTUVUORI J S, STRATFORD K, CATES M E. Colloids in cholesterics: Size-dependent defects and non-Stokesian microrheology[J/OL]. *Physical Review Letters*, 2010, 105(17): 1-4.
- [44] USHA Z R, BABIKER D M D, YU R. Super hydrophilic modified biaxially

REFERENCES

- oriented polypropylene microporous membrane for excellent gravity-driven oil/water emulsion separation[J/OL]. *Journal of Membrane Science*, 2022, 660(August): 120840.
- [45] LIN X, HONG J. Recent Advances in Robust Superwetable Membranes for Oil–Water Separation[J/OL]. *Advanced Materials Interfaces*, 2019, 6(12): 1-23.
- [46] LI X, WANG M, WANG C. Facile immobilization of Ag nanocluster on nanofibrous membrane for oil/water separation[J/OL]. *ACS Applied Materials and Interfaces*, 2014, 6(17): 15272-15282.
- [47] ZHANG N, YANG X, WANG Y. A review on oil/water emulsion separation membrane material[J/OL]. *Journal of Environmental Chemical Engineering*, 2022, 10(2).
- [48] DHYANI A, WANG J, HALVEY A K. Design and applications of surfaces that control the accretion of matter[J/OL]. *Science*, 2021, 373(6552).
- [49] CHEN H, SHEN Y, HE Z. Facilely fabricating superhydrophobic coated-mesh materials for effective oil-water separation: Effect of mesh size towards various organic liquids[J/OL]. *Journal of Materials Science and Technology*, 2020, 51: 151-160.
- [50] LV W, MEI Q, XIAO J. 3D Multiscale Superhydrophilic Sponges with Delicately Designed Pore Size for Ultrafast Oil/Water Separation[J/OL]. *Advanced Functional Materials*, 2017, 27(48): 1-9.
- [51] XI J, LOU Y, JIANG S. Robust paper-based materials for efficient oil–water emulsion separation[J/OL]. *Cellulose*, 2021, 28(16): 10565-10578.
- [52] ZHAO X, ZHANG R, LIU Y. Antifouling membrane surface construction: Chemistry plays a critical role[M/OL]//*Journal of Membrane Science*. (2018).
- [53] YANG H, ZHU B, ZHU L. Efficient Fenton-Like Catalysis Boosting the Antifouling Performance of the Heterostructured Membranes Fabricated via Vapor-

REFERENCES

- Induced Phase Separation and in Situ Mineralization[J/OL]. ACS Applied Materials and Interfaces, 2021.
- [54] SONG C, RUTLEDGE G C. Electrospun polyimide fiber membranes for separation of oil-in-water emulsions[J/OL]. Separation and Purification Technology, 2021, 270(December 2020): 118825.
- [55] JUNAIDI N F D, OTHMAN N H, FUZIL N S. Recent development of graphene oxide-based membranes for oil–water separation: A review[J/OL]. Separation and Purification Technology, 2021, 258.
- [56] YAO Y, DANG X, QIAO X. Crosslinked biomimetic coating modified stainless-steel-mesh enables completely self-cleaning separation of crude oil/water mixtures[J/OL]. Water Research, 2022, 224(August): 119052.
- [57] YONG J, CHEN F, LI M. Remarkably simple achievement of superhydrophobicity, superhydrophilicity, underwater superoleophobicity, underwater superoleophilicity, underwater superaerophobicity, and underwater superaerophilicity on femtosecond laser ablated PDMS surfaces[J/OL]. Journal of Materials Chemistry A, 2017, 5(48): 25249-25257.
- [58] CHEN C, LIN K, WU M. Micro-Nano Dual-Scale All-Polymer particles for construction of superwetting surface with controllable wettability and Hot-Water-Repellency[J/OL]. Chemical Engineering Journal, 2022, 445(February): 136810. <https://doi.org/10.1016/j.cej.2022.136810>.
- [59] ZANG L, ZHENG S, WANG L. Zwitterionic nanogels modified nanofibrous membrane for efficient oil/water separation[J/OL]. Journal of Membrane Science, 2020, 612.
- [60] ZHAN Y, HE S, WAN X. Thermally and chemically stable poly(arylene ether nitrile)/halloysite nanotubes intercalated graphene oxide nanofibrous composite membranes for highly efficient oil/water emulsion separation in harsh environment[J/OL]. Journal of Membrane Science, 2018, 567(August): 76-88.

REFERENCES

- [61] LI Y, FAN T, CUI W. Harsh environment-tolerant and robust PTFE@ZIF-8 fibrous membrane for efficient photocatalytic organic pollutants degradation and oil/water separation[J/OL]. *Separation and Purification Technology*, 2023, 306(PA): 122586.
- [62] QIN Y, SHEN H, HAN L. Mechanically Robust Janus Poly(lactic acid) Hybrid Fibrous Membranes toward Highly Efficient Switchable Separation of Surfactant-Stabilized Oil/Water Emulsions[J/OL]. *ACS Applied Materials and Interfaces*, 2020, 12(45): 50879-50888.
- [63] SUN C, CHEN K, WIAFE BINEY B. Switchable wettability of grain-stacked filter layers from polyurethane plastic waste for oil/water separation[J/OL]. *Journal of Colloid and Interface Science*, 2022, 610: 970-981.
- [64] ZUO J, LIU Z, ZHOU C. A durable superwetting clusters-inlayed mesh with high efficiency and flux for emulsion separation[J/OL]. *Journal of Hazardous Materials*, 2021, 403(May 2020): 123620.
- [65] LI J, XU C, GUO C. Underoil superhydrophilic desert sand layer for efficient gravity-directed water-in-oil emulsions separation with high flux[J/OL]. *Journal of Materials Chemistry A*, 2017, 6(1): 223-230.
- [66] YUE X, LI Z, ZHANG T. Design and fabrication of superwetting fiber-based membranes for oil/water separation applications[J/OL]. *Chemical Engineering Journal*, 2019, 364(January): 292-309.
- [67] JUNAIDI N F D, OTHMAN N H, FUZIL N S. Recent development of graphene oxide-based membranes for oil–water separation: A review[J/OL]. *Separation and Purification Technology*, 2021, 258(P1): 118000.
- [68] ZOUBEIK M, SALAMA A, HENNI A. Investigation of Oily Wastewater Filtration Using Polymeric Membranes: Experimental Verification of the Multicontinuum Modeling Approach[J/OL]. *Industrial and Engineering Chemistry Research*, 2018, 57(33): 11452-11464.
- [69] BANDEHALI S, SANAEPUR H, EBADI AMOOGHIN A. Biodegradable

REFERENCES

- Polymers for Membrane Separation[J/OL]. Separation and Purification Technology, 2021.
- [70] PANDEY R P, RASHEED P A, GOMEZ T. A fouling-resistant mixed-matrix nanofiltration membrane based on covalently cross-linked Ti₃C₂TX (MXene)/cellulose acetate[J/OL]. Journal of Membrane Science, 2020, 607.
- [71] HAN G, DE WIT J S, CHUNG T S. Water reclamation from emulsified oily wastewater via effective forward osmosis hollow fiber membranes under the PRO mode[J/OL]. Water Research, 2015, 81.
- [72] DU Y, LI Y, WU T. A superhydrophilic and underwater superoleophobic chitosan-TiO₂ composite membrane for fast oil-in-water emulsion separation[J/OL]. RSC Advances, 2017, 7(66): 41838-41846.
- [73] THAKUR K, RAJHANS A, KANDASUBRAMANIAN B. Starch/PVA hydrogels for oil/water separation[J/OL]. Environmental Science and Pollution Research, 2019, 26(31).
- [74] WANG Y, HE Y, YU J. Alginate-based nanofibrous membrane with robust photo-Fenton self-cleaning property for efficient crude oil/water emulsion separation[J/OL]. Separation and Purification Technology, 2022, 287(December 2021).
- [75] LI T, LIU F, ZHANG S. Janus Polyvinylidene Fluoride Membrane with Extremely Opposite Wetting Surfaces via One Single-Step Unidirectional Segregation Strategy[J/OL]. ACS Applied Materials and Interfaces, 2018, 10(29): 24947-24954.
- [76] ZHANG W, LI X, QU R. Janus membrane decorated: Via a versatile immersion-spray route: Controllable stabilized oil/water emulsion separation satisfying industrial emission and purification criteria[J/OL]. Journal of Materials Chemistry A, 2019, 7(9): 4941-4949.
- [77] XIE A, CUI J, YANG J. Photo-Fenton self-cleaning PVDF/NH₂-MIL-88B(Fe) membranes towards highly-efficient oil/water emulsion separation[J/OL]. Journal

REFERENCES

- of Membrane Science, 2020, 595(September 2019): 117499.
- [78] ZINADINI S, ROSTAMI S, VATANPOUR V. Preparation of antibiofouling polyethersulfone mixed matrix NF membrane using photocatalytic activity of ZnO/MWCNTs nanocomposite[J/OL]. Journal of Membrane Science, 2017, 529(January): 133-141.
- [79] AYYARU S, AHN Y H. Application of sulfonic acid group functionalized graphene oxide to improve hydrophilicity, permeability, and antifouling of PVDF nanocomposite ultrafiltration membranes[J/OL]. Journal of Membrane Science, 2017, 525(August 2016): 210-219.
- [80] XU Y, YUAN D, GUO Y. Superhydrophilic and polyporous nanofibrous membrane with excellent photocatalytic activity and recyclability for wastewater remediation under visible light irradiation[J/OL]. Chemical Engineering Journal, 2022, 427(June 2021): 131685. [81] XIE A, CUI J, YANG J等. Photo-Fenton self-cleaning membranes with robust flux recovery for an efficient oil/water emulsion separation[J/OL]. Journal of Materials Chemistry A, 2019, 7(14): 8491-8502.
- [82] FENG Q, ZHAN Y, YANG W. Layer-by-layer construction of super-hydrophilic and self-healing polyvinylidene fluoride composite membrane for efficient oil/water emulsion separation[J/OL]. Colloids and Surfaces A: Physicochemical and Engineering Aspects, 2021, 629(June): 127462.
- [83] RIZZELLO L, POMPA P P. Nanosilver-based antibacterial drugs and devices: Mechanisms, methodological drawbacks, and guidelines[J/OL]. Chemical Society Reviews, 2014, 43(5): 1501-1518.
- [84] CHEN S, LV C, HAO K. Multifunctional negatively-charged poly (ether sulfone) nanofibrous membrane for water remediation[J/OL]. Journal of Colloid and Interface Science, 2019, 538: 648-659.
- [85] VÁSQUEZ L, DAVIS A, GATTO F. Multifunctional PDMS polyHIPE filters for oil-water separation and antibacterial activity[J/OL]. Separation and Purification

REFERENCES

- Technology, 2021, 255(May 2020).
- [86] WANG K, HE H, ZHANG T C. Self-Locked and Self-Cleaning Membranes for Efficient Removal of Insoluble and Soluble Organic Pollutants from Water[J/OL]. ACS Applied Materials and Interfaces, 2021, 13(5): 6906-6918.
- [87] WANG K, HE H, WEI B. Multifunctional switchable nanocoated membranes for efficient integrated purification of oil/water emulsions[J/OL]. ACS Applied Materials and Interfaces, 2021, 13(45): 54315-54323.
- [88] WANG Y X, LI Y J, YANG H. Super-wetting, photoactive TiO₂ coating on amino-silane modified PAN nanofiber membranes for high efficient oil-water emulsion separation application[J/OL]. Journal of Membrane Science, 2019, 580(January): 40-48.
- [89] CAI Y, CHEN D, LI N. Self-healing and superwetable nanofibrous membranes for efficient separation of oil-in-water emulsions[J/OL]. Journal of Materials Chemistry A, 2019, 7(4): 1629-1637.
- [90] MA W, LI Y, GAO S. Self-Healing and Superwetable Nanofibrous Membranes with Excellent Stability toward Multifunctional Applications in Water Purification[J/OL]. ACS Applied Materials and Interfaces, 2020, 12(20): 23644-23654.
- [91] WU Y, XU G, WANG T. Janus Nanofiber Antibacterial Membrane for Switchable Separation of Oil/Water Emulsions[J/OL]. ACS Applied Nano Materials, 2022, 5(9): 13037-13046.
- [92] SURESH D, GOH P S, ISMAIL A F. Surface design of liquid separation membrane through graft polymerization: A state of the art review[J/OL]. Membranes, 2021, 11(11): 1-40.
- [93] DATTA P, GENZER J. “ Grafting Through ” Polymerization Involving Surface-Bound Monomers[J/OL]. 2016: 263-274.

REFERENCES

- [94] LI L, XIANG Y, YANG W. Embedded polyzwitterionic brush-modified nanofibrous membrane through subsurface-initiated polymerization for highly efficient and durable oil/water separation[J/OL]. *Journal of Colloid and Interface Science*, 2020, 575: 388-398.
- [95] ZHU Y, WANG J, ZHANG F. Zwitterionic Nanohydrogel Grafted PVDF Membranes with Comprehensive Antifouling Property and Superior Cycle Stability for Oil-in-Water Emulsion Separation[J/OL]. *Advanced Functional Materials*, 2018, 28(40).
- [96] CHEN X, HUANG G, AN C. Plasma-induced PAA-ZnO coated PVDF membrane for oily wastewater treatment: Preparation, optimization, and characterization through Taguchi OA design and synchrotron-based X-ray analysis[J/OL]. *Journal of Membrane Science*, 2019, 582(April): 70-82.
- [97] GAO S, SUN J, LIU P. A Robust Polyionized Hydrogel with an Unprecedented Underwater Anti-Crude-Oil-Adhesion Property[J/OL]. *Advanced Materials*, 2016, 28(26): 5307-5314.
- [98] LIU Y, WANG L, LU H. Achieving Effective Oil/Water Separation with Bicomponent Supramolecular Hydrogel Paint Coated Metal Mesh[J/OL]. *ACS Applied Polymer Materials*, 2020, 2(11): 4770-4778.
- [99] MA Z Y, XUE Y R, YANG H C. Surface and Interface Engineering of Polymer Membranes: Where We Are and Where to Go[J/OL]. *Macromolecules*, 2021.
- [100] ZHANG G, LI Y, GAO A. Bio-inspired underwater superoleophobic PVDF membranes for highly-efficient simultaneous removal of insoluble emulsified oils and soluble anionic dyes[J/OL]. *Chemical Engineering Journal*, 2019, 369(January): 576-587.
- [101] YANG X, HE Y, ZENG G. Bio-inspired method for preparation of multiwall carbon nanotubes decorated superhydrophilic poly(vinylidene fluoride) membrane for oil/water emulsion separation[J/OL]. *Chemical Engineering Journal*, 2017, 321:

REFERENCES

245-256.

- [102] YU Z, SHAO L, LI X. One-step preparation of sepiolite/graphene oxide membrane for multifunctional oil-in-water emulsions separation[J/OL]. *Applied Clay Science*, 2019, 181: 105208.
- [103] WANG M, XU Z, HOU Y. Fabrication of a superhydrophilic PVDF membrane with excellent chemical and mechanical stability for highly efficient emulsion separation[J/OL]. *Separation and Purification Technology*, 2020, 251(June): 117408.
- [104] DU X, LI L, LI J. Uv-triggered dopamine polymerization: Control of polymerization, surface coating, and photopatterning[J/OL]. *Advanced Materials*, 2014, 26(47): 8029-8033.
- [105] WANG J, MA G, HUANG W. Visible-light initiated polymerization of dopamine in a neutral environment for surface coating and visual protein detection[J/OL]. *Polymer Chemistry*, 2018, 9(42): 5242-5247.
- [106] WANG Q, CUI J, XIE A. PVDF composite membrane with robust UV-induced self-cleaning performance for durable oil/water emulsions separation[J/OL]. *Journal of the Taiwan Institute of Chemical Engineers*, 2020, 110: 130-139. <https://doi.org/10.1016/j.jtice.2020.02.024>.
- [107] YE J, ZHANG B, GU Y. Tailored Graphene Oxide Membranes for the Separation of Ions and Molecules[J/OL]. *ACS Applied Nano Materials*, 2019, 2(10): 6611-6621.
- [108] GUPTA O, ROY S, MITRA S. Microwave Induced Membrane Distillation for Enhanced Ethanol-Water Separation on a Carbon Nanotube Immobilized Membrane[J/OL]. *Industrial and Engineering Chemistry Research*, 2019, 58(39): 18313-18319.
- [109] LAM M P Y, LAU E, LIU X. Sample preparation for glycoproteins[J/OL]. *Comprehensive Sampling and Sample Preparation: Analytical Techniques for Scientists*, 2012, 3: 307-322.

REFERENCES

- [110] YI Y, TU H, ZHOU X. Acrylic acid-grafted pre-plasma nanofibers for efficient removal of oil pollution from aquatic environment[J/OL]. *Journal of Hazardous Materials*, 2019, 371: 165–174.
- [111] LI R, LI J, RAO L. Inkjet printing of dopamine followed by UV light irradiation to modify mussel-inspired PVDF membrane for efficient oil-water separation[J/OL]. *Journal of Membrane Science*, 2021, 619(September 2020): 118790.
- [112] GU Y, ZHANG B, FU Z. Poly (vinyl alcohol) modification of poly(vinylidene fluoride) microfiltration membranes for oil/water emulsion separation via an unconventional radiation method[J/OL]. *Journal of Membrane Science*, 2021, 619: 118792.
- [113] ZHANG J, QU W, LI X. Surface engineering of filter membranes with hydrogels for oil-in-water emulsion separation[J/OL]. *Separation and Purification Technology*, 2023, 304(September 2022): 122340.
- [114] GAO S, ZHU Y, WANG J. Layer-by-Layer Construction of Cu²⁺/Alginate Multilayer Modified Ultrafiltration Membrane with Bioinspired Superwetting Property for High-Efficient Crude-Oil-in-Water Emulsion Separation[J/OL]. *Advanced Functional Materials*, 2018, 28(49): 1-11.
- [115] GUO Y, GONG L, GAO S. Cupric phosphate mineralized polymer membrane with superior cycle stability for oil/water emulsion separation[J/OL]. *Journal of Membrane Science*, 2020, 612(June): 118427.
- [116] JIA Y, GUAN K, ZHANG L. Enabling polyketone membrane with underwater superoleophobicity via a hydrogel-based modification for high-efficiency oil-in-water emulsion separation[J/OL]. *Journal of Membrane Science*, 2021, 618(September 2020): 118705.
- [117] CUI J, XIE A, YAN Z. Fabrication of crosslinking modified PVDF/GO membrane with acid, alkali and salt resistance for efficient oil-water emulsion separation[J/OL]. *Separation and Purification Technology*, 2021, 265(118528).

REFERENCES

- [118] ZHU Y, XIE W, ZHANG F. Superhydrophilic In-Situ-Cross-Linked Zwitterionic Polyelectrolyte/PVDF-Blend Membrane for Highly Efficient Oil/Water Emulsion Separation[J/OL]. ACS Applied Materials and Interfaces, 2017, 9(11): 9603-9613.
- [119] LI C, ZHANG H, WANG F. PVA and CS cross-linking combined with: In situ chimeric SiO₂ nanoparticle adhesion to enhance the hydrophilicity and antibacterial properties of PTFE flat membranes[J/OL]. RSC Advances, 2019, 9(33): 19205-19216.
- [120] LIU D, ZHU J, QIU M. Antifouling performance of poly(lysine methacrylamide)-grafted PVDF microfiltration membrane for solute separation[J/OL]. Separation and Purification Technology, 2016, 171: 1-10.
- [121] BAI Z, WANG L, LIU C. Interfacial coordination mediated surface segregation of halloysite nanotubes to construct a high-flux antifouling membrane for oil-water emulsion separation[J/OL]. Journal of Membrane Science, 2021, 620(July 2020): 118828.
- [122] ZHANG F, GAO S, ZHU Y. Alkaline-induced superhydrophilic/underwater superoleophobic polyacrylonitrile membranes with ultralow oil-adhesion for high-efficient oil/water separation[J/OL]. Journal of Membrane Science, 2016, 513: 67-73.
- [123] ZHANG J, XUE Q, PAN X. Graphene oxide/polyacrylonitrile fiber hierarchical-structured membrane for ultra-fast microfiltration of oil-water emulsion[J/OL]. Chemical Engineering Journal, 2017, 307: 643-649.
- [124] SHI H, HE Y, PAN Y. A modified mussel-inspired method to fabricate TiO₂ decorated superhydrophilic PVDF membrane for oil/water separation[J/OL]. Journal of Membrane Science, 2016, 506: 60-70.
- [125] ZANG L, ZHENG S, WANG L. Zwitterionic nanogels modified nanofibrous membrane for efficient oil/water separation[J/OL]. Journal of Membrane Science, 2020, 612(118379).

REFERENCES

- [126] ZHENG Y, ZHANG C, WANG L. Tannic acid-based complex coating modified membranes with photo-Fenton self-cleaning property for sustainable oil-in-water emulsion separation[J/OL]. *Separation and Purification Technology*, 2021, 272(December 2020): 118893.
- [127] ZHANG N, YANG N, ZHANG L. Facile hydrophilic modification of PVDF membrane with Ag/EGCG decorated micro/nanostructural surface for efficient oil-in-water emulsion separation[J/OL]. *Chemical Engineering Journal*, 2020, 402: 126200.
- [128] ZARGHAMI S, MOHAMMADI T, SADRZADEH M. Bio-inspired anchoring of amino-functionalized multi-wall carbon nanotubes (N-MWCNTs) onto PES membrane using polydopamine for oily wastewater treatment[J/OL]. *Science of the Total Environment*, 2020, 711: 134951.
- [129] ZARGHAMI S, MOHAMMADI T, SADRZADEH M. Preparation, characterization and fouling analysis of in-air hydrophilic/underwater oleophobic bio-inspired polydopamine coated PES membranes for oily wastewater treatment[J/OL]. *Journal of Membrane Science*, 2019, 582(February): 402-413.
- [130] MA W, ZHANG M, LI Y. Flexible, durable and magnetic nanofibrous membrane with pH-switchable wettability for efficient on-demand oil/water separation[J/OL]. *Environmental Science: Nano*, 2019, 6(12): 3699-3711.
- [131] MA W, SAMAL S K, LIU Z. Dual pH- and ammonia-vapor-responsive electrospun nanofibrous membranes for oil-water separations[J/OL]. *Journal of Membrane Science*, 2017, 532: 12-23.
- [132] SONG Y Z, KONG X, YIN X. Tannin-inspired superhydrophilic and underwater superoleophobic polypropylene membrane for effective oil/water emulsions separation[J/OL]. *Colloids and Surfaces A: Physicochemical and Engineering Aspects*, 2017, 522: 585-592.
- [133] GU Y, ZHANG B, FU Z. Poly (vinyl alcohol) modification of poly(vinylidene

REFERENCES

- fluoride) microfiltration membranes for oil/water emulsion separation via an unconventional radiation method[J/OL]. *Journal of Membrane Science*, 2021, 619(118792).
- [134] ADIB H, RAISI A. Surface modification of a PES membrane by corona air plasma-assisted grafting of HB-PEG for separation of oil-in-water emulsions[J/OL]. *RSC Advances*, 2020, 10(29): 17143-17153.
- [135] LIN Y, SALEM M S, ZHANG L. Development of Janus membrane with controllable asymmetric wettability for highly-efficient oil/water emulsions separation[J/OL]. *Journal of Membrane Science*, 2020, 606(April): 118141.
- [136] WANG D, YANG H, WANG Q. Composite membranes of polyacrylonitrile cross-linked with cellulose nanocrystals for emulsion separation and regeneration[J/OL]. *Composites Part A: Applied Science and Manufacturing*, 2023, 164(November 2022): 1-10.
- [137] MENG H, LIANG H, XU T. Crosslinked electrospinning membranes with contamination resistant properties for highly efficient oil–water separation[J/OL]. *Journal of Polymer Research*, 2021, 28(9).
- [138] CHENG X, SUN Z, YANG X. Construction of superhydrophilic hierarchical polyacrylonitrile nanofiber membranes by: In situ asymmetry engineering for unprecedentedly ultrafast oil-water emulsion separation[J/OL]. *Journal of Materials Chemistry A*, 2020, 8(33): 16933-16942.
- [139] DENG Y, ZHANG G, BAI R. Fabrication of superhydrophilic and underwater superoleophobic membranes via an in situ crosslinking blend strategy for highly efficient oil/water emulsion separation[J/OL]. *Journal of Membrane Science*, 2019, 569(August 2018): 60-70.
- [140] ZHANG H, HE Q, LUO J. Sharpening Nanofiltration: Strategies for Enhanced Membrane Selectivity[J/OL]. *ACS Applied Materials and Interfaces*, 2020, 12(36): 39948-39966.

REFERENCES

- [141] S E, G A, A F I. Review on characteristics of biomaterial and nanomaterials based polymeric nanocomposite membranes for seawater treatment application[J/OL]. *Environmental research*, 2021, 197(March): 111177. <https://doi.org/10.1016/j.envres.2021.111177>.
- [142] CHOUDHURY R R, GOHIL J M, MOHANTY S. Antifouling, fouling release and antimicrobial materials for surface modification of reverse osmosis and nanofiltration membranes[J/OL]. *Journal of Materials Chemistry A*, 2018, 6(2): 313-333.
- [143] VAN DER BRUGGEN B, MÄNTTÄRI M, NYSTRÖM M. Drawbacks of applying nanofiltration and how to avoid them: A review[J/OL]. *Separation and Purification Technology*, 2008, 63(2): 251-263.
- [144] BICY K, KALARIKKAL N, STEPHEN A M. Facile fabrication of microporous polypropylene membrane separator for lithium-ion batteries[J/OL]. *Materials Chemistry and Physics*, 2020, 255(June): 123473.
- [145] MENG L pu, CHEN X wei, LIN Y fei. Improving the softness of BOPP films: From laboratory investigation to industrial processing[J/OL]. *Chinese Journal of Polymer Science (English Edition)*, 2017, 35(9): 1122-1131.
- [146] CHANGANI Z, RAZMJOU A, TAHERI-KAFRANI A. Surface modification of polypropylene membrane for the removal of iodine using polydopamine chemistry[J/OL]. *Chemosphere*, 2020, 249: 126079.
- [147] LI R, LIU J, SHI A. A facile method to modify polypropylene membrane by polydopamine coating via inkjet printing technique for superior performance[J/OL]. *Journal of Colloid and Interface Science*, 2019, 552: 719-727. <https://doi.org/10.1016/j.jcis.2019.05.108>.
- [148] LIN Y, MENG L, WU L. A semi-quantitative deformation model for pore formation in isotactic polypropylene microporous membrane[J/OL]. *Polymer*, 2015, 80: 214-227.

REFERENCES

- [149] SHAO S, LIU Y, SHI D. Control of organic and surfactant fouling using dynamic membranes in the separation of oil-in-water emulsions[J/OL]. *Journal of Colloid and Interface Science*, 2020, 560: 787-794. <https://doi.org/10.1016/j.jcis.2019.11.013>.
- [150] MILLER D J, DREYER D R, BIELAWSKI C W. Surface Modification of Water Purification Membranes[J/OL]. *Angewandte Chemie - International Edition*, 2017, 56(17): 4662-4711.
- [151] FENG R, WANG C, XU X. Highly effective antifouling performance of N-vinyl-2-pyrrolidone modified polypropylene non-woven fabric membranes by ATRP method[J/OL]. *Journal of Membrane Science*, 2011, 369: 233-242.
- [152] MENG J, LI J, ZHANG Y. A novel controlled grafting chemistry fully regulated by light for membrane surface hydrophilization and functionalization[J/OL]. *Journal of Membrane Science*, 2014, 455: 405-414.
- [153] ROY D, GUTHRIE J T, PERRIER S. Synthesis of natural-synthetic hybrid materials from cellulose via the RAFT process[J/OL]. *Soft Matter*, 2007, 4(1): 145-155.
- [154] SAFFAR A, CARREAU P J, KAMAL M R. Hydrophilic modification of polypropylene microporous membranes by grafting TiO₂ nanoparticles with acrylic acid groups on the surface[J/OL]. *Polymer*, 2014, 55: 6069-6075.
- [155] LONG X, HE L, ZHANG Y. Surface modification of polypropylene non-woven fabric for improving its hydrophilicity[J/OL]. *Surface Engineering*, 2018, 34: 818-824.
- [156] XU Y, WANG G, ZHU L. Multifunctional superhydrophobic adsorbents by mixed-dimensional particles assembly for polymorphic and highly efficient oil-water separation[J/OL]. *Journal of Hazardous Materials*, 2021, 407: 124374.
- [157] WANG S, ZHANG X, JIANG C. Polymer Solid-Phase Grafting at Temperature Higher than the Polymer Melting Point through Selective Heating[J/OL].

REFERENCES

- Macromolecules, 2019, 52: 3222–3230.
- [158] ZHANG M, CHEN J, WANG M. Electron beam-induced preparation of AIE non-woven fabric with excellent fluorescence durability[J/OL]. Applied Surface Science, 2021, 541(October): 148382.
- [159] ELSABEE M Z, ABDOU E S, NAGY K S A. Surface modification of polypropylene films by chitosan and chitosan/pectin multilayer[J/OL]. Carbohydrate Polymers, 2008, 71: 187-195.
- [160] JALEH B, PARVIN P, WANICHAPICHART P. Induced super hydrophilicity due to surface modification of polypropylene membrane treated by O₂ plasma[J/OL]. Applied Surface Science, 2010, 257: 1655-1659.
- [161] CHALYKH A E, TVERSKOY V A, ALIEV A D. Mechanism of post-radiation-chemical graft polymerization of styrene in polyethylene[J/OL]. Polymers, 2021, 13(15).
- [162] GAO Y, CHEN Y, YANG L. Effect of two different RAFT reactions on grafting MMA from pre-irradiated PP film[J/OL]. Radiation Physics and Chemistry, 2019, 159(January): 222-230.
- [163] XING L, LIU L, XIE F. Mutual irradiation grafting on indigenous aramid fiber-3 in diethanolamine and epichlorohydrin and its effect on interfacially reinforced epoxy composite[J/OL]. Applied Surface Science, 2016, 375: 65-73. <http://dx.doi.org/10.1016/j.apsusc.2016.03.073>.
- [164] ISHIHARA R, ASAI S, SAITO K. Recent progress in charged polymer chains grafted by radiation-induced graft polymerization; adsorption of proteins and immobilization of inorganic precipitates[J/OL]. Quantum Beam Science, 2020, 4(2).
- [165] KUMARI M, GUPTA B, IKRAM S. Characterization of N -isopropyl acrylamide / acrylic acid grafted polypropylene nonwoven fabric developed by radiation-induced graft polymerization[J/OL]. Radiation Physics and Chemistry, 2012, 81(11): 1729-1735.

REFERENCES

- [166] ZHANG S, WANG W, WANG H. Synthesis and characterisation of starch grafted superabsorbent via 10 MeV electron-beam irradiation[J/OL]. Carbohydrate Polymers, 2014, 101: 798-803.
- [167] LIU F, ZHU B K, XU Y Y. Improving the hydrophilicity of poly(vinylidene fluoride) porous membranes by electron beam initiated surface grafting of AA/SSS binary monomers[J/OL]. Applied Surface Science, 2006, 253(4): 2096-2101.
- [168] GOVENDER T, EHTEZAZI T, STOLNIK S. Complex formation between the anionic polymer (PAA) and a cationic drug (procaine HCl): Characterization by microcalorimetric studies[J/OL]. Pharmaceutical Research, 1999, 16: 1125–1131.
- [169] SAFFAR A, CARREAU P J, AJJI A. Development of polypropylene microporous hydrophilic membranes by blending with PP-g-MA and PP-g-AA[J/OL]. Journal of Membrane Science, 2014, 462: 50-61.
- [170] TIAN L, GU J, ZHANG H. Preparation of functionalized poly(1-butene) from 1,2-polybutadiene: Via sequential thiol-ene click reaction and ring-opening polymerization[J/OL]. RSC Advances, 2020, 10(70): 42799-42803.
- [171] ZHENG X Y, SONG S Y, YANG J R. 4-Formyl Dibenzo-18-Crown-6 Grafted Polyvinyl Alcohol As Anion Exchange Membranes for Fuel Cell[J/OL]. European Polymer Journal, 2019, 112(October 2018): 581-590.
- [172] PARK M J, GONZALES R R, ABDEL-WAHAB A. Hydrophilic polyvinyl alcohol coating on hydrophobic electrospun nanofiber membrane for high performance thin film composite forward osmosis membrane[J/OL]. Desalination, 2018, 426(October 2017): 50-59.
- [173] BOLTO B, TRAN T, HOANG M. Crosslinked poly(vinyl alcohol) membranes[J/OL]. Progress in Polymer Science (Oxford), 2009, 34(9): 969-981.
- [174] RAY S S, CHEN S S, NGUYEN N C. Poly(vinyl alcohol) incorporated with surfactant based electrospun nanofibrous layer onto polypropylene mat for improved desalination by using membrane distillation[J/OL]. Desalination, 2017,

REFERENCES

414: 18-27.

- [175] LIU H, YU H, YUAN X. Amino-functionalized mesoporous PVA/SiO₂ hybrids coated membrane for simultaneous removal of oils and water-soluble contaminants from emulsion[J/OL]. *Chemical Engineering Journal*, 2019, 374(April): 1394-1402.
- [176] LI H, ZHANG J, ZHU L. Reusable membrane with multifunctional skin layer for effective removal of insoluble emulsified oils and soluble dyes[J/OL]. *Journal of Hazardous Materials*, 2021, 415(February): 125677.
- [177] ZHANG X, TIAN J, XU R. In Situ Chemical Modification with Zwitterionic Copolymers of Nanofiltration Membranes: Cure for the Trade-Off between Filtration and Antifouling Performance[J/OL]. *ACS Applied Materials and Interfaces*, 2022, 14(25): 28842-28853.
- [178] LIU T, CHEN D, CAO Y. Construction of a composite microporous polyethylene membrane with enhanced fouling resistance for water treatment[J/OL]. *Journal of Membrane Science*, 2021, 618(June 2020): 118679.
- [179] CHEN F, XIE L. Enhanced fouling-resistance performance of polypropylene hollow fiber membrane fabricated by ultrasonic-assisted graft polymerization of acrylic acid[J/OL]. *Applied Surface Science*, 2020, 502: 144098.
- [180] ZHU T, JIANG C, WU J. Eco-friendly and one-step modification of poly(vinylidene fluoride) membrane with underwater superoleophobicity for effective emulsion separation[J/OL]. *Colloids and Surfaces A: Physicochemical and Engineering Aspects*, 2021, 610: 125939.
- [181] ZHU T, JIANG C, WU J. Eco-friendly and one-step modification of poly(vinylidene fluoride) membrane with underwater superoleophobicity for effective emulsion separation[J/OL]. *Colloids and Surfaces A: Physicochemical and Engineering Aspects*, 2021, 610: 125939.
- [182] ZHOU F, WANG Y, DAI L. Anchoring metal organic frameworks on nanofibers via etching-assisted strategy: Toward water-in-oil emulsion separation

REFERENCES

- membranes[J/OL]. *Separation and Purification Technology*, 2022, 281(August 2021): 119812.
- [183] LIU C, GUO Y, ZHOU Y. High-hydrophilic and antifouling reverse osmosis membrane prepared based an unconventional radiation method for pharmaceutical plant effluent treatment[J/OL]. *Separation and Purification Technology*, 2022, 280(3688): 119838.
- [184] WANG X, HUANG W, LI X. Superhydrophilic mixed matrix membranes by using strategy of internal and external coupling for oil-in-water emulsion separation[J/OL]. *Journal of Water Process Engineering*, 2021, 43(May): 102276.
- [185] WANG N, WANG X, ZHANG Y. All-in-one flexible asymmetric supercapacitor based on composite of polypyrrole-graphene oxide and poly(3,4-ethylenedioxythiophene)[J/OL]. *Journal of Alloys and Compounds*, 2020, 835: 155299.
- [186] ZHU X, YANG Z, GAN Z. Toward tailoring nanofiltration performance of thin-film composite membranes: Novel insights into the role of poly(vinyl alcohol) coating positions[J/OL]. *Journal of Membrane Science*, 2020, 614(July): 118526.
- [187] XU J, CUI J, SUN H. Facile preparation of hydrophilic PVDF membrane via tea polyphenols modification for efficient oil-water emulsion separation[J/OL]. *Colloids and Surfaces A: Physicochemical and Engineering Aspects*, 2023, 657(PB): 130639.
- [188] XIANG B, SUN Q, ZHONG Q. Current research situation and future prospect of superwetting smart oil/water separation materials[J/OL]. *Journal of Materials Chemistry A*, 2022, 10(38): 20190-20217.
- [189] LI F, WANG S, ZHAO X. Durable Superoleophobic Janus Fabric with Oil Repellence and Anisotropic Water-Transport Integration toward Energetic-Efficient Oil-Water Separation[J/OL]. *ACS Applied Materials and Interfaces*, 2022, 14(32): 37170-37181.

REFERENCES

- [190] LI Y, YANG X, WEN Y. Progress reports of mineralized membranes: Engineering strategies and multifunctional applications[J/OL]. Separation and Purification Technology, 2023, 304(October 2022): 122379. <https://doi.org/10.1016/j.seppur.2022.122379>.
- [191] LI H, ZHONG Q, SUN Q. Upcycling Waste Pine nut Shell Membrane for Highly Efficient Separation of Crude Oil-in-Water Emulsion[J/OL]. Langmuir, 2022, 38(11): 3493-3500.
- [192] ZHANG T, KONG F xin, LI X chen. Comparison of the performance of prepared pristine and TiO₂ coated UF/NF membranes for two types of oil-in-water emulsion separation[J/OL]. Chemosphere, 2020, 244: 125386.
- [193] TURK B, KAZAK O, AKKAYA G K. A simple and green preparation of red mud-coated membrane for efficient separation of oil-in-water emulsions[J/OL]. Journal of Environmental Chemical Engineering, 2022, 10(1).
- [194] WU M, XIANG B, MU P. Janus nanofibrous membrane with special micro-nanostructure for highly efficient separation of oil–water emulsion[J/OL]. Separation and Purification Technology, 2022, 297(March): 121532.
- [195] TANUDJAJA H J, HEJASE C A, TARABARA V V. Membrane-based separation for oily wastewater: A practical perspective[J/OL]. Water Research, 2019, 156: 347-365.
- [196] FENG L, GAO Y, XU Y. A dual-functional layer modified GO@SiO₂ membrane with excellent anti-fouling performance for continuous separation of oil-in-water emulsion[J/OL]. Journal of Hazardous Materials, 2021, 420(June): 126681.
- [197] XIONG Q, CHEN H, TIAN Q. Waste PET derived Janus fibrous membrane for efficient oil/water emulsions separation[J/OL]. Journal of Environmental Chemical Engineering, 2022, 10(5): 108459.
- [198] MODI A, JIANG Z, KASHER R. Hydrostable ZIF-8 layer on polyacrylonitrile membrane for efficient treatment of oilfield produced water[J/OL]. Chemical

REFERENCES

- Engineering Journal, 2022, 434: 133513.
- [199] SHAKIBA M, ABDOUSS M, MAZINANI S. Super-hydrophilic electrospun PAN nanofibrous membrane modified with alkaline treatment and ultrasonic-assisted PANI in-situ polymerization for highly efficient gravity-driven oil / water separation[J/OL]. Separation and Purification Technology, 2023, 309(November 2022): 123032.
- [200] HAN L, LI X, LI F. Superhydrophilic/air-superoleophobic diatomite porous ceramics for highly-efficient separation of oil-in-water emulsion[J/OL]. Journal of Environmental Chemical Engineering, 2022, 10(5): 108483.
- [201] CUI J, ZHOU Z, XIE A. Separation and Purification Technology Bio-inspired fabrication of superhydrophilic nanocomposite membrane based on surface modification of SiO₂ anchored by polydopamine towards effective oil-water emulsions separation[J/OL]. Separation and Purification Technology, 2019, 209(December 2017): 434-442.
- [202] GUO Y, LI M, WEN X. Silica-Modified Electrospun Membrane with Underwater Superoleophobicity for Effective Gravity-driven Oil/Water Separation[J/OL]. Fibers and Polymers, 2022, 23(7): 1906-1914.
- [203] ESCOBAR I C, VAN DER BRUGGEN B. Microfiltration and ultrafiltration membrane science and technology[J/OL]. Journal of Applied Polymer Sciencefile:///C:/Users/USER/Downloads/fmech-06-00029.pdf, 2015, 132(21).
- [204] ZHANG S, JIANG G, GAO S. Cupric Phosphate Nanosheets-Wrapped Inorganic Membranes with Superhydrophilic and Outstanding Anticrude Oil-Fouling Property for Oil/Water Separation[J/OL]. ACS Nano, 2018, 12(1): 795-803.
- [205] CHEN X, WAN C, YU R. A novel carboxylated polyacrylonitrile nanofibrous membrane with high adsorption capacity for fluoride removal from water[J/OL]. Journal of Hazardous Materials, 2021, 411: 125113.
- [206] MASLAKOV K I, TETERIN Y A, STEFANOVSKY S V.. XPS study of uranium-

REFERENCES

- containing sodium-aluminum-iron-phosphate glasses[J/OL]. *Journal of Alloys and Compounds*, 2017, 712: 36-43.
- [207] CINAT P, GNECCO G, PAGGI M. Multi-Scale Surface Roughness Optimization Through Genetic Algorithms[J/OL]. *Frontiers in Mechanical Engineering*, 2020, 6(May).
- [208] CHICHE A, PAREIGE P, CRETON C. Role of surface roughness in controlling the adhesion of a soft adhesive on a hard surface[J/OL]. *Comptes Rendus de l'Academie des Sciences - Series IV: Physics, Astrophysics*, 2000, 1(9): 1197-1204.
- [209] CHEN X, ZHANG Y, YU F. DFT calculations on hydrogen-bonded complexes formed between guanine and acrylamide[J/OL]. *Journal of Solution Chemistry*, 2010, 39: 1341–1349.
- [210] YAN L, YANG X, ZENG H. Nanocomposite hydrogel engineered hierarchical membranes for efficient oil/water separation and heavy metal removal[J/OL]. *Journal of Membrane Science*, 2023, 668(October 2022): 121243.
- [211] MA W, DING Y, LI Y. Durable, self-healing superhydrophobic nanofibrous membrane with self-cleaning ability for highly-efficient oily wastewater purification[J/OL]. *Journal of Membrane Science*, 2021, 634(May): 119402.
- [212] LI H, ZHU L, ZHU X. Dual-functional membrane decorated with flower-like metal-organic frameworks for highly efficient removal of insoluble emulsified oils and soluble dyes[J/OL]. *Journal of Hazardous Materials*, 2021, 408(124444).
- [213] ONG C, SHI Y, CHANG J. Tannin-inspired robust fabrication of superwettability membranes for highly efficient separation of oil-in-water emulsions and immiscible oil/water mixtures[J/OL]. *Separation and Purification Technology*, 2019, 227(April): 115657.
- [214] SHIJIE F, JIEFENG Z, PENGYU Z. Superhydrophilic/underwater superoleophobic oil-in-water emulsion separation membrane modified by the co-deposition of polydopamine and chitosan-tripolyphosphate nanoparticles[J/OL]. *Journal of*

REFERENCES

- Environmental Chemical Engineering, 2022, 10(3): 107407.
- [215] DOU Y le, YUE X, LV C jiang. Dual-responsive polyacrylonitrile-based electrospun membrane for controllable oil-water separation[J/OL]. Journal of Hazardous Materials, 2022, 438(July): 129565.
- [216] GAO J, CAI M, NIE Z. Superwetting PVDF membrane prepared by in situ extraction of metal ions for highly efficient oil/water mixture and emulsion separation[J/OL]. Separation and Purification Technology, 2021, 275(April): 119174.
- [217] WANG X, SUN K, ZHANG G. Robust zirconia ceramic membrane with exceptional performance for purifying nano-emulsion oily wastewater[J/OL]. Water Research, 2022, 208(August 2021): 117859.
- [218] GAO Y, LI Z, CHENG B. Superhydrophilic poly(p-phenylene sulfide) membrane preparation with acid/alkali solution resistance and its usage in oil/water separation[J/OL]. Separation and Purification Technology, 2018, 192: 262–270.
- [219] LU H, SHA S, YANG S. The coating and reduction of graphene oxide on meshes with inverse wettability for continuous water/oil separation[J/OL]. Applied Surface Science, 2021, 538(June 2020): 147948.
- [220] LI Z, ZHANG T C, MOKOBA T. Superwetting Bi₂MoO₆/Cu₃(PO₄)₂Nanosheet-Coated Copper Mesh with Superior Anti-Oil-Fouling and Photo-Fenton-like Catalytic Properties for Effective Oil-in-Water Emulsion Separation[J/OL]. ACS Applied Materials and Interfaces, 2021, 13(20): 23662-23674.
- [221] MATINDI C N, HU M, KADANYO S. Tailoring the morphology of polyethersulfone/sulfonated polysulfone ultrafiltration membranes for highly efficient separation of oil-in-water emulsions using TiO₂ nanoparticles[J/OL]. Journal of Membrane Science, 2021, 620(May): 118868.
- [222] ZHONG Q, SHI G, SUN Q. Robust PVA-GO-TiO₂ composite membrane for efficient separation oil-in-water emulsions with stable high flux[J/OL]. Journal of

REFERENCES

- Membrane Science, 2021, 640(July): 119836.
- [223] ZHAO Y, GUO J, LI Y. Superhydrophobic and superoleophilic PH-CNT membrane for emulsified oil-water separation[J/OL]. Desalination, 2022, 526(January): 115536.
- [224] WANG S, ZHANG X, XI Z. Design and preparation of polypropylene ultrafiltration membrane with ultrahigh flux for both water and oil[J/OL]. Separation and Purification Technology, 2020, 238: 116455.
- [225] DMITRIEVA E S, ANOKHINA T S, NOVITSKY E G. Polymeric Membranes for Oil-Water Separation: A Review[J/OL]. Polymers, 2022, 14(5): 1-25.
- [226] RAHIMPOUR A, MADAENI S S. Improvement of performance and surface properties of nano-porous polyethersulfone (PES) membrane using hydrophilic monomers as additives in the casting solution[J/OL]. Journal of Membrane Science, 2010, 360: 371-379.
- [227] XU MAO, HU SHIRU, GUAN JIAYU, SUN XIANMING, WU WEI, ZHU WEI, ZHANG XIAN, MA ZIMIAN, HAN QI, LIU SHANGQI. Polypropylene Microporous Film[M]//U.S. Patent, 5,134,174,.
- [228] FANG W, LIANG G, LI J. Microporous formation and evolution mechanism of PTFE fibers/isotactic polypropylene membranes by interface separation[J/OL]. Journal of Membrane Science, 2021, 631(April): 119333.
- [229] ZHANG L, HE Y, LUO P. Photocatalytic GO/M88A “interceptor plate” assembled nanofibrous membrane with photo-Fenton self-cleaning performance for oil/water emulsion separation[J/OL]. Chemical Engineering Journal, 2022, 427(March 2021).
- [230] WEI P, LOU H, XU X. Preparation of PP non-woven fabric with good heavy metal adsorption performance via plasma modification and graft polymerization[J/OL]. Applied Surface Science, 2021, 539(April 2020): 148195.
- [231] QU F, CAO A, YANG Y. Hierarchically superhydrophilic poly(vinylidene fluoride)

REFERENCES

- membrane with self-cleaning fabricated by surface mineralization for stable separation of oily wastewater[J/OL]. *Journal of Membrane Science*, 2021, 640(August): 119864.
- [232] CHEN X, HUANG G, AN C. Plasma-induced poly(acrylic acid)-TiO₂ coated polyvinylidene fluoride membrane for produced water treatment: Synchrotron X-Ray, optimization, and insight studies[J/OL]. *Journal of Cleaner Production*, 2019.
- [233] SADEGHI I, AROUJALIAN A, RAISI A. Surface modification of polyethersulfone ultrafiltration membranes by corona air plasma for separation of oil/water emulsions[J/OL]. *Journal of Membrane Science*, 2013, 430: 24-36.
- [234] ZHANG S, JIANG G, GAO S. Cupric Phosphate Nanosheets-Wrapped Inorganic Membranes with Superhydrophilic and Outstanding Anticrude Oil-Fouling Property for Oil/Water Separation[J/OL]. *ACS Nano*, 2018, 12: 795-803.
- [235] ZHAO Z, NING Y, JIN X. Molecular-structure-induced under-liquid dual superlyophobic surfaces[J/OL]. *ACS Nano*, 2020, 14(11): 14869-14877.
- [236] CUI J, ZHOU Z, XIE A. Bio-inspired fabrication of superhydrophilic nanocomposite membrane based on surface modification of SiO₂ anchored by polydopamine towards effective oil-water emulsions separation[J/OL]. *Separation and Purification Technology*, 2019, 209(March 2018): 434-442.
- [237] XU Y, WANG G, ZHU L. Multifunctional superhydrophobic adsorbents by mixed-dimensional particles assembly for polymorphic and highly efficient oil-water separation[J/OL]. *Journal of Hazardous Materials*, 2021, 407: 124374.
- [238] WU J, HOU Z, YU Z. Facile preparation of metal-polyphenol coordination complex coated PVDF membrane for oil/water emulsion separation[J/OL]. *Separation and Purification Technology*, 2021, 258(P2): 118022.
- [239] DENG Y, PENG C, DAI M. Recent development of super-wettable materials and their applications in oil-water separation[J/OL]. *Journal of Cleaner Production*, 2020, 266: 121624.

REFERENCES

- [240] CHEN J, ZHOU Y, ZHOU C. A durable underwater superoleophobic and underoil superhydrophobic fabric for versatile oil/water separation[J/OL]. *Chemical Engineering Journal*, 2019, 370.
- [241] CONG Y, ZHANG W, LIU C. Composition and Oil-Water Interfacial Tension Studies in Different Vegetable Oils[J/OL]. *Food Biophysics*, 2020, 15(2): 229-239.
- [242] CHEN S, LIU Y, WANG Y. Dual-functional superwetable nano-structured membrane: From ultra-effective separation of oil-water emulsion to seawater desalination[J/OL]. *Chemical Engineering Journal*, 2021, 411: 128042.
- [243] ZHAN Y, HE S, HU J. Robust super-hydrophobic/super-oleophilic sandwich-like UIO-66-F4@rGO composites for efficient and multitasking oil/water separation applications[J/OL]. *Journal of Hazardous Materials*, 2020, 388(August 2019): 121752.
- [244] CHEN C, WENG D, MAHMOOD A. Separation Mechanism and Construction of Surfaces with Special Wettability for Oil/Water Separation[J/OL]. *ACS Applied Materials and Interfaces*, 2019, 11(11): 11006-11027.
- [245] CHEN L, YE F, LIU H. Demulsification of oily wastewater using a nano carbon black modified with polyethyleneimine[J/OL]. *Chemosphere*, 2022, 295(December 2021): 133857.
- [246] YIN Y, ZHU L, CHANG X. Bioinspired Anti-Oil-Fouling Hierarchical Structured Membranes Decorated with Urchin-Like α -FeOOH Particles for Efficient Oil/Water Mixture and Crude Oil-in-Water Emulsion Separation[J/OL]. *ACS Applied Materials and Interfaces*, 2020, 12(45): 50962-50970.
- [247] HE L, LEI W, LIU D. One-step facile fabrication of mechanical strong porous boron nitride nanosheets–polymer electrospun nanofibrous membranes for repeatable emulsified oil/water separation[J/OL]. *Separation and Purification Technology*, 2021, 264(February).
- [248] LU T, DENG Y, CUI J. Multifunctional Applications of Blow-Spinning *Setaria*

REFERENCES

- viridis Structured Fibrous Membranes in Water Purification[J/OL]. ACS Applied Materials and Interfaces, 2021, 13: 22874–22883.
- [249] YU T, HALOUANE F, MATHIAS D. Preparation of magnetic, superhydrophobic/superoleophilic polyurethane sponge: Separation of oil/water mixture and demulsification[J/OL]. Chemical Engineering Journal, 2020, 384(123339).
- [250] SIVEBAEK I M, JAKOBSEN J. The viscosity of dimethyl ether[J/OL]. Tribology International, 2007, 40(4): 652-658.
- [251] RATHNAM M V., MANKUMARE S, KUMAR M S S. Density, viscosity, and speed of sound of (Methyl Benzoate + Cyclohexane), (Methyl Benzoate + n-Hexane), (Methyl Benzoate + Heptane), and (Methyl Benzoate + Octane) at temperatures of (303.15, 308.15, and 313.15) K[J/OL]. Journal of Chemical and Engineering Data, 2010, 55(3): 1354-1358.
- [252] ASSAEL M J, DALAOUTI N K, POLIMATIDOU S. Viscosity of toluene in the temperature range from 210 to 370 K at pressures up to 30 MPa[J/OL]. International Journal of Thermophysics, 1999, 20(5): 1367-1377.
- [253] DIAMANTE L M, LAN T. Absolute Viscosities of Vegetable Oils at Different Temperatures and Shear Rate Range of 64.5 to 4835 s⁻¹ [J/OL]. Journal of Food Processing, 2014, 2014: 1-6.
- [254] AL-WAHAIBI T, AL-WAHAIBI Y, AL-HASHMI A A R. Experimental investigation of the effects of various parameters on viscosity reduction of heavy crude by oil–water emulsion[J/OL]. Petroleum Science, 2015, 12(1): 170-176.
- [255] GONG Z, YANG N, CHEN Z. Fabrication of meshes with inverse wettability based on the TiO₂ nanowires for continuous oil/water separation[J/OL]. Chemical Engineering Journal, 2020, 380(122524).
- [256] AO C, YUAN W, ZHAO J. Superhydrophilic graphene oxide@electrospun cellulose nanofiber hybrid membrane for high-efficiency oil/water separation[J/OL].

REFERENCES

- Carbohydrate Polymers, 2017, 175: 216-222.
- [257] XIONG Z, LIN H, ZHONG Y. Robust superhydrophilic polylactide (PLA) membranes with a TiO₂ nano-particle inlaid surface for oil/water separation[J/OL]. Journal of Materials Chemistry A, 2017, 5(14): 6538-6545.
- [258] ZHANG C, ZHANG Y, XIAO X. Correction: Efficient separation of immiscible oil/water mixtures using a perforated lotus leaf[J/OL]. Green Chemistry, 2020, 22(2): 6579–6584.
- [259] LIAO Y, TIAN M, WANG R. A high-performance and robust membrane with switchable super-wettability for oil/water separation under ultralow pressure[J/OL]. Journal of Membrane Science, 2017, 543: 123-132.
- [260] YANG S, CHEN L, LIU S. Facile and sustainable fabrication of high-performance cellulose sponge from cotton for oil-in-water emulsion separation[J/OL]. Journal of Hazardous Materials, 2021, 408(October): 124408.
- [261] VENAULT A, CHEN L A, MAGGAY I V. Simultaneous amphiphilic polymer synthesis and membrane functionalization for oil/water separation[J/OL]. Journal of Membrane Science, 2020, 604(118069).
- [262] LI H, ZHU L, ZHANG J. High-efficiency separation performance of oil-water emulsions of polyacrylonitrile nanofibrous membrane decorated with metal-organic frameworks[J/OL]. Applied Surface Science, 2019, 476: 61-69.
- [263] LIU Z, WU W, LIU Y. A mussel inspired highly stable graphene oxide membrane for efficient oil-in-water emulsions separation[J/OL]. Separation and Purification Technology, 2018, 199: 37-46.
- [264] FAN Z, ZHOU S, MAO H. A novel ceramic microfiltration membrane fabricated by anthurium andraeanum-like attapulgite nanofibers for high-efficiency oil-in-water emulsions separation[J/OL]. Journal of Membrane Science, 2021, 630(119291).

REFERENCES

- [265] GE J, JIN Q, ZONG D. Biomimetic Multilayer Nanofibrous Membranes with Elaborated Superwettability for Effective Purification of Emulsified Oily Wastewater[J/OL]. ACS Applied Materials and Interfaces, 2018, 10(18): 16183-16192.
- [266] LIU M, SHEN L, WANG J. Continuous separation and recovery of high viscosity oil from oil-in-water emulsion through nondispersive solvent extraction using hydrophobic nanofibrous poly(vinylidene fluoride) membrane[J/OL]. Journal of Membrane Science, 2022, 660(July): 120876.
- [267] XIE H, CHEN B, LIN H. Efficient oil-water emulsion treatment via novel composite membranes fabricated by CaCO₃-based biomineralization and TA-Ti(IV) coating strategy[J/OL]. Science of the Total Environment, 2023, 857(August 2022): 159183.
- [268] DAN H, JI K, GAO Y. Fabrication of superhydrophobic Enteromorpha-derived carbon aerogels via NH₄H₂PO₄ modification for multi-behavioral oil/water separation[J/OL]. Science of the Total Environment, 2022, 837(May): 155869.
- [269] WANG S, ZENG J, LI P. Rechargeable nanofibrillated cellulose aerogel with excellent biocidal properties for efficient oil/water separation[J/OL]. Separation and Purification Technology, 2022, 301(August): 121955.
- [270] HOU X, ZHANG R, FANG D. Flexible and robust polyimide membranes with adjustable surface structure and hierarchical pore distribution for oil/water emulsion and heavy oil separation[J/OL]. Journal of Membrane Science, 2021, 640(June): 119769.
- [271] GEORGE J K, VERMA N. Super-hydrophobic/super-oleophilic carbon nanofiber-embedded resorcinol-formaldehyde composite membrane for effective separation of water-in-oil emulsion[J/OL]. Journal of Membrane Science, 2022, 654(April): 120538.
- [272] CHEN Y, LIU H, XIA M. Green multifunctional PVA composite hydrogel-membrane for the efficient purification of emulsified oil wastewater containing

REFERENCES

- Pb²⁺ ions[J/OL]. *Science of the Total Environment*, 2023, 856(July 2022).
- [273] LI F, BHUSHAN B, PAN Y. Bioinspired superoleophobic/superhydrophilic functionalized cotton for efficient separation of immiscible oil-water mixtures and oil-water emulsions[J/OL]. *Journal of Colloid and Interface Science*, 2019, 548: 123-130.
- [274] ZHU X, ZHU L, LI H. Enhancing oil-in-water emulsion separation performance of polyvinyl alcohol hydrogel nanofibrous membrane by squeezing coalescence demulsification[J/OL]. *Journal of Membrane Science*, 2021, 630(March): 119324.
- [275] SUN Y, LIU Y, XU B. Simultaneously achieving high-effective oil-water separation and filter media regeneration by facile and highly hydrophobic sand coating[J/OL]. *Science of the Total Environment*, 2021, 800: 149488.
- [276] RICHARDSON J J, BJÖRNMALM M, CARUSO F. Technology-driven layer-by-layer assembly of nanofilms[J/OL]. *Science*, 2015, 348(6233).
- [277] ZIN G, WU J, REZZADORI K. Modification of hydrophobic commercial PVDF microfiltration membranes into superhydrophilic membranes by the mussel-inspired method with dopamine and polyethyleneimine[J/OL]. *Separation and Purification Technology*, 2019, 212: 641-649.
- [278] KRISHNAMOORTHY R, ANBAZHAGAN R, TSAI H C. Preparation of caffeic acid-polyethyleneimine modified sponge for emulsion separation and dye adsorption[J/OL]. *Journal of the Taiwan Institute of Chemical Engineers*, 2021, 118: 325-333.
- [279] LIU W, HUANG X, PENG K. PDA-PEI copolymerized highly hydrophobic sponge for oil-in-water emulsion separation via oil adsorption and water filtration[J/OL]. *Surface and Coatings Technology*, 2021, 406(September 2020): 126743.
- [280] PULIKKALPURA H, KURUP R, MATHEW P J. Levodopa in *Mucuna pruriens* and its degradation[J/OL]. *Scientific Reports*, 2015, 5: 2-10.

REFERENCES

- [281] HUANG Q, LIU M, GUO R. Facile synthesis and characterization of poly(levodopa)-modified silica nanocomposites via self-polymerization of levodopa and their adsorption behavior toward Cu^{2+} [J/OL]. *Journal of Materials Science*, 2016, 51(21): 9625-9637.
- [282] BENFICA J, MORAIS E S, MIRANDA J S. Aqueous solutions of organic acids as effective solvents for levodopa extraction from *Mucuna pruriens* seeds[J/OL]. *Separation and Purification Technology*, 2021, 274(May).
- [283] DING L, WANG Y, ZHU P. One-step plant-inspired reaction that transform membrane hydrophobicity into high hydrophilicity and underwater super oleophobicity for oil-in-water emulsion separation[J/OL]. *Applied Surface Science*, 2019, 479.
- [284] ZHANG H, YU L, MA X. Self-cleaning poly(L-dopa)-based coatings with exceptional underwater oil repellency for crude oil/water separation[J/OL]. *Applied Surface Science*, 2020, 510(December 2019).
- [285] MU L, YUE X, HAO B. Facile preparation of melamine foam with superhydrophobic performance and its system integration with prototype equipment for the clean-up of oil spills on water surface[J/OL]. *Science of the Total Environment*, 2022, 833(April): 155184.
- [286] LONG X, ZHAO G, HU J. Cracked-earth-like titanium carbide MXene membranes with abundant hydroxyl groups for oil-in-water emulsion separation[J/OL]. *Journal of Colloid and Interface Science*, 2022, 607: 378-388.
- [287] WANG D, ZANG J, WANG Q. Hierarchical composite membrane with multiscale roughness structures for water-in-oil emulsion separation[J/OL]. *Applied Surface Science*, 2021, 566(June): 150666.
- [288] LI J, QIN Q H, SHAH A. Oil droplet self-transportation on oleophobic surfaces[J/OL]. *Science Advances*, 2016, 2(6): 1-7.
- [289] TAN Z, HU L, YANG D. Lignin: Excellent hydrogel swelling promoter used in

REFERENCES

- cellulose aerogel for efficient oil/water separation[J/OL]. *Journal of Colloid and Interface Science*, 2023, 629: 422-433.
- [290] ZHAO J, CHE Y, MAN S. Stimuli-responsive wettability quartz sand filter material for efficient separation of oil/water mixture and controllable demulsification of oil/water emulsion[J/OL]. *Journal of Water Process Engineering*, 2022, 46(October 2021): 102596.
- [291] ZHANG G, LIU Y, CHEN C. Applied Surface Science Green , robust self-cleaning superhydrophilic coating and on-demand oil – water separation[J]. 2022, 595(April).
- [292] HU J, ZHAN Y, ZHANG G. Durable and super-hydrophilic/underwater super-oleophobic two-dimensional MXene composite lamellar membrane with photocatalytic self-cleaning property for efficient oil/water separation in harsh environments[J/OL]. *Journal of Membrane Science*, 2021, 637(March): 119627.
- [293] CHEN S, LIU Y, WANG Y. Dual-functional superwetable nano-structured membrane: From ultra-effective separation of oil-water emulsion to seawater desalination[J/OL]. *Chemical Engineering Journal*, 2021, 411(November 2020): 128042.
- [294] YIN Z, YUAN F, XUE M. A multifunctional and environmentally safe superhydrophobic membrane with superior oil/water separation, photocatalytic degradation and anti-biofouling performance[J/OL]. *Journal of Colloid and Interface Science*, 2022, 611(December 2021): 93-104.
- [295] ZHANG H L. Viscosity and density for binary mixtures of carbon tetrachloride + chloroform, carbon tetrachloride + dichloromethane, and chloroform + dichloromethane and one ternary mixture of chloroform + 1:1 (carbon tetrachloride + dichloromethane) at 303.15 K[J/OL]. *Journal of Chemical and Engineering Data*, 2003, 48(1): 52-55.
- [296] LEE S L, THOMAS J, LIU C L. A greener approach to design Janus PVDF membrane with polyphenols using one-pot fabrication for emulsion

REFERENCES

- separation[J/OL]. *Journal of Membrane Science*, 2022, 656(May): 120616.
- [297] CAO M, XIAO F, YANG Z. Construction of Polytetrafluoroethylene nanofiber membrane via continuous electrospinning/electrospraying strategy for oil-water separation and demulsification[J/OL]. *Separation and Purification Technology*, 2022, 287(November 2021): 120575.
- [298] GAO D, FENG Y, ZHANG X. Cellulosic paper-based membrane for oil-water separation enabled by papermaking and in-situ gelation[J/OL]. *Cellulose*, 2022, 29(7): 4057-4069.